# Factor Graph Based Detection Schemes for Mobile Terrestrial DVB Systems with Long OFDM Blocks


Pello Ochandiano Campo

*Supervisors:*

**Mikel Mendicute Errasti**

*and*

**Jon Altuna Iraola**


MONDRAGON
UNIBERTSITATEA

A thesis submitted for the degree of

**Doctor by Mondragon Unibertsitatea**


Department of Electronics and Computer Science

Mondragon Goi Eskola Politeknikoa

Mondragon Unibertsitatea


April 2012

*Zuontzat guztiontzat...*

*eta zuretzat bereziki.*

# Eskertza

Lau urteko ibilbidearen ondoren jende askoren laguntza eskertu behar dut, beraiei esker izan ez balitz ez nintzateke hona iritsiko eta. Lantaldean eta elkarrekintzan nire burua aberastu dut eta modu baten edo beste baten jende askok izan du zerikusirik lan honen emaitzan. Nire esker ona erakutsi nahi diet bereziki:

- Nire tesi zuzendari Mikel Mendikute doktore jaunari lehenengo eta behin, beti hor egon delako. Bere zuzendaritza lanak eta gomendioek egin dute posible ikerketa lan hau. Eskerrak baita ere Jon Altuna doktore jaunari lan honen zuzendaritzan parte hartu duelako.

- Eusko Jaurlaritzako Industria, Berrikuntza, Merkataritza eta Turismo sailari eta Fagor Elektronikari IKERTU programako bekaren bidez emandako laguntzagatik.

- Mondragon Unibertsitateko Goi Eskola Politeknikoari bertan tesia egiteko aukera eman izanagatik.

- Goteborg-eko (Suedia) *Chalmers University*-ko *Communications Systems and Information Theory* sailari bertan zortzi hilabeteko estantzia egiteko aukera ematearren.

- Henk Wymeersch doktore jaunari Suedian egindako estantzian zehar nire ikerketa lana zuzendu zuelako.

- Nire lankide izan diren Iker Sobrón eta Lorena Martínez-i. Hirurok batera elkarlanean garatu dugu DVB-T2 simulatzailea eta horrekin batera ehundaka eztabaida izan ditugu bidean aurkitzen joan garen arazo teknikoen inguruan.

- Departamentuan lankide izan ditudanei: Maitane Barrenetxea, Idoia Jimenez, Aritz, Maite, Lorea, Iñaki... kafe orduak ere ikerketa lanaren parte direlako.

- Chalmers-en lankide izan nituenei: bereziki Alex Graell-i bere konpainiak Suediako egun ilunak argitu zituelako. Nire esker ona baita ere Alex Alvaradori.

# Acknowledgments

It is four years since I began to work on this research work. After this long journey I would like to express my gratitude to the people who have support me in many different ways:

- First of all, my supervisor Dr. Mikel Mendikute for his unconditional help and support. Without his guidance, I would not reach this point. I also want to thank Dr. Jon Altuna for his advice.
- The Department of Industry and Innovation of the Basque Government and Fagor Electrónica for the funding received through a IKERTU program grant.
- The High Polytechnical School of the University of Mondragon, for the chance to develop the PhD.
- Communications Systems and Information Theory division of Chalmers University, and specially to Dr. Henk Wymeersch for his help and support during my internship in Sweden.
- To my current and past colleges Lorena Martínez and Iker Sobrón. We have jointly developed the DVB-T2 simulator and we have had hundreds of technical discussions.
- To my PhD colleges who accompanied me along the last four years: Maitane Barrenetxea, Idoia Jimenez, Aritz, Maite, Lorea, Iñaki... coffee breaks are fundamental part of the research work.
- To the people I met in Chalmer University for their kindness and confidence. Especially to Alex Graell, for his joyful presence in Gothenburg, and to Alex Alvarado.

# Laburpena

Doktoretza tesi honek bigarren belaunaldiko telebista digitalaren eraginkortasuna aztertzen du eskenatoki mugikorrean, eta faktoreen grafoetan oinarritzen den hartzaile iteratibo bat proposatzen du denboran aldakorra den kanalak sortzen duen distortsioa leundu eta seinalea errorerik gabe hartzea ahalbidetzen duena. Proposatutako detektorea BICM-OFDM komunikazio eskema orokor baten gainean ebaluatu da lurreko *broadcasting* kanalaren baldintzak kontutan hartuz. Simulazio emaitzek algoritmo honen eraginkortasuna frogatzen dute Doppler frekuentzia handietan. Ikerketa lanaren bigarren zatian, faktoreen grafoetan oinarritutako detektorea eskema turbo zabalago baten baitan txertatu da LDPC dekodifikatzaile batekin batera. Hartzaile diseinu honen abantaila nagusia da OFDM simbolo luzeetara ondo egokitzen dela. Azkenik, proposatutako algoritmoa DVB-T2 katearen baitan inplementatu da, bi hartzaile eskema proposatu direlarik seinaleak duen dibertsitate tenporal eta frekuentziala probesteko, beti ere eraginkortasunaren, konplexutasunaren eta latentziaren arteko konpromisoa mantenduz.

# Resumen

Este trabajo de tesis analiza el rendimiento de la segunda generación de la televisión digital terreste en escenarios móviles y propone un algoritmo iterativo basado en grafos de factores para la detección de la señal y la reducción de la distorsión causada por la variación temporal del canal, permitiendo así recibir la señal libre de errores. El detector basado en grafos de factores propuesto es evaluado sobre un esquema de comunicaciones general BICM-OFDM en condiciones de transmisión propios de canales de difusión terrestres. Los resultados de simulación presentados muestran la eficiencia del algoritmo de detección propuesto en presencia de frecuencias Doppler muy altas. En una segunda parte del trabajo de investigación, el detector propuesto es incorporado a un esquema turbo junto con un decodificador LDPC, dando lugar a un receptor iterativo que presenta características especialmente apropiadas para su implementación en sistemas OFDM con longitudes de símbolo elevadas. Por último, se analiza la implementación del algoritmo propuesto sobre la cadena de recepción de DVB-T2. Se presentan dos esquemas de recepción que explotan la diversidad temporal y frecuencial presentes en la señal afectada por canales variantes en el tiempo, consiguiendo un compromiso razonable entre rendimiento, complejidad y latencia.

# Abstract

This PhD dissertation analyzes the performance of second generation digital video broadcasting (DVB) systems in mobile terrestrial environments and proposes an iterative detection algorithm based on factor graphs (FG) to reduce the distortion caused by the time variation of the channel, providing error-free communication in very severe mobile conditions. The research work focuses on mobile scenarios where the intercarrier interference (ICI) is very high: high vehicular speeds when long orthogonal frequency-division multiplexing (OFDM) blocks are used.

As a starting point, we provide the theoretical background on the main topics behind the transmission and reception of terrestrial digital television signals in mobile environments, along with a general overview of the main signal processing techniques included in last generation terrestrial DVB systems. The proposed FG-based detector design is then assessed over a simplified bit-interleaved coded modulation (BICM)-OFDM communication scheme for a wide variety of mobile environments. Extensive simulation results show the effectiveness of the proposed belief propagation (BP) algorithm over the channels of interest in this research work. Moreover, assuming that low density parity-check (LDPC) codes are decoded by means of FG-based algorithms, a high-order FG is defined in order to accomplish joint signal detection and decoding into the same FG framework, offering a fully parallel structure very suitable when long OFDM blocks are employed.

Finally, the proposed algorithms are analyzed over the physical layer of DVB-T2 specification. Two reception schemes are proposed which exploit the frequency and time-diversity inherent in time-varying channels with the aim of achieving a reasonable trade-off among performance, complexity and latency.

# Declaration of Originality

I hereby declare that the research recorded in this thesis and the thesis itself were developed entirely by myself at the Signal Theory and Communications Area, Department of Electronics and Computer Science, at the University of Mondragon.

The software used to perform the simulations was developed entirely by myself, with the following exceptions: the Matlab implementation of the basic transmission-reception chain of the DVB-T2 simulator has been jointly developed by Lorena Martínez, Iker Sobrón and myself. The implementation of the channel estimation algorithm employed in Chapter 5 has been carried out by Lorena Martínez.

Pello Ochandiano Campo
Department of Electronics and Computer Science
Mondragon Goi Eskola Politeknikoa
Mondragon Unibertsitatea
April, 2012

# Contents


Acknowledgments . . . iii
Abstract . . . v
Declaration of Originality . . . viii
Contents . . . ix
List of Figures . . . xi
List of Tables . . . xv
List of Symbols . . . xxi

**1 Introducción** **1**
1.1 Motivación . . . 2
1.2 Objetivos . . . 3
1.3 Contribuciones de la Tesis . . . 4
1.4 Estructura de la Tesis . . . 4

**2 Background and Related Work** **6**
2.1 Introduction . . . 6
2.2 Fundamentals of the wireless channel . . . 6
2.3 BICM-OFDM communication scheme . . . 8
2.3.1 Bit-interleaved coded modulation . . . 9
2.3.1.1 An information-theoretical view . . . 10
2.3.2 Orthogonal frequency-division multiplexing . . . 12
2.3.2.1 Frequency-diversity through coding and interleaving . . . 13
2.4 Low-density parity-check codes . . . 14
2.4.1 LDPC codes in DVB . . . 15
2.4.2 Decoding algorithms . . . 16
2.5 Time-varying fading channels . . . 18
2.5.1 Performance degradation of OFDM systems due to Doppler spreading 20
2.5.1.1 Intercarrier interference . . . 21
2.5.2 Exploiting time-domain diversity . . . 24

2.6 Terrestrial digital television . . . 25
2.6.1 DVB-T2 . . . 26
2.6.2 Multipath channel models for terrestrial television . . . 28
2.7 The turbo principle in mobile communications . . . 29
2.7.1 BICM-ID . . . 30
2.8 Intercarrier interference cancellation schemes . . . 31
2.9 Chapter Summary . . . 33

**3 Factor graph-based detection for channels affected by ICI 34**
3.1 Introduction . . . 34
3.2 Basic concepts . . . 35
3.2.1 Factor graphs and inference . . . 35
3.2.2 Building a factor graph . . . 36
3.2.3 SP algorithm . . . 38
3.2.4 Messages and their representation . . . 39
3.2.4.1 Message-scaling . . . 40
3.3 Loopy factor graphs . . . 41
3.4 System description . . . 42
3.5 Maximum a posteriori symbol detection based on factor graphs . . . 44
3.5.1 Optimal maximum a posteriori symbol detection . . . 45
3.5.2 Forney approach . . . 46
3.5.2.1 Convergence analysis . . . 47
3.5.2.2 Exploiting frequency-diversity . . . 48
3.5.2.3 BER and FER analysis . . . 49
3.5.3 Ungerboeck approach . . . 51
3.5.4 Forney approach vs Ungerboeck approach . . . 52
3.5.4.1 Kullback-Leibler divergence analysis . . . 53
3.5.5 BP detection vs MAP detection with ICI cancellation . . . 56
3.6 Complexity analysis . . . 58
3.7 Chapter Summary . . . 58

**4 Turbo approach for intercarrier interference cancellation 60**
4.1 Introduction . . . 60
4.2 System description . . . 61
4.3 Pilot-assisted factor graph based detection . . . 64
4.4 Classical approach . . . 65
4.4.1 EXIT chart analysis . . . 66
4.4.1.1 Numerical results . . . 67
4.5 Graphical approach . . . 69

4.6 Chapter Summary . . . . . 73

**5 Impact of BP-based ICI cancellation in mobile DVB-T2 74**

5.1 Introduction . . . . . 74

5.2 DVB-T2 to pave the way of DVB-NGH . . . . . 75

5.2.1 The benefits of employing long OFDM blocks in terrestrial broadcasting systems . . . . . 76

5.3 DVB-T2 performance in mobile scenarios . . . . . 77

5.4 Belief propagation detection over DVB-T2 . . . . . 79

5.4.1 First proposed reception scheme (PS1) . . . . . 80

5.4.1.1 Performance with ideal CSI . . . . . 80

5.4.1.2 Performance with channel estimation . . . . . 81

5.4.2 Second proposed reception scheme (PS2) . . . . . 83

5.4.2.1 Performance with ideal CSI . . . . . 84

5.4.2.2 Performance with channel estimation . . . . . 84

5.5 Chapter Summary . . . . . 85

**6 Conclusions and Further Research 87**

6.1 Summary . . . . . 87

6.2 Thesis Contributions . . . . . 88

6.3 Suggestions for Further Research . . . . . 89

**A Publications 91**

**References 94**

# List of Figures


2.1 Signal transmission over a multipath channel. . . . . 7

2.2 bit-interleaved coded modulation (BICM) transmitter. . . . . 9

2.3 BICM receiver with a turbo-like binary code. . . . . 9

2.4 Equivalent parallel channel model for BICM in the case of ideal interleaving. 10

2.5 Capacity of BICM over AWGN (a) and Rayleigh block fading (b) channels. . 12

2.6 Representation of five orthogonal subcarriers in orthogonal frequency-division multiplexing (OFDM) transmission. . . . . 13

2.7 Information outage probability for BICM over block Rayleigh fading channel with 16quadrature-amplitude modulation (QAM) modulation. . . . . 14

2.8 Tanner graph for an example low density parity check (LDPC) code. Round nodes represent variable nodes and square nodes represent check nodes. . . . 15

2.9 Message passing in the LDPC decoder. $f_j$ represents a variable node and $c_i$ represents a check node. . . . . 17

2.10 Clarke's model for time-varying Rayleigh fading channels. . . . . 18

2.11 Representation of the time-varying frequency response of the channel $\breve{\mathbf{H}}$ (a) and the frequency response matrix $\mathbf{H}$ describing the ICI power distribution (b). $f_d = 0.8$ and TU6 channel has been considered. . . . . 23

2.12 The main three diagonals of $\mathbf{H}$ for $f_d = 0.1$ (a) and $f_d = 0.4$ (b). The blue line represents the main diagonal, and the red one and the green one represent the first diagonal on the right side and the first diagonal on the left side, respectively. 23

2.13 Histogram of the LLRs affected by intercarrier interference (ICI). . . . . 24

2.14 DVB-T2 signal transmission over multipath channel profile with 100 Hz of Doppler frequency. 16QAM and code rate (CR)= 2/3 is considered. . . . . 25

2.15 Elementary transmission chain of DVB-T2. . . . . 26

2.16 Available modes in DVB-T and DVB-T2. . . . . 27

2.17 bit error rate (BER) performance of Digital Video Broadcasting-Terrestrial (DVB-T) and DVB-T2 systems over additive white Gaussian noise (AWGN) (a) and Rayleigh (b) channels. . . . . 28
2.18 Example of a turbo receiver. . . . . 29
2.19 DVB.T2 performance with iterative demapping over the 6-tap typical urban (TU6) channel. In the iterative case, 3 turbo iterations are considered and 20 LDPC iterations in each turbo iteration. In the non-iterative case, 50 LDPC iterations are carried out. . . . . 31
2.20 Summary of the main ICI suppressing schemes. . . . . 32

3.1 Simplified discrete channel model, where neither OFDM modulation nor interleaving has been considered for simplicity. . . . . 35
3.2 FG representing function $f(s_1, s_2, s_3, s_4) = f_1(s_1) f_2(s_1, s_2, s_3) f_3(s_3, s_4)$. . . 37
3.3 The sum-product (SP) algorithm: message computation rule from function node $f_k$ to variable node $s_m$ (a), and from variable node $s_n$ to function node $f_l$ (b). . . . . 38
3.4 Block diagram of the BICM-OFDM reception scheme including the belief propagation (BP) detector. . . . . 43
3.5 Frequency-domain system input-output relation after CP removal. . . . . 43
3.6 Representation of part of the channel frequency response $\mathbf{H}$ for $f_d = 0.13$ (a) and $f_d = 0.4$ (b). Higher power is represented by lighter color. TU6 channel has been considered. . . . . 44
3.7 The SP algorithm on a hidden-Markov model (HMM) with forward and backward phases. . . . . 46
3.8 Factor Graph for the Forney approach-based maximum a posteriori (MAP) symbol detection. . . . . 47
3.9 Convergence analysis by means of BER performance vs number of iterations for SP (a) and max-sum (MS) (b) algorithms at turbo cliff region. TU6 channel is assumed. . . . . 48
3.10 Percentages of suppressed ICI, non-suppressed ICI and residual ICI for different $f_d$ (a) and SNR vs $f_d$ at BER = $10^{-4}$ (b). MS algorithm is assumed. . . 49
3.11 BER vs SNR and FER vs SNR performance. . . . . 50
3.12 BER vs $f_d$ at SNR=7dB (a) and BER vs SNR for different iterations when MS algorithm is assumed ($f_d = 0.5$) (b). . . . . 51
3.13 Factor Graph for the Ungerboeck approach-based MAP symbol detection. . . 53
3.14 Ungerboeck approach vs Forney approach for $f_d = 0.16$ (a) $f_d = 0.4$ (b). . . . 54
3.15 Kullback-Leibler divergence $D(P||Q)$, where $P$ refers to the optimal FB algorithm and $Q$ represents the Forney approach BP algorithm and the Ungerboeck approach BP algorithm in each case. . . . . 55

3.16 SNR vs $f_d$ for the Forney approach BP detector, Ungerboeck approach BP detector and optimal FB algorithm. . . . . 55
3.17 Structure of the ICI suppressing soft demapper. . . . . 56
3.18 Stage 1 computes symbol estimates using a Viterbi-like algorithm. . . . . 57
3.19 MAP ICI canceler [Peng06] vs proposed BP detector for $f_d = 0.1$ and 0.3. . . 57

4.1 Turbo receiver consisting of the concatenation of the detector and the decoder, where the ICI channel works as a rate-1 inner code. . . . . 62
4.2 Block diagram of the BICM iterative receiver chain including the BP detector. 62
4.3 Example of a variable node processing a priori information of the corresponding symbol. . . . . 63
4.4 Pilot processing in the factor graph. . . . . 64
4.5 Example of a variable node processing a priori information of the corresponding symbol in the classical turbo approach. . . . . 66
4.6 Modeling a serial concatenated system with extrinsic information transfer (EXIT) functions. . . . . 67
4.7 Detector EXIT function for QPSK modulation (a) and detector and decoder EXIT functions for 16QAM modulation with different mapping schemes when $f_d = 0.22$ (b). TU6 channel has been considered in both cases. . . . . 68
4.8 EXIT chart (a) and BER vs LDPC iterations (b). QPSK modulation, TU6 channel, $f_d = 0.5$ and SNR = 8 dB has been considered. . . . . 69
4.9 High order FG performing joint data detection and decoding following the graphical approach for turbo reeption. . . . . 70
4.10 Performance comparison of non-turbo reception, classical turbo approach and the graphical turbo approach for TU6 (a) and RA6 (b) channels. $f_d = 0.5$ has been considered. . . . . 70
4.11 BER vs SNR performance of the graphical approach for the five turbo iterations. 71
4.12 Graphical turbo approach performance for different Doppler frequencies over TU6 channel (a) and RA6 channel (b) when QPSK modulation is considered. 72
4.13 Graphical turbo approach performance for different Doppler frequencies over TU6 channel (a) and RA6 channel (b) when 16QAM modulation is considered. 72

5.1 Bitrate vs robustness trade-off. . . . . 75
5.2 Simplified block diagram of the conventional DVB-T2 receiver (CONV). . . . 77
5.3 DVB-T2 performance versus different number of FEC blocks in the TI-block (time interleaving depth) at high SNR regime (SNR=30dB) for QPSK (a) and 16QAM (b). . . . . 79
5.4 Simplified block diagram of the first proposed scheme (PS1). . . . . 80

5.5 PS1 BER performance comparison for different number of BP iterations, with $f_d = 0.5$ over TU6 channel, considering ideal and partial CSI. 10 FEC blocks per TI-block are assumed (a). PS1 BER performance for different number of FEC blocks per TI-block, with $f_d = 0.5$ over TU6 channel, considering 3 BP iterations (b). . . . . 81
5.6 PS1 BER performance comparison for different numbers of BP iterations, with $f_d = 0.5$ over RA6 channel, considering ideal and partial CSI. 10 FEC blocks per TI-block are assumed (a). PS1 BER performance for different number of FEC blocks per TI-block, with $f_d = 0.5$ over RA6 channel, considering 3 BP iterations (b). . . . . 82
5.7 Simplified block diagram of the second proposed scheme (PS2). . . . . 83
5.8 PS2 BER performance for 3 BP iterations. $f_d = 0.5$ over TU6 channel (a) and RA6 channel (b). . . . . 84

# List of Tables

2.1 Serial concatenated systems with iterative detection/decoding. . . . . 30

3.1 Simulation parameters in Chapter 3. . . . . 45
3.2 Complexity analysis. . . . . 58

5.1 Simulation parameters in Chapter 5. . . . . 78

# Acronyms

**BICM** bit-interleaved coded modulation

**CSI** channel state information

**AMI** average mutual information

**AWGN** additive white Gaussian noise

**CM** coded modulation

**eIRA** extended irregular repeat-accumulate

**BP** belief propagation

**CP** cyclic prefix

**DFT** discrete Fourier transform

**DTV** digital television

**ASTC** advanced television system committee

**DTMB** digital terrestrial multimedia broadcast

**DVB** Digital Video Broadcasting

**DVB-T** Digital Video Broadcasting-Terrestrial

**DVB-NGH** Digital Video Broadcasting-Next Generation Handheld

**CR** code rate

**BER** bit error rate

**BCH** Bose-Chaudhuri-Hocquegham

**BICM-ID** bit-interleaved coded modulation-iterative demapping

**BILCM** bit-interleaved LDPC coded modulation

**BCJR** Bahl Cocke Jelinek Raviv

**CSI** channel state information

**BEM** basic expansion model

**EXIT** extrinsic information transfer

**BPSK** binary phase-shift keying

**LOS** line-of-sight

**LTE** long term evolution

**LLR** log-likelihood ratio

**FDM** frequency-division multiplexing

**ISI** intersymbol interference

**FER** frame error rate

**LDPC** low density parity check

**FEC** forward error correction

**ICI** intercarrier interference

**GI** guard interval

**IDFT** inverse discrete Fourier transform

**ISDB-T** integrated services digital broadcasting-terrestrial

**HDTV** high definition television

**GSM** global system for mobile communication

**FG** factor graph

**HMM** hidden-Markov model

**FFT** fast Fourier transform

**FB** forward-backward

**IFFT** inverse fast Fourier transform

**KL** Kullback-Leibler

**HD** high definition

**i.i.d.** independent and identically distributed

**OFDM** orthogonal frequency-division multiplexing

**MLC** multilevel coding

**ML** maximum likelihood

**MAP** maximum a posteriori

**QAM** quadrature-amplitude modulation

**RS** Reed-Solomon

**MP** message-passing

**MS** max-sum

**MP** max-product

**MSPCF** max-sum plus-correction factor

**PSK** phase-shift keying

**PDF** probability density function

**MPEG** moving picture experts group

**RQD** rotated constellations and Q-delay

**PAPR** peak-to-average power ratio

**QEF** quasi error free

**RA6** 6-tap typical rural area

**NLOS** non line-of-sight

**MMSE** minimum mean-square error

**MUI** multiuser interference

**PIC** parallel interference cancellation

**ML** maximum likelihood

**QPSK** quadrature phase-shift keying

**RSSD** Reduced state sequence detection

**MSEW** maximum squared euclidian weight

**SNR** signal to noise ratio

**SP** sum-product

**SISO** soft-in/soft-out

**SIC** successive interference cancellation

**SAGE** generalized expectation maximization

**SD** sphere decoding

**SER** symbol error rate

**SFN** single frequency networks

**TCM** trellis coded modulation

**TU6** 6-tap typical urban

**ZF** zero-forcing

**VA** Viterbi algorithm

# List of Symbols

| | |
|---|---|
| $\Delta_f$ | Subcarrier spacing |
| $c$ | Speed of light |
| $C_{BICM}$ | Bit interleaved coded modulation capacity |
| $C_{CM}$ | Coded modulation capacity |
| CR | Code rate |
| $d_{free}$ | Minimum Hamming distance |
| $E(s)$ | Average energy per symbol |
| $\mathrm{E}(x)$ | Expectation of $x$ |
| $f$ | frequency |
| $F_c$ | Carrier frequency |
| $f_c$ | 3-dB-cutoff frequency |
| $F_d$ | Absolute Doppler frequency |
| $f_d$ | Normalized Doppler frequency |
| $\mathbf{G}$ | Hermitian matrix |
| $\Gamma$ | Constellation size |
| $\mathbf{H}$ | Frequency-domain channel matrix |
| $h$ | Channel impulse response |
| $\breve{\mathbf{H}}$ | Time-varying frequency response of the channel |

| | |
|---|---|
| $\bar{\mathbf{H}}$ | Time-domain channel matrix |
| $\mathbf{H}_c$ | Parity-check matrix |
| $K_c$ | Number of message bits in the codeword |
| $L$ | Number of taps or paths of a multipath channel |
| $M$ | Number of bits per symbol |
| $M_c$ | Number of parity bits in the codeword |
| $N$ | OFDM symbol length |
| $N_0$ | Noise power spectral density |
| $N_c$ | Codeword length |
| $P_0$ | Outage probability |
| $P(a)$ | Probability of event a |
| $\mathbf{r}$ | Time-domain received signal column vector |
| $R$ | Coded modulation rate |
| $\mathbf{s}$ | Frequency-domain transmitted signal column vector |
| $\hat{s}$ | Hard estimate of symbol s |
| $\sigma_n^2$ | Variance of noise per real component |
| $\tilde{s}$ | Soft estimate of symbol s |
| $S_X$ | Power spectral density |
| $\tau$ | Tap delay |
| $T_C$ | Coherence time of the channel |
| $T_{IL}$ | Interleaver time span |
| $T_s$ | Sampling rate |
| $T_u$ | Length of the OFDM block |
| $w_c$ | uniform column weight |
| $w_r$ | uniform row weight |

| | |
|---|---|
| $\mathbf{x}$ | Time-domain transmitted signal column vector |
| $\mathbf{y}$ | Frequency-domain received signal column vector |
| $\mathbf{z}$ | Time-domain additive white Gaussian noise column vector |
| $\mathbf{z}_f$ | Frequency-domain additive white Gaussian noise column vector |

# Capítulo 1

# Introducción

La incorporación de la tecnología digital al mundo de la televisión supuso la apertura de un horizonte plagado de oportunidades relacionadas con el tratamiento digital de la señal. No obstante, más allá de lo estrictamente técnico, la televisión digital sentó las bases para revolucionar el concepto de televisión. Nuevas características como el pago por visión, la interactividad con el espectador, la integración de los aparatos audiovisuales domésticos, etc. son los cimientos de este nuevo concepto. En este contexto, Digital Video Broadcasting (DVB) se ha convertido en referencia mundial como consorcio encargado de crear y proponer los procedimientos de estandarización para la televisión digital. Los estándares de mayor repercusión comercial en la última década han sido DVB-C (televisión digital por cable, 1994) [ETSI94], DVB-S (televisión digital por satélite, 1995) [ETSI95], DVB-T (televisión digital terrestre, 1997) [ETSI97] y DVB-H (televisión digital terrestre para recepción en dispositivos móviles, 2004) [ETSI04]. Los estándares propuestos por DVB han sido adoptados en gran parte del mundo. No obstante, EEUU, China, Corea y Japón han desarrollado sus propias especificaciones.

Desde la definición de esta primera generación de la televisión digital, la electrónica ha experimentado un avance sustancial en cuanto a técnicas de procesamiento de señal se refiere. Una década después se conocen nuevas técnicas de modulación y protección contra errores que mejoran notablemente la capacidad y la robustez de la señal. Conjuntamente, los últimos años han sido testigos de la emersión de demandas comerciales como el video bajo demanda o la televisión de alta definición (HDTV), los cuales requieren de mayor eficiencia espectral. Todo ello ha dado lugar a la definición de la segunda generación de estándares para la televisión digital. DVB-T2 [ETSI09] fue lanzada al mercado en 2009 incluyendo las técnicas de codificación de canal más potentes, los códigos *low density parity-check* (LDPC), y etapas de procesamiento de señal opcionales como la rotación de constelaciones, o la codificación espacio-frecuencial. Estos avances han permitido acercarse considerablemente al límite teórico de capacidad de Shannon.

En general, la variedad de escenarios de difusión puede ser muy diversa, más aún si se añade como variable la movilidad del receptor, la cual es un requisito fundamental en los receptores modernos. La cada vez mayor demanda y oferta de información en el mercado

de las telecomunicaciones, incluida la televisión, y la tendencia a acceder a la información en cualquier momento y/o lugar, genera una continua necesidad de evolución hacia sistemas móviles que soporten mayores tasas de información con la misma o mayor robustez en su recepción. En el Plan Técnico Nacional Español de la televisión digital terrestre (RD 944/2005) ya se hablaba de la televisión en movilidad a través de DVB-H. No obstante, en el estado español, estas emisiones nunca llegaron más allá de algunos proyectos piloto aislados. Otros países con emisiones estables las abandonaron a lo largo de 2011. La causa del fracaso quizás haya que buscarla en la parte comercial: demasiadas incógnitas para un modelo de negocio que fue sustituido por el streaming a través de las redes 3G.

Con la introducción de la segunda familia de especificaciones de televisión digital, la recepción móvil vuelve a ser uno de los temas principales de estudio. De hecho, la movilidad fue uno de los requisitos comerciales para el diseño de DVB-T2, y actualmente nos encontramos inmersos en el proceso de definición de la segunda generación de televisión digital terrestre para dispositivos móviles (DVB-NGH), cuyo diseño se está basando en el primero.

## 1.1 Motivación

Hoy en día convivimos con múltiples sistemas de comunicaciones inalámbricas tales como redes de telefonía móvil, redes de área local WLAN (Wireless Local Area Network), redes de área metropolitana (Wireless Metropolitan Area Network) o redes de difusión de señales de radio y televisión. Este gran mercado se renueva constantemente con nuevos estándares que optimizan el uso del limitado espectro electromagnético basándose en el procesado digital de la señal. En este sentido, las redes de frecuencia única (SFN) juegan un papel fundamental.

Por otra parte, el estándar DVB-T2 introduce la posibilidad de transmitir múltiples flujos de entrada (PLP) ajustando los parámetros de transmisión a cada servicio específico. Ahondando en este sentido, la aparición reciente del perfil Lite de la norma DVB-T2 puede suponer un cambio cualitativo en el panorama de la televisión en movilidad, especialmente para aquellos países que ya hayan adoptado el estándar DVB-T2. Se abre la posibilidad de transmitir señales DVB-T2-Lite a través de un mismo canal de radiofrecuencia (RF) por donde se emite contenido en DVB-T2. Se hace uso así de diferentes niveles de robustez para cada tipo de señal, siendo la bondad del sistema que ambas tramas se pueden transmitir al mismo tiempo por el mismo canal de RF. A modo de ejemplo, se podría realizar el lanzamiento de un nuevo *múltiplex* DVB-T2 con servicios de calidad de imagen estándar (SDTV) o alta definición (HDTV) que incorporara un PLP específico DVB-T2 Lite para recepción en movilidad, renunciando a parte del ancho de banda en detrimento de un PLP más robusto. Por lo tanto, no sería necesario invertir en el despliegue de una nueva red específica para dispositivos móviles.

Tanto para extender la cobertura en redes SFN, contribuyendo así a la optimización de las

infraestructuras, como para aumentar la tasa efectiva de transmisión sin perder robustez, se está imponiendo la utilización de longitudes elevadas de bloque *orthogonal frequency-division multiplexing* (OFDM) (hasta 32K portadoras). No obstante, el uso de longitudes largas de bloque OFDM presenta dos desafíos desde el punto de vista técnico: por una parte, la distorsión que introduce la variación del canal puede resultar devastadora, ya que depende de la separación entre portadoras en frecuencia. Por lo tanto, se requiere de técnicas de procesamiento de señal avanzadas que reduzcan el nocivo efecto de la interferencia interportadora (ICI). Por otra parte, aumenta la complejidad de la implementación de los algoritmos en *hardware*, lo que conlleva un potencial aumento de la latencia y el coste en los receptores de televisión. En este sentido, desde el punto de vista de la implementación práctica, resulta vital disenar algoritmos de baja complejidad que permitan el procesamiento de la señal a alta velocidad.

## 1.2 Objetivos

Teniendo en cuenta lo expuesto anteriormente, los objetivos principales de esta tesis son los siguientes:

- Análisis del estándar DVB-T2, como referencia fundamental de la segunda generación de la televisión digital terrestre, en escenarios de movilidad.
- Diseño de un algoritmo de detección que permita la comunicación libre de errores considerando una longitud de bloque OFDM elevada (e.g., 32K) y que el receptor se mueve a alta velocidad, respetando las citadas restricciones de complejidad y latencia.

Para la consecución de estos objetivos se han abordado los siguientes objetivos parciales:

- Definición de los modelos y condiciones de propagación de la señal de televisión digital terrestre en movilidad.
- Evaluación de técnicas de detección de señal diseñadas específicamente para canales variantes en el tiempo que puedan ajustarse a los requisitos de diseño de estándares de televisión digital de última generación.
- Búsqueda de alternativas de algoritmos iterativos de detección en combinación con los códigos LDPC, restringiendo la complejidad del diseño de cara a su implementación en *hardware*.

## 1.3 Contribuciones de la Tesis

A continuación se listan las principales contribuciones de esta tesis doctoral:

- Análisis del rendimiento de la cadena física de DVB-T2 sobre modelos de canal propios de condiciones de radiodifusión terrestre. Se ha analizado la detección iterativa propuesta en [DVB09]. Este trabajo ha sido publicado en [Mendicute10].

- Estudio de las técnicas de detección de señal y supresión de interferencia interportadora adecuadas para su implementación en la cadena de recepción de DVB-T2. Concretamente, se ha analizado el rendimiento del detector propuesto en [Peng06] para una longitud de bloque OFDM de 128 subportadoras. Este trabajo ha sido publicado en [Ochandiano10].

- Diseño de un novedoso algoritmo iterativo basado en grafos de factores para la detección de la señal de televisión digital terrestre en receptores móviles. El detector ha sido evaluado sobre un esquema *bit-interleaved coded modulation* (BICM)-OFDM. Este trabajo ha sido publicado en [Ochandiano11b, Ochandiano11a].

- Se han analizado dos técnicas para la detección *maximum a posteriori* (MAP) en el grafo de factores, comprobando que la propuesta en esta tesis obtiene mejores resultados de rendimiento que la alternativa propuesta en [Haselmayr11]. Además, se ha analizado el comportamiento del detector como parte de un esquema *turbo* junto con el decodificador de LDPC. El receptor ha sido evaluado sobre un esquema BICM-OFDM. Este trabajo ha sido propuesto para su publicación en [Ochandiano12b]. Actualmente se encuentra en revisión.

- Implementación del receptor propuesto sobre la cadena de recepción de DVB-T2. Análisis del rendimiento del detector junto con el entrelazador de tiempo incluido en la especificación DVB-T2. Este trabajo ha sido propuesto para su publicación en [Ochandiano12a]. Actualmente se encuentra en revisión.

## 1.4 Estructura de la Tesis

La memoria de la tesis está estructurada en seis capítulos. Este primer capítulo introduce al lector en la temática de la tesis y presenta la motivación de la misma junto a los objetivos más destacados. También se presentan las contribuciones más notables, señalándose las publicaciones a los que han dado lugar.

El segundo capítulo recoge los fundamentos científicos sobre los que se desarrolla el trabajo de investigación. En primera instancia se introduce el canal inhalámbrico variante en el

tiempo y los efectos de dicho canal tanto en el dominio temporal como en el frecuencial. A continuación se describe el sistema de comunicaciones en el que se basa la nueva generación de televisión digital, BICM-OFDM, y los códigos LDPC, responsables en gran parte del incremento de capacidad en DVB-T2. Acto seguido se analiza el efecto de la variación del canal sobre una señal OFDM y se describe la ICI como fuente de diversidad frecuencial. En la segunda parte, se introducen las principales características de la capa física de DVB-T2, se analiza el principio de funcionamiento del esquena *turbo*, y se hace un repaso bibliográfico de las técnicas de cancelación de ICI más relevantes propuestas en los últimos años.

En el tercer capítulo se presenta la contribución central de la tesis: el diseño del detector basado en grafos de factores para receptores de elevada movilidad. En la primera parte se exponen los fundamentos de los algoritmos iterativos basados en grafos de factores y la problemática que esconde la presencia de bucles en dichos grafos. En la segunda parte se describe la detección MAP de la señal afectada por ICI en base al algoritmo suma-producto (SP) ejecutado sobre un grafo de factores. Para ello, se analizan dos modelos conocidos actualmente para la ejecución de la detección MAP así como su efecto sobre el rendimiento del detector: Ungerboeck y Forney. Se demuestra que la detección MAP en base al modelo de Forney supera en rendimiento al modelo de Ungerboeck en las condiciones de canal que interesan en este trabajo de investigación. Además, se realiza un análisis comparativo del rendimiento del algoritmo y un potencial candidato propuesto anteriormente en la bibliografía. Por último, se aborda la cuestión de la complejidad.

El cuarto capítulo se centra en el análisis del rendimiento del algoritmo propuesto como parte integrante de un esquema *turbo* de nivel superior en el que se intercambia información *soft* entre el detector y el decodificador LDPC. Se toman en cuenta dos procedimientos para la ejecución del esquema *turbo*: el clásico, según el cual se intercambia información *soft* entre dos procesadores independientes; y el gráfico, que comprende la visión de un único grafo en el que se intercambian mensajes entre nodos. Se analiza el comportamiento del primero a través de la curva de transferencia de información extrínseca (EXIT) y se muestran resultados comparativos de rendimiento.

El quinto capítulo analiza el detector propuesto sobre la capa física de DVB-T2. Para ello se proponen dos esquemas de recepción combinando el empleo del entrelazador de tiempo y el esquema *turbo* introducido en el capítulo cuarto. Se considera tanto el conocimiento ideal del canal como no ideal, analizando así el efecto del error de estimación sobre el detector. Se muestran resultados de rendimiento para modelos de canal típicos de radiodifusión terrestre.

Por último, el sexto capítulo resume el trabajo realizado y las principales conclusiones obtenidas, así como las líneas futuras que el autor plantea como posible extensión del trabajo presentado en esta tesis.

# Chapter 2
# Background and Related Work

## 2.1 Introduction

Commercial requirements based on the demand of higher data rates, greater spectral efficiencies and improved data integrity have triggered the specification of recent broadband high-speed communications standards. This is the case of IEEE's 802.16 family, long term evolution (LTE) project, or the recently standardized Digital Video Broadcasting (DVB) specifications. Mobility support is one of the key features of these new technologies, dealing with the challenge of enabling mobile broadband services at high vehicular speeds. Either the second generation DVB standards, with both terrestrial and handheld versions, or the IEEE 802.16m are good examples of the mobility requirements of new wireless communication standards.

As a starting point, this chapter offers the theoretical background on the main topics behind the transmission and reception of terrestrial digital television signals in mobile environments. First of all, the fundamentals of wireless communication channels are reviewed, along with their effects on the performance of received signals. On the other hand, a general overview of the main signal processing techniques included in last generation terrestrial DVB systems is drawn, giving a brief look at the diversity sources available in such communication scenarios.

In the second part, we review the 'turbo principle', which is a basic mechanism in the development of factor graph (FG)-based algorithms, and discuss the most remarkable ICI suppressing techniques proposed in the recent literature, paying special attention to those ones suitable for being implemented in terrestrial DVB systems.

## 2.2 Fundamentals of the wireless channel

The channel model plays a key role in communication systems design. A common approach is to define a statistical model based on a large set of measurements, in a way that the performance can be assessed by simulation, averaging over a large amount of channel realizations.

In a wireless system, the signal from transmitter to receiver usually experiments several reflections due to scatterers. Therefore, the channel can be modeled as a multipath channel where the line-of-sight (LOS) component may or not be available depending on the propagation environment.

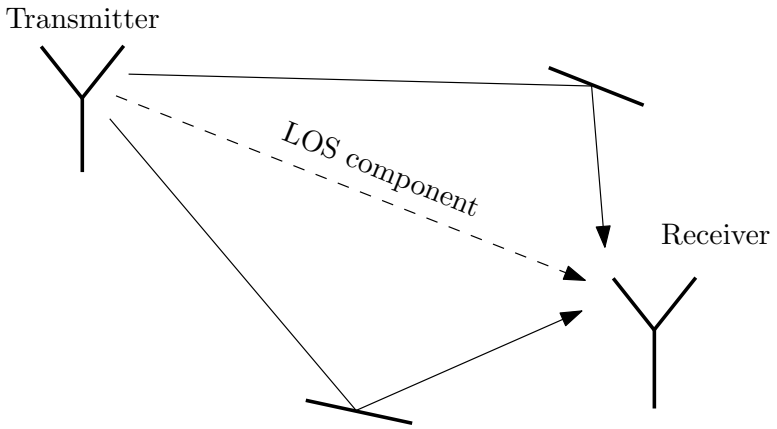


Figure 2.1: Signal transmission over a multipath channel.

The multipath channel model can be mathematically expressed as follows:

$$h(t) = \sum_{l=1}^{L} A_l \exp(j\theta_l)\, \delta(t - \tau_l), \tag{2.1}$$

where $A_l$ is the amplitude, $\theta_l$ is the phase of the $l$th component and $\tau_l$ is the relative delay. Note that the phases $\theta_l$ are modeled as independent and identically distributed (i.i.d.) random variables, uniformly distributed in $[0, 2\pi)$. For the moment, we do not consider any time variation of the channel impulse response, therefore, the amplitudes and the delays are constant. Applying the Fourier transform to (2.1), we get the frequency response of the channel

$$H(f) = \sum_{l=1}^{L} A_l \exp(j\theta_l) \exp(-j2\pi f \tau_l). \tag{2.2}$$

Let us assume that the channel is flat-fading or frequency-nonselective, which means that the frequency response of the channel remains constant over the signal band. In this case, it can be modeled as a scalar gain $g$ described as

$$g \approx H(f_0) = \sum_{l=1}^{L} A_l \exp(j\theta_l) \exp(-j2\pi f_0 \tau_l). \tag{2.3}$$

If the number of channel taps is large, and the contributions of all of them are small, central limit theorem can be invoked, and the channel $g$ can be considered as a complex Gaussian, i.e., $g \sim \mathcal{CN}(0, \sum_l A_l^2)$, which implies that the envelope, given by the absolute value of $g$, is

a Rayleigh random variable. Moreover, in wireless communication channels, it is very common to have a LOS component which corresponds to the smallest delay and is significantly stronger than the other taps. In this case, the sum of the components apart from the LOS path, $g_{rest}$, can be modeled as zero mean Gaussian, so that the channel gain is

$$g = A_1 \exp\left(j\left(\theta_1 - 2\pi f_1 \tau_1\right)\right) + g_{rest}. \tag{2.4}$$

The envelope $|g|$, is a Rician random process and the channel is termed as Rician fading:

$$g \sim \mathcal{CN}\left(A_1 \exp\left(j\left(\theta_1 - 2\pi f_1 \tau_1\right)\right), \sum_{l=2}^{L} A_l^2\right) \tag{2.5}$$

Now, let assume that the transmitted signal has a bandwidth larger than the channel coherence bandwidth, so that the channel is considered frequency-selective. Considering the transmitted signal has bandwidth $B_W$, we must modify the mathematical channel model in (2.1) in a way that $1/B_W$-spaced taps are considered:

$$h\left(t\right) = \sum_{i=1}^{\infty} \alpha_i \delta\left(t - \frac{i}{B_W}\right), \tag{2.6}$$

where each of the $\alpha_i$ taps is obtained by means of summing a large number of unresolvable taps as

$$\alpha_i \approx \sum_{k:\tau_k \approx \frac{i}{B_W}} A_k \exp j\theta_k. \tag{2.7}$$

The $\alpha_i$ taps are independent, zero mean Gaussian random variables, and as a consequence, the amplitudes $|\alpha_i|$ are independent Rayleigh random variables. Note that, in the case of LOS presence, the direct path is modeled as Rician rather than Rayleigh.

## 2.3 BICM-OFDM communication scheme

The BICM-OFDM communication scheme has been adopted by most of the last-generation communication standards due to its simplicity, flexibility and performance in wireless environments. This is the case of IEEE's 802.16 family [IEEE05, IEEE06], the LTE project, or the recently standardized second generation DVB specifications [ETSI05, ETSI09]. In this section, BICM-OFDM scheme is analyzed with the aim of offering a general overview of the key features which make this communication scheme so robust in wireless channels.

### 2.3.1 Bit-interleaved coded modulation

Massey proposed in 1974 [Massey74] to jointly design coding and modulation, thus founding the field of coded modulation. The goal was to efficiently combine high-order modulation (high data rates) with strong channel coding schemes for high reliability. Two years later, Ungerboeck presented trellis coded modulation (TCM) [Ungerboeck76] and Imai proposed multilevel coding (MLC) [Imai77] as powerful coded modulation schemes. In contrast to traditional approaches which tried to optimize the Hamming distance measure, in both TCM and MLC schemes, the design strategy was to improve the Euclidean distance. Afterwards, in 1992, BICM was introduced by Zehavi [Zehavi92], which consists of nothing but a serial concatenation of a code, a bit-wise interleaver and a mapper. Caire, Taricco and Biglieri [Caire98] proved that it is possible to achieve very close to capacity performance with BICM when Gray mapping is used.

The information bits are encoded by a single encoder and interleaved by a random interleaver $\prod$. The coded and interleaved sequence $\mathbf{c}$ is partitioned in $N_s$ subsequences $\mathbf{c}_n$ of length $M$, where

$$\mathbf{c}_n = (c_{n,1}, ..., c_{n,m}, ..., c_{n,M}) \,. \tag{2.8}$$

The bits $\mathbf{c}_n$ are mapped at time index $n$ to a symbol $s_n$ chosen from the $2^M$-ary signal constellation $\chi$ according to the binary labeling map $\mu : \{0,1\}^M \rightarrow \chi$.

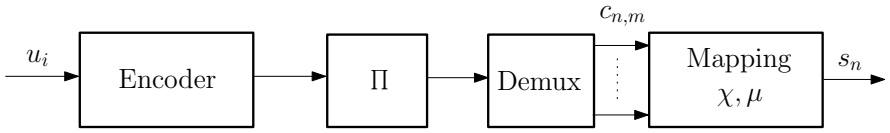


Figure 2.2: BICM transmitter.

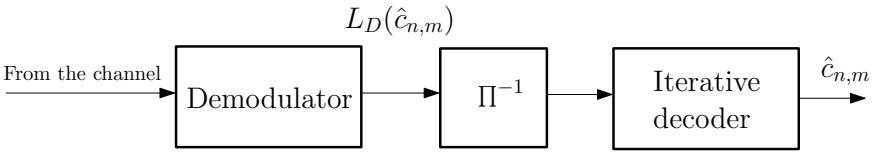


Figure 2.3: BICM receiver with a turbo-like binary code.

The optimum BICM receiver is the joint maximum likelihood (ML) decoder. However, the complexity of a joint ML demapper and decoder is not manageable. Therefore, demapping and decoding tasks are separated (Fig. 2.3) and the MAP soft demapping is performed which uses the received value $y_n$ of the transmitted symbol $s_n$ to obtain estimates about the corresponding bits $c_{n,m}$. The log-likelihood ratio (LLR) for the bit estimate $\hat{c}_{n,m}$ is described as follows,

$$L_D\left(\hat{c}_{n,m}\right) = \log \frac{\sum_{\forall \mathbf{c}_n : c_{n,m}=0} \exp \Lambda\left(\mathbf{c}_n\right)}{\sum_{\forall \mathbf{c}_n : c_{n,m}=1} \exp\left[\Lambda\left(\mathbf{c}_n\right)\right]}, \tag{2.9}$$

with the metric

$$\Lambda\left(\mathbf{c}_n\right) = \log P\left(y_n | s_n\right) + \sum_{m=1}^{M} \log P\left(c_{n,m}\right), \tag{2.10}$$

where $P\left(y|s\right)$ is the channel transition probability. Considering no a priori information and omitting the terms that are independent of the sequence $\mathbf{c}_n$, we can rewrite the LLR for the bit estimate $\hat{c}_{n,m}$ as

$$L_D\left(\hat{c}_{n,m}\right) = \log \frac{\sum_{\forall \mathbf{c}_n : c_{n,m}=0} P\left(y_n|s_n\right) \prod_{j=1; j\neq m}^{M} P\left(c_{n,j}\right)}{\sum_{\forall \mathbf{c}_n : c_{n,m}=1} P\left(y_n|s_n\right) \prod_{j=1; j\neq m}^{M} P\left(c_{n,j}\right)}. \tag{2.11}$$

Commonly, an equivalent channel model is defined for the BICM communication scheme with ideal interleaving. It consists of a set of $M$ parallel independent and memoryless binary input channels connected to the encoder output through a random switch, which models ideal interleaving. Each channel corresponds to a position in the label of $\chi$. For every symbol $c_{n,m}$ of a coded sequence, the switch selects randomly a position index as it is shown in Fig. 2.4.

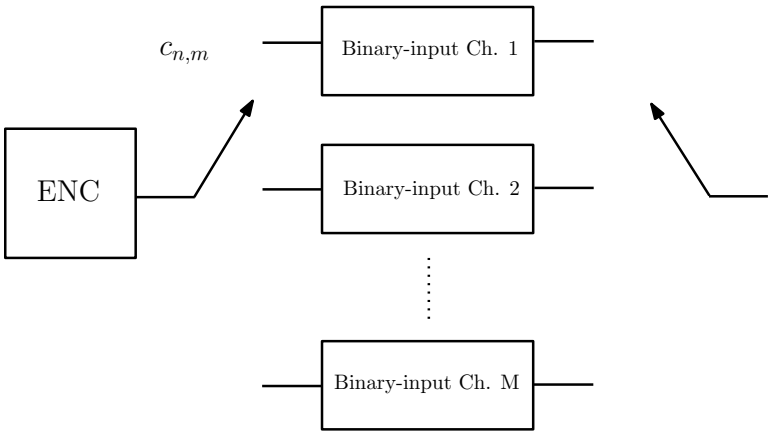


Figure 2.4: Equivalent parallel channel model for BICM in the case of ideal interleaving.

#### 2.3.1.1 An information-theoretical view

Under the constraint of uniform input probabilities and assuming ideal interleaving, we can compute the capacity of CM and BICM communication systems. Consider the memoryless discrete-input continuous-output channel with input $\mathbf{s}$, output $\mathbf{y}$, and transition distribution $P_{\boldsymbol{\theta}}\left(\mathbf{y}|\mathbf{s}\right)$. Due to ideal interleaving, the sequence of channel state parameters $\boldsymbol{\theta}$ is i.i.d.. Hence, the coded modulation (CM) capacity constrained to uniform inputs and perfect channel state

information (CSI) is given by the conditional average mutual information (AMI) [Caire98]

$$C_{CM} = I\left(\mathbf{s};\mathbf{y}|\boldsymbol{\theta}\right) = M - E_{\mathbf{s},\mathbf{y},\boldsymbol{\theta}}\left[\log_2 \frac{\sum_{\upsilon\in\chi} P_{\boldsymbol{\theta}}\left(\mathbf{y}|\boldsymbol{\upsilon}\right)}{P_{\boldsymbol{\theta}}\left(\mathbf{y}|\boldsymbol{\upsilon}\right)}\right], \tag{2.12}$$

where capacity is expressed in information bits per complex dimensions (bit/dim). It is stated that CM communication system can achieve spectral efficiencies $R \leq C_{CM}$.

In order to compute the capacity achievable by BICM, we are going to take into account the parallel channel model described in Fig. 2.4. Let $b$ denote a binary input, $\mathbf{y}$ the vector channel output, and $\check{S}$ the random variable whose output determines the switch position (which we consider i.i.d., uniformly distributed and known to the receiver). Assuming perfect CSI and uniform inputs, and since there are $M$ parallel independent channels, the conditional mutual information of $b$ and $\mathbf{y}$ given $S$ can be expressed as [Caire98]

$$C_{BICM} = M \cdot I\left(b;\mathbf{y}|\boldsymbol{\theta},\check{S}\right) = M - \sum_{i=1}^{M} E_{b,\mathbf{y},\boldsymbol{\theta}}\left[\log_2 \frac{\sum_{\upsilon\in\chi} P_{\boldsymbol{\theta}}\left(\mathbf{y}|\boldsymbol{\upsilon}\right)}{\sum_{\upsilon\in\chi_b^i} P_{\boldsymbol{\theta}}\left(\mathbf{y}|\boldsymbol{\upsilon}\right)}\right], \tag{2.13}$$

where it is shown that the capacity of the BICM channel is the average over the equivalent channels of the bit positions. Expectations in (2.12) and (2.13) cannot be calculated in closed form. Thus, numerical integration based on Monte Carlo method is used and the next inequality can be proven:

$$C_{BICM} \leq C_{CM}. \tag{2.14}$$

BICM capacity strongly depends on the applied mapping. Fig. 2.5 depicts the capacity of a standard BICM receiver using different mappings over AWGN channel. As it is shown, when Gray mapping is used, since the bit positions in the symbol labels are independent, BICM capacity is closed to CM's capacity. However, a significant loss is obtained for mappings different from Gray as it is shown in Fig. 2.5. Capacity curves are also depicted for a Rayleigh fading channel with coherent detection and it is shown that the sub-optimality of BICM with respect to CM is maintained.

However, it is widely accepted that the analysis based on the cutoff rate $R_0$ is more sensible for comparing channels for which a finite-complexity coding scheme is required. The cutoff rate specifies the highest information rate beyond which sequential decoding becomes impractical. Again in [Caire98], simulation results based on cutoff rate are shown over AWGN and Rayleigh channels, where it is concluded that, for a given complexity, BICM outperforms CM over Rayleigh fading channel, especially for high rates. As a consequence, if the channel obeys a Rician fading channel model and fluctuates in time between the extremes of Rayleigh and AWGN (as is the case for mobile radio), the BICM scheme is more robust than CM.

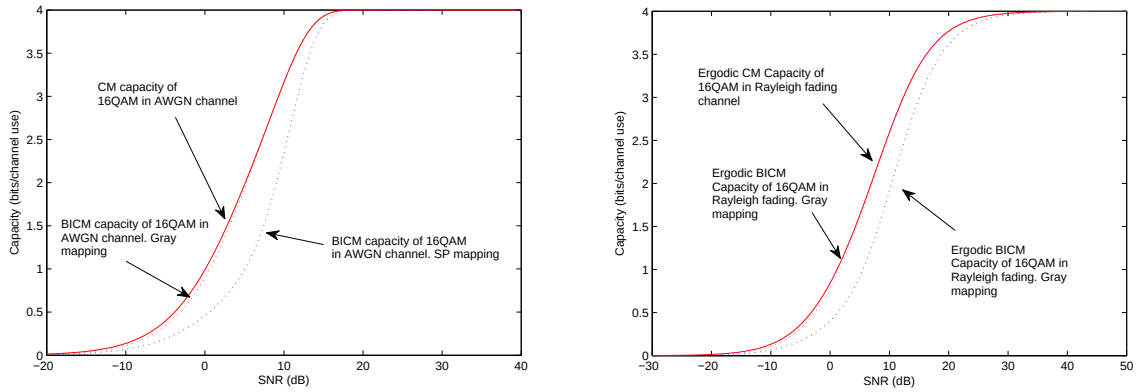


(a) (b)

Figure 2.5: Capacity of BICM over AWGN (a) and Rayleigh block fading (b) channels.

On the other hand, it is easy to realize intuitively which are the benefits of using coding and interleaving. Since multipath fading channels vary across frequency, when a wide enough bandwidth is employed, there can be good channel realizations as well as bad fades. Usually, the former are more likely than the latter. Therefore, employing error correction coding over a large enough frequency span prevents from a dramatical performance loss due to the small fraction of symbols that experiment bad fades. Since typical codes are optimized to correct random errors, the bit interleaver scrambles the errors along the entire codeword, thus improving the system performance.

### 2.3.2 Orthogonal frequency-division multiplexing

OFDM is a frequency-division multiplexing (FDM) scheme used as a digital multi-carrier modulation method. A large number of closely-spaced orthogonal subcarriers are used to carry data (see Fig, 2.6), which are divided into several parallel data streams or channels, one for each subcarrier. Each subcarrier is modulated with a conventional modulation scheme (such as QAM) at a low symbol rate, maintaining total data rates similar to conventional single-carrier modulation schemes in the same bandwidth.

The primary advantage of OFDM over single-carrier schemes is its ability to cope with severe channel conditions (i.e., narrowband interference and frequency-selective fading due to multipath) without complex equalization filters. Channel equalization is simplified because OFDM may be viewed as using many slowly-modulated narrowband signals rather than one wideband signal. A guard interval (GI) is included to avoid intersymbol interference (ISI) between consecutive blocks. In order to make the channel convolution circulant and simplify frequency-domain equalization, cyclic prefix (CP) is used as GI scheme.

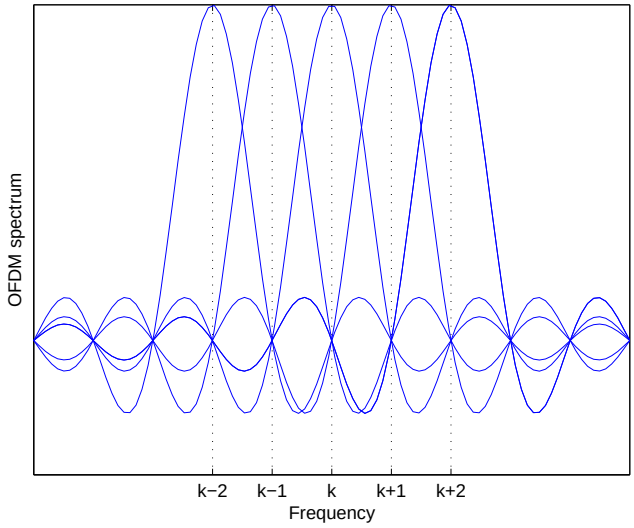


Figure 2.6: Representation of five orthogonal subcarriers in OFDM transmission.

#### 2.3.2.1 Frequency-diversity through coding and interleaving

One of the key features that explains the good performance of OFDM in wireless communication systems is that the channel turns out to be a set of parallel flat-fading channels. On the other hand, as it has been described in Section 2.3.1.1, BICM shows high performance for flat-fading channels. Hence, it is natural to combine BICM and OFDM in order to exploit the common grounds of both techniques and improve the robustness of the overall system in demanding wireless channels. In fact, BICM-OFDM has been shown to exploit the diversity that is inherent within the frequency-selective fading channels. In other words, BICM-OFDM is a very effective technique to provide diversity gain employing frequency-diversity.

In [May04] it is formally proven that the diversity order achieved by BICM-OFDM systems is $\min(d_{free}, L)$, where $d_{free}$ is the minimum Hamming distance of the channel code. Hence, in practice, the larger the delay spread is, in other words, the more selective the channel is, the higher is the diversity order that the system can achieve for a given channel code. The following example shows how the diversity order increases depending on the selectivity of the channel: let assume a BICM single-carrier scheme over a block Rayleigh fading channel. The codeword is broken into $B$ equal-length blocks and the signal to noise ratio (SNR) changes randomly from block to block. The instantaneous SNR for block $b$ is $\gamma_b$. Note that the system equals to a BICM-OFDM system over a multipath channel. We consider that the codeword's mutual information $I^B$ is the sum of the block's $I_b = \log(1 + \gamma_b)$, $I^B = \sum_{b=1}^{B} I_b$. An information outage occurs after $B$ blocks if $I^B < R$, where $R \leq \log_2 \Gamma$ is the rate of the coded modulation, and means that no code can be reliable for the particular channel instantiation. The information outage probability is given by

$$P_0 = P\left[I^B < R\right]. \tag{2.15}$$

Fig. 2.7 shows that as the block number $B$ increases (more selective is the channel), the information outage probability, considered as a practical bound of frame error rate (FER), curves become steeper, gaining diversity order.

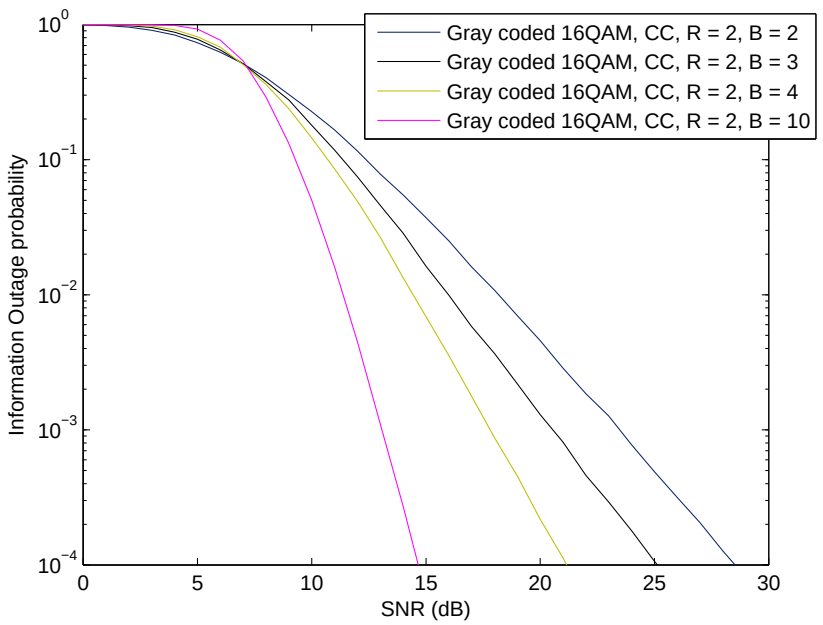


Figure 2.7: Information outage probability for BICM over block Rayleigh fading channel with 16QAM modulation.

## 2.4 Low-density parity-check codes

LDPC codes are a class of linear block codes which provide near-capacity performance on a large collection of data transmission channels while simultaneously admitting implementable decoders. They were first introduced by Gallager during his PhD thesis in 1963 [Gallager63], but due to computational complexity of the coding and decoding processes, they were ignored until about twenty years ago. Although LDPC codes can be generalized to non-binary alphabets, we shall consider only binary LDPC codes. An LDPC code is defined by a sparse parity-check matrix $\mathbf{H}_c$ that contains mostly zeros and only a small number of ones, i.e., it has low density of ones. If the parity check matrix $\mathbf{H}_c$ has $N_c$ columns and $M_c$ rows, the codewords consist of sequences $\mathbf{c}$ of $N_c$ bits that satisfy a set of $M_c$ parity checks defined by the equation $\mathbf{H}_c \cdot \mathbf{c}^{\mathrm{T}} = 0$. The number of message bits is $K_c = N_c - M_c$ and the rate of the code is CR$= K_c/N_c$. LDPC codes can be classified broadly into two types: regular and irregular. Regular LDPC codes have a parity check matrix with uniform column weight $w_c$

as well as uniform row weight $w_r$, where the column (row) weight refers to the number of "1"s in a column (row). In irregular LDPC codes the column and row weight are not constant.

In 1981, Tanner generalized LDPC codes and introduced a graphical representation [Tanner81], now called Tanner graphs. The Tanner graph is a bipartite graph which describes the code by two types of nodes (variable and check nodes) and edges connecting two nodes of different types (see Fig. 2.8).

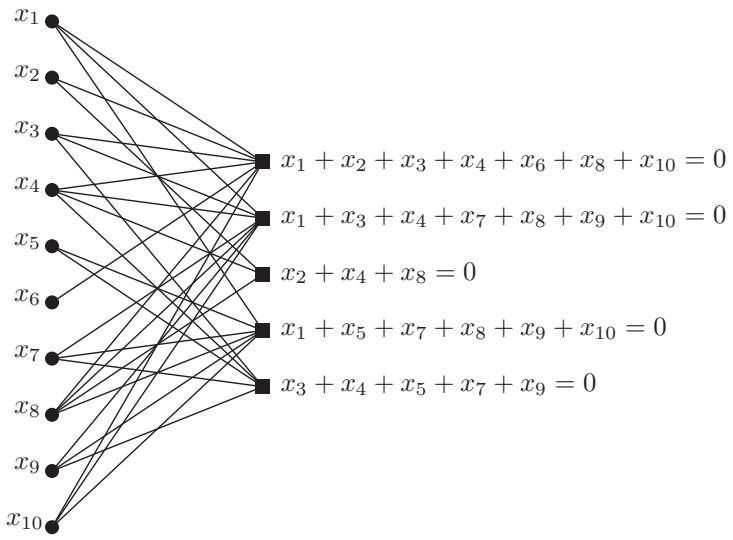


Figure 2.8: Tanner graph for an example LDPC code. Round nodes represent variable nodes and square nodes represent check nodes.

Generally, Tanner graphs are a specific case of FGs. In Tanner's original formulation, all variables are codeword symbols and hence "visible". Wiberg et al. [Wiberg96], introduced "hidden" state variables and also suggested applications beyond coding. FGs take these graph theoretic models one step further, by applying them to functions. From the FG perspective (as we will describe in Section 3.2), a Tanner graph represents a particular factorization of the characteristic function of a code. Hence, from now on and without loss of generality, we will refer to Tanner graphs as FGs.

### 2.4.1 LDPC codes in DVB

The first generation of DVB specifications use concatenated convolutional and Reed-Solomon (RS) codes. In the second generation standards, this forward error correction (FEC) techniques have been replaced by LDPC and Bose-Chaudhuri-Hocquegham (BCH) codes. These codes, which are tens of thousands bits long, can realize a substantial throughput increase and improve both the performance and the encoding complexity. The well-known extended irregular repeat-accumulate (eIRA) codes have been adopted for this purpose [Yang04]. The

parity-check matrix is of the form

$$\mathbf{H}_c = \left[\mathbf{H}^1_{(N_c-K_c)\times K_c}\mathbf{H}^2_{(N_c-K_c)\times(N_c-K_c)}\right], \tag{2.16}$$

where $\mathbf{H}^1$ is a submatrix corresponding to information and $\mathbf{H}^2$ is a staircase lower triangular submatrix corresponding to parity:

$$H^2 = \begin{pmatrix} 1 & & & & & & \\ 1 & 1 & & & & & \\ & 1 & 1 & & & & \\ & & & \ddots & & & \\ & & & & 1 & 1 & \\ & & & & & 1 & 1 \end{pmatrix} \tag{2.17}$$

Encoding procedure is given by the parity bits calculation as

$$p_1 = \sum_{k=1}^{K_c} u_k h_{1,k} \tag{2.18}$$

$$p_m = p_{m-1} + \sum_{k=1}^{K_c} u_k h_{m,k}, \tag{2.19}$$

where $h_{i,j}$ is the $(i,j)$th element of parity check matrix $\mathbf{H}_c$, with $1 \leq i \leq M_c$ and $1 \leq j \leq N_c$. Note that $M_c = N_c - K_c$. Calculating each parity bit recursively, we can obtain the whole codeword $\mathbf{c}$ using the parity check matrix directly, that is, without the generator matrix. Since $\mathbf{H}^1$ is sparse, encoding has linear complexity with respect to the codeword length.

### 2.4.2 Decoding algorithms

In addition to introducing LDPC codes, Gallager proposed a near-optimal decoding algorithm. Since then, many research works have proposed similar algorithms, albeit for other applications. The algorithm iteratively computes the distributions of variables in a graph-based model, and it is known under different names depending on the context, such as SP, BP or max-product (MP). We will take the SP algorithm as a reference, but there are approximations of the SP that are popular for reducing complexity like MS or max-sum plus-correction factor (MSPCF). A further explanation on iterative algorithms based on graph models is given in Section 3.2.

With the aim of avoiding numerical instability, it is common to use the logarithmic domain version of the SP. Following the graph theory basis, local computations are performed in the nodes and updated messages are exchanged between variable and check nodes. After a finite number of iterations or after some stopping criteria has been met, the decoder

computes the output LLRs from which decisions on the bits $c_i$ are made. One example of such stopping criteria is to stop iterating when $\hat{\mathbf{c}}\mathbf{H}_c^{\mathrm{T}} = 0$, where $\hat{\mathbf{c}}$ is a tentative decoded codeword.

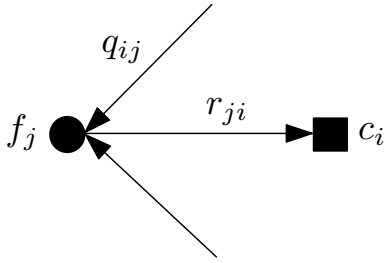


Figure 2.9: Message passing in the LDPC decoder. $f_j$ represents a variable node and $c_i$ represents a check node.

The logarithmic domain SP decoder is summarized as follows:

1. For $i = 1, ..., N_c$, initialize $L(q_{ij})$ with channel LLRs $L(c_i)$ calculated in (2.11). Note that index $n$ and $m$ in (2.11) have been replaced by $i$.

2. Update $\{L(r_{ji})\}$ using the next equation

$$L(r_{ji}) = \prod_{i' \in V_j \backslash i} \alpha_{i'j} \phi \left( \sum_{i' \in V_j \backslash i} \phi(\beta_{i'j}) \right), \tag{2.20}$$

   where $\alpha_{ij} = \mathrm{sign}[L(q_{ij})]$, $\beta_{ij} = |L(q_{ij})|$ and $\phi(x) = -\log[\tanh(x/2)] = \log\left(\frac{\exp(x)+1}{\exp(x)-1}\right)$.

3. Update $\{L(q_{ij})\}$ using the next equation

$$L(q_{ij}) = L(c_i) + \sum_{j' \in C_i \backslash j} L(r_{j'i}), \tag{2.21}$$

4. Update $\{L(Q_i)\}$ using the next equation

$$L(Q_i) = L(c_i) + \sum_{j \in C_i} L(r_{ji}). \tag{2.22}$$

5. For $i = 1, ..., N_c$ set $\hat{c}_i = 1$ if $L(Q_i) < 0$ and $\hat{c}_i = 0$ otherwise. If the stopping criteria is not fulfilled or the number of iterations is less than the maximum limit go to step 2, else stop.

## 2.5 Time-varying fading channels

In Section 2.2 we have referred to the fading experienced by a signal due to multipath time delay spread. Depending on the relation between the signal bandwidth and the coherence bandwidth of the channel (or the delay spread and the symbol period), the channel can be frequency-flat fading or frequency-selective fading. On the other hand, a wireless channel can also be characterized by channel time variation induced by relative mobility between transmitter and receiver, which imposes fundamental limitations on the performance of the wireless communication systems.

The time-varying nature of the channel is described by the coherence time and the Doppler spread. The coherence time refers to the time duration over which the channel impulse response remains essentially invariant, whereas the Doppler spread is the frequency-domain dual of the coherence time, and describes how much a pure sinusoid is spread out when it undergoes a mobile channel. On the basis of broadcasting communication scenarios considered in this dissertation, Clarke's model for mobile systems is adopted, where the transmitter is fixed and the receiver is moving around at a certain speed $v$ as depicted in Fig 2.10.

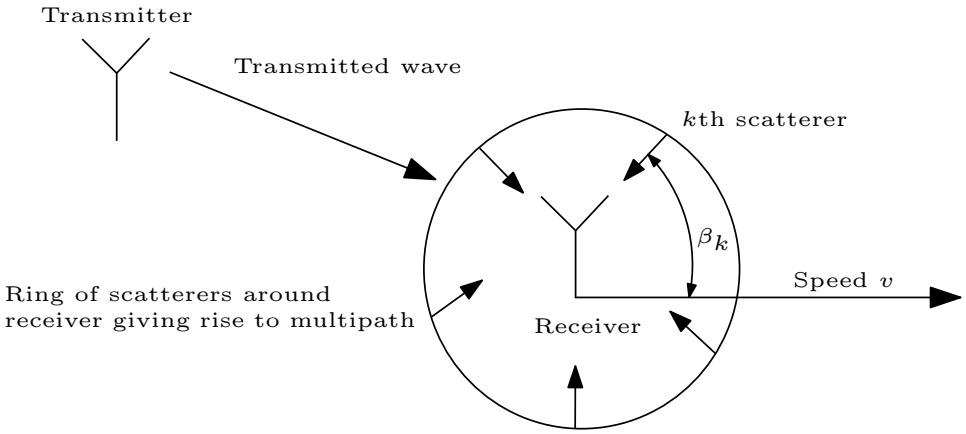


Figure 2.10: Clarke's model for time-varying Rayleigh fading channels.

Clarke defined a well-known model for channel variations in a typical urban environment characterized by fast-fading and multipath [Clarke68]. The mathematical model describes a time-varying complex gain that is a sum of a finite number of gains of complex exponentials (scatterers) as

$$X(t) = \sum_k \exp\left(j\left(2\pi f_k t + \theta_k\right)\right), \tag{2.23}$$

where $f_k$ is the Doppler shift suffered by the $k$th component. This mathematical model is represented graphically in Fig. 2.10, where the Doppler spread for each of the components or scatterers is $f_k = \frac{vF_c}{c}\cos\beta_k$, where $F_c$ is the carrier frequency, and $c$ denotes the speed of light.

The maximum Doppler spread (also called absolute Doppler frequency) is $F_d = \frac{vF_c}{c}$. Based on the central limit theorem, $X(t)$ can be modeled as a complex Gaussian random process with zero mean, so that we need to specify the power spectral density. The derivation of the Clarke power spectral density (sometimes better known as Jakes power spectral density) is based on the following three assumptions:

1. The propagation of the electromagnetic waves takes place in the two-dimensional (horizontal) plane, and the receiver is located in the center of an isotropic scattering area.
2. The angles of arrival $\beta_k$ are uniformly distributed in the interval $[-\pi, \pi)$.
3. The antenna radiation pattern of the receiving antenna is omnidirectional.

The power spectral density is defined as

$$S_X(f) = \frac{1}{\pi F_d \sqrt{1 - \left(\frac{f}{F_d}\right)^2}} \qquad |f| \leq F_d, \tag{2.24}$$

which is normalized so that

$$E\left[|X(t)|^2\right] = \int_{-F_d}^{F_d} S_X(f)\,\mathrm{d}f = 1. \tag{2.25}$$

The power spectral density is the Fourier transform of the time-domain autocorrelation function described as $R_X(\tau) = J_0(2\pi F_d \tau)$, where $J_0(\cdot)$ is the zero-order Bessel function of the first kind. The "bowl shape" is the classical shape of this spectrum. The procedure described above is widely used to model frequency-selective time-varying channels, since each tap in (2.6) can be thought of as a sum of a number of unresolvable components arriving from different directions.

It is worth noting that the Doppler power spectral density of far echoes deviates considerably from the Clarke power spectral density and it is better described by the so-called Gaussian power spectral density:

$$S_X(f) = \frac{1}{f_c}\sqrt{\frac{\ln 2}{\pi}} \exp\left(-\ln 2 \left(\frac{f}{f_c}\right)^2\right), \tag{2.26}$$

where $f_c$ is the 3-dB-cutoff frequency. The Gaussian power spectral densities are generally shifted from the origin of the frequency plane because far echoes mostly dominate from a certain direction of preference.

After having incorporated the mobility factor to the channel model described in Section 2.2, we can sum up the whole effects produced by the channel as follows: the time dispersion and the frequency dispersion mechanisms (they are independent of each other) in a mobile radio channel lead to four possible distinct effects, which are manifested depending on the

nature of the transmitted signal, the channel, and the vehicular speed. Multipath delay spread leads to time dispersion and frequency-selective fading, whereas the Doppler spread leads to frequency dispersion and time-selective fading. Consequently, we can identify four different types of fading:

1. The channel is frequency-flat fading if the bandwidth of the signal is smaller than the channel bandwidth, or, from the time-domain point of view, the delay spread is smaller than the symbol period.

2. The channel is frequency-selective if the bandwidth of the signal is bigger than the channel bandwidth, or, from the time-domain point of view, the delay spread is bigger than the symbol period.

3. The channel is slow-fading if the coherence time of the channel is bigger than the symbol period, which happens when the Doppler spread is low.

4. The channel is fast-fading if the coherence time of the channel is smaller than the symbol period, which happens when the Doppler spread is high.

The scope of this work covers the challenging radio channels where the high vehicular speed in a multipath environment leads to fast frequency-selective fading, also termed as double selective fading channels.

### 2.5.1 Performance degradation of OFDM systems due to Doppler spreading

As it has been pointed in Section 2.3.2, OFDM yields high spectral efficiency and reduces the effects of the multipath channel by making the symbol period much larger than the delay spread of the channel. If $1/T_s$ is the symbol rate of the input data, the symbol interval in the OFDM system is increased to $NT_s$, where $N$ is the number of total subcarriers. Consequently, each subchannel transmits at a bit rate of $\frac{\log_2 \Gamma}{NT_s}$ bits/s, where $\Gamma$ refers to the constellation size. The subcarriers are orthogonal to each other, satisfying

$$\frac{1}{NT_s}\int_0^{NT_s} \exp\left(j2\pi f_i t\right)\exp\left(j2\pi f_j t\right)\mathrm{d}t = \begin{cases} 1 & i = j \\ 0 & i \neq j \end{cases}, \tag{2.27}$$

where $f_i = \frac{i-1}{NT_s}$, $(i = 1, 2, ..., N)$. For conventional OFDM receivers, it is assumed that the channel remains static in an OFDM symbol period. In this case, equalization can be drastically simplified by turning the frequency-selective channel into several parallel flat-fading channels, whose channel impulse response $h_k\left(t, \tau\right)$ for the $k$th subchannel is denoted as

$$h_k(t,\tau) = \beta k(t)\,\delta(\tau), \tag{2.28}$$

and it is assumed that the processes $\{\beta_k(t), -\infty < t < \infty\}$ are complex jointly stationary and jointly Gaussian with zero means and cross covariance function

$$R_{\beta_k,\beta_l(\tau)} := E\left[\beta_k(t+\tau)\,\beta_l^*(t)\right], \qquad k,l = 1,...,N. \tag{2.29}$$

However, when the channel is time-variant and it varies within an OFDM block, the subcarriers are not longer orthogonal and the system performance drops down severely. In fact, it is well-known that one of the main drawbacks of OFDM is its susceptibility to the loss of orthogonality among subcarriers due to Doppler frequency shifts (i.e., mobile reception) or oscillator offsets, which lead to the so-called ICI. If it is not compensated, the ICI will result in an error floor. It is widely assumed in the literature [Wang06] that the correlation function expressed in (2.29) has the following factorable form

$$R_{\beta_k,\beta_l(\tau)} = R_1(\tau)\,R_2(k-l), \tag{2.30}$$

which is sufficient to represent both the frequency-selectivity and the time-varying effects of the channel. $R_1(\tau)$ is the same autocorrelation function defined in the previous section which describes the temporal correlation and is identical for all subchannels. The corresponding power spectral density is modeled by the Jakes' spectrum (2.24). On the other hand, $R_2(k)$ represents the correlation in frequency across subcarriers and is conditioned by the power profile of the channel impulse response and the subcarrier spacing $\Delta_f = \frac{1}{NT_s}$. Throughout this dissertation, we will assume that the delay spread of the channel is much smaller than the CP duration, and therefore, the received signal is not affected by ISI.

#### 2.5.1.1 Intercarrier interference

We now turn our attention to describing the ICI. Let us represent the channel impulse response in discrete form as $h_{n,l}$ for the $l$th channel tap and $n$th time instant, so that the channel can be approximated by an equivalent, discrete-time, baseband model. The received signal in time-domain (before applying the discrete Fourier transform (DFT)), under the effect of time-varying fading channel and AWGN is given by

$$r_n = \sum_{l=0}^{L-1} h_{n,l}x_{n-l} + z_n, \tag{2.31}$$

where $\mathbf{x}$ is the transmitted signal in time-domain (after applying the inverse discrete Fourier transform (IDFT)), and $\mathbf{z}$ is the AWGN. Demodulation implies taking DFT of the received block after removing the CP to get $[y_0, y_1, ..., y_{N-1}]^T$. The demodulated signal at the $k$th

tone becomes

$$y_k = \frac{1}{\sqrt{N}} \sum_{n=0}^{N-1} r_n e^{-j2\pi nk/N} = \frac{1}{\sqrt{N}} \sum_{n=0}^{N-1} \sum_{l=0}^{L-1} h_{n,l} x_{n-l} e^{-j2\pi nk/N} + \sum_{n=0}^{N-1} z_n e^{-j2\pi nk/N}. \tag{2.32}$$

This on solving yields

$$y_k = \sum_{m=0}^{N-1} H_{k,m} s_m + \hat{z}_k = g_k s_k + \sum_{m=0, m\neq k}^{N-1} H_{k,m} s_m + \hat{z}_k, \tag{2.33}$$

where $\mathbf{H}$ is the $N \times N$ frequency response of the channel, $\mathbf{s}$ is the transmitted signal in frequency-domain, $g_k = H_{k,k}$ represents the gain of the desired symbol, and $\hat{z}_k$ is the noise on the $k$th subcarrier which has the same statistics as the noise in time-domain. The second term on the right hand side in (2.33) describes the ICI affecting the $y_k$ received symbol, where

$$H_{k,m} = \frac{1}{N} \sum_{n=0}^{N-1} \breve{H}_{n,m} e^{j2\pi(m-k)n/N}, \tag{2.34}$$

and $\breve{H}_{n,m}$ is the time-varying frequency response of the channel, defined as

$$\breve{H}_{n,m} = \frac{1}{\sqrt{N}} \sum h_{n,l} e^{-2\pi ml/N} \qquad 0 \leq m \leq N-1. \tag{2.35}$$

From 2.33, it is clear that each of the received symbols $y_k$ has information of all the transmitted symbols $\mathbf{s}$. In other words, due to the Doppler spread, the transmitted symbols $\mathbf{s}$ are modulated in all the subcarriers with different weights defined by the $\mathbf{H}$ matrix, giving rise to a new form of frequency-diversity. Let focus on the $\mathbf{H}$ matrix, which will be used to exploit the frequency-diversity given by the ICI in further sections. It is worth noting that when the channel is time-invariant the frequency response matrix is diagonal, which means that the off-diagonal elements describing the ICI become zero. This fact makes possible the low complexity per-subcarrier equalization that characterizes OFDM systems. However, when the channel is time-variant, the off-diagonal elements of $\mathbf{H}$ are not longer zero, which makes necessary to cope with high complexity detection.

Fig. 2.11a and 2.11b show the first 100 samples of $\breve{\mathbf{H}}$ and $\mathbf{H}$ respectively. As it can be seen, $\breve{\mathbf{H}}$ reflects the variation of the channel over time and frequency, while $\mathbf{H}$ shows that although the $\mathbf{H}$ matrix is not diagonal, most of the energy is concentrated around the main diagonal, where higher power is represented by lighter color. For example, more than the 64% of the energy is located in the three main neighboring subcarriers for normalized Doppler frequency $f_d = 0.13$, where the normalized Doppler is defined as $f_d = F_d/\Delta f$ and $\Delta f$ refers to the subcarrier spacing. As a result of increasing the vehicular speed, or the

OFDM block size, more energy leaks into the off-diagonal elements of $\mathbf{H}$, increasing the ICI power that affects each subcarrier as it is shown in Fig. 2.12.

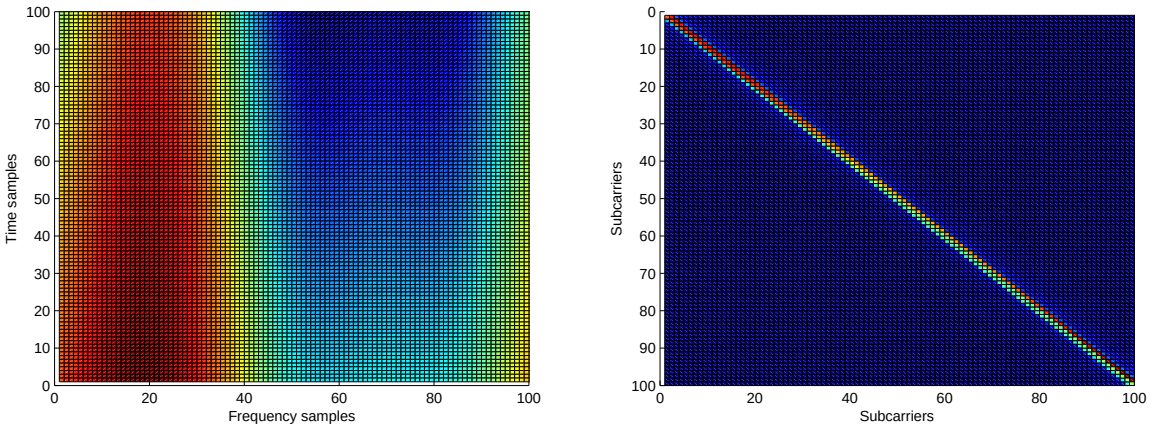


(a) (b)

Figure 2.11: Representation of the time-varying frequency response of the channel $\breve{\mathbf{H}}$ (a) and the frequency response matrix $\mathbf{H}$ describing the ICI power distribution (b). $f_d = 0.8$ and TU6 channel has been considered.

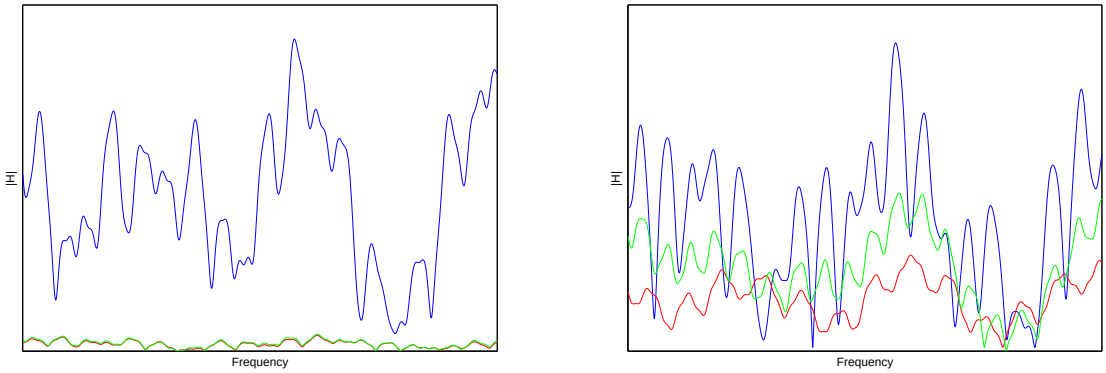


(a) (b)

Figure 2.12: The main three diagonals of $\mathbf{H}$ for $f_d = 0.1$ (a) and $f_d = 0.4$ (b). The blue line represents the main diagonal, and the red one and the green one represent the first diagonal on the right side and the first diagonal on the left side, respectively.

Russel and Stüber [Russell95] derived the ICI power as

$$P_{ICI} = E_s - \frac{E_s}{N^2}\left\{N + 2\sum_{i=1}^{N-1}(N-i)\,J_0\left(2\pi F_d T_s i\right)\right\}, \tag{2.36}$$

where $\sum_{l=0}^{L-1} E\left[|h_{n,l}|^2\right] = 1$ has been assumed. Note that the degradation due to ICI is only a function of $E_s$, $N$, $T_s$ and $F_d$, and is independent of the signal constellation. That is to

say, apart from signal power criteria, the ICI power is determined by the normalized Doppler frequency $f_d$.

For $N$ sufficiently large, the central limit theorem can be invoked and the ICI can be modeled as an additive Gaussian random process leading to an error floor determined analytically by means of the normalized Doppler frequency [Russell95]. In [Wang06], it is proven that, for conventional modulation methods, such as phase-shift keying (PSK) and QAM, the bivariate probability density function (PDF) of the ICI is shown to be a weighted Gaussian mixture. Fig. 2.13 depicts the histogram of the LLRs at the input of the decoder affected by ICI, where it is clearly shown that it presents a Gaussian-like distribution centered around zero.

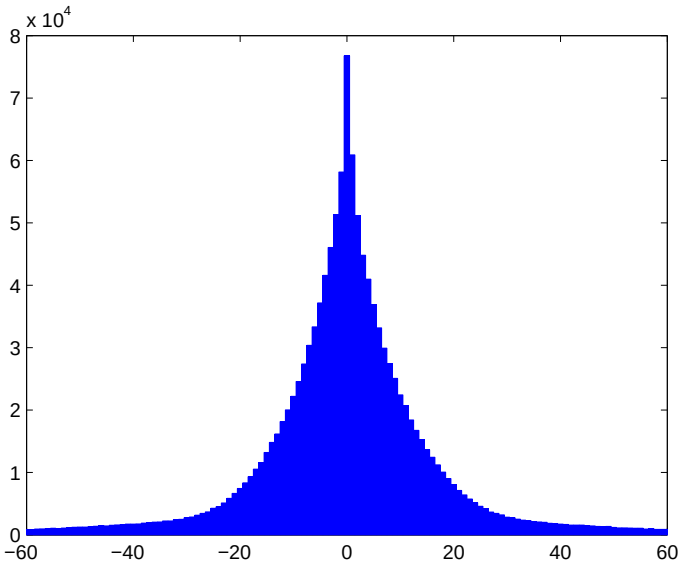


Figure 2.13: Histogram of the LLRs affected by ICI.

### 2.5.2 Exploiting time-domain diversity

Most of wireless communication standards make use of symbol interleavers. In this section, the attributes of a symbol interleaver in mobile scenarios are described. For that purpose, the time interleaver of the DVB-T2 standard is taken as reference. The primary benefit of this time interleaver is to provide time-diversity when used along with error correction coding. If the interleaver time span $T_{IL}$ is much larger than the coherence time of the channel $T_C$, there is a great chance that contiguous symbols are subjected to uncorrelated fading values, which leads to achieve effective diversity. Therefore, it is of interest to enlarge the ratio $T_{IL}/T_C$. Moreover, although communications degrade as the vehicle speed increases (the channel becomes more selective), the benefit of an interleaver can be higher for higher vehicular speeds. However, in a real-time communication system, there should be a maximum limit

of this ratio in order to limit the time delay associated with the interleaver.

Fig. 2.14 shows the effect of the time interleaver in a DVB-T2 signal transmission over a multipath channel profile with 100 Hz of Doppler frequency where different time interleaving depths (time span) have been adopted. When the interleaving depth is set to 1 FEC block, the BER curve tends to the typical error floor due to Doppler spreading. However, increasing the interleaving depth leads to a substantial enhancement of system performance, removing the error floor, and thus, making it possible to have an acceptable communication quality. The time interleaving, in conjunction with LDPC codes, makes the DVB-T2 specification very robust in a wide range of mobile communication scenarios.

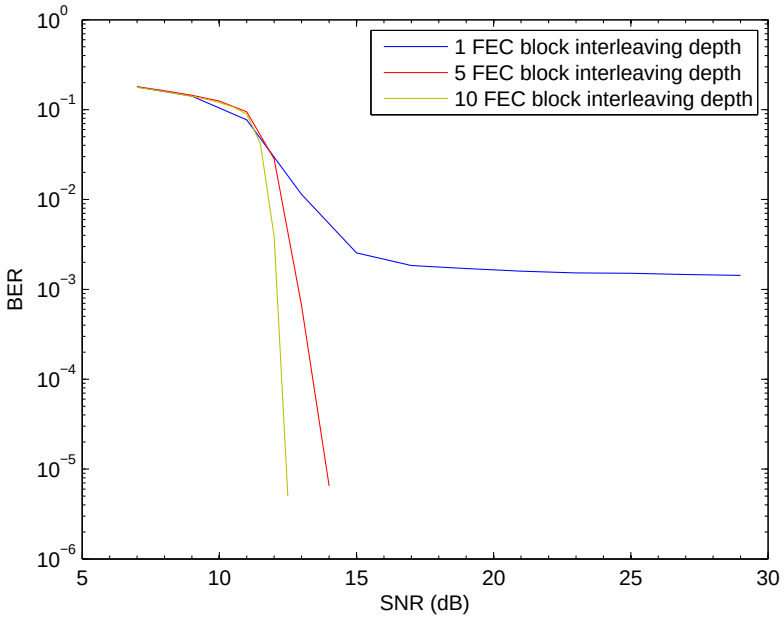


Figure 2.14: DVB-T2 signal transmission over multipath channel profile with 100 Hz of Doppler frequency. 16QAM and CR= 2/3 is considered.

Take not that, throughout this work, the amount of bits to be simulated in BER vs SNR simulations (max trials) has been calculated as follows

$$\text{max trials} = \frac{\text{arbitrary amount of errors to be assumed}}{\text{target BER} \times \text{CR}} \tag{2.37}$$

where the arbitrary amount of errors to be assumed is set to 100, and the target BER is usually $10^{-5}$. The BER will be measured at the output of the inner decoder.

## 2.6 Terrestrial digital television

Television services can be delivered through different means of transmission. Nowadays, there coexist three main television networks: satellite, cable and terrestrial. The last one is

one of the most extended since the direct evolution of the analogue television yielded the popularity of its digital counterpart. Several standards of terrestrial digital television (DTV) are adopted all around the world, being the following four considered the most important: the American advanced television system committee (ASTC) [ATSC05], the Japanese integrated services digital broadcasting-terrestrial (ISDB-T) [ARIB01], the Chinese digital terrestrial multimedia broadcast (DTMB) [SAC06] and the European DVB-T [ETSI97]. In this work, we are going to focus on the European standards, namely on the second generation of terrestrial DVB specifications: DVB-T2 [DVB08] and Digital Video Broadcasting-Next Generation Handheld (DVB-NGH). A decade after having published the first generation DVB standards, the second generation terrestrial counterpart was issued, which thanks to novel signal processing techniques, has noteworthy increased robustness and spectral efficiency comparing with its predecessor. Recently, the DVB consortium has issued a Call for Technologies for DVB-NGH with the aim of providing an advanced mobile broadcasting system.

### 2.6.1 DVB-T2

Based on recent research results and a set of commercial requirements, the DVB consortium concluded that there were suitable technologies which could provide increased capacity and robustness in the terrestrial environment, mainly for high definition television (HDTV) transmission. Therefore, a new standard named DVB-T2 has been designed primarily for fixed receptors, although it must allow mobile reception in certain conditions with the same spectrum characteristics as DVB-T. Fig. 2.15 shows the main stages of a DVB-T2 transmitter, where dashed lines represent optional blocks.

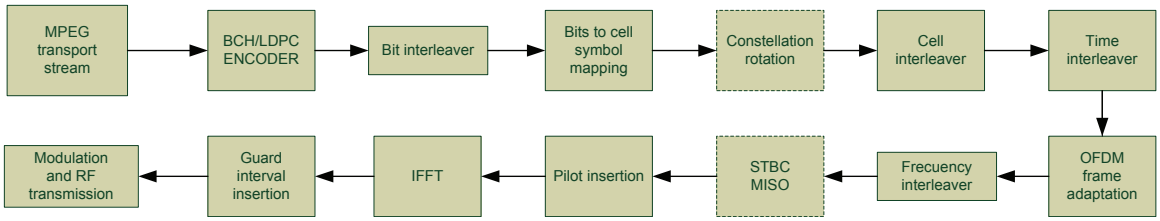


Figure 2.15: Elementary transmission chain of DVB-T2.

Considering the physical layer, the digital data sequences, which contain moving picture experts group (MPEG) video, audio and other information streams, are transmitted using OFDM modulation. The first remarkable novelty comparing with DVB-T lies on the error correction strategy, since DVB-T2 uses the same channel codes that were designed for DVB-S2. The coding algorithms, based on the serial concatenation of LDPC and BCH codes, offer excellent performance, resulting in a very robust signal reception. LDPC-based FEC techniques can offer a significant improvement compared with the convolutional error

correcting scheme used in DVB-T. Regarding the modulation, as it has been already mentioned, DVB-T2 uses the same OFDM technique as DVB-T. Maintaining the 2K and 8K modes, the new standard has introduced longer symbols with 16K and 32K carriers in order to increase the length of the GI without decreasing the spectral efficiency of the system. The new specification offers a large set of modulation parameters by combining different numbers of carriers and GI lengths, making it a very flexible standard as it is shown in Fig. 2.16. Furthermore, the highest constellation size has been increased to 256 symbols.

| | **DVB-T** | **DVB-T2** |
|---|---|---|
| FEC | Convolutional + Reed-Solomon<br>1/2, 2/3, 3/4, 5/6, 7/8 | LDPC + BCH<br>1/2, 3/5, 2/3, 3/4, 4/5, 5/6 |
| Modes | QPSK, 16QAM, 64QAM | QPSK, 16QAM, 64QAM, 256QAM |
| Guard intervals | ¼, 1/8, 1/16, 1/32 | 1/4, 19/256, 1/8, 19/128, 1/16, 1/32, 1/128 |
| FFT size | 2K, 8K | 1K, 2K, 4K, 8K, 16K, 32K |
| Scattered pilots | 8% of total | 1%, 2%, 4% and 8% of total |
| Continual pilots | 2.6% of total | 0.35% of total |

Figure 2.16: Available modes in DVB-T and DVB-T2.

On the other hand, a new technique called rotated constellations and Q-delay (RQD) is provided as optional, which comes to offer additional robustness and diversity in challenging terrestrial broadcasting scenarios. Furthermore, a mechanism has been introduced to separately adjust the robustness of each delivered service within a channel in order to meet the required reception conditions (in-door antenna/roof-top antenna, etc.). DVB-T2 also specifies a transmitter diversity method, known as Alamouti coding, which improves coverage in small scale single frequency networks (SFN)s.

Finally, the DVB-T2 standard takes into account one of the main drawbacks of OFDM, the peak-to-average power ratio (PAPR) of the signal and its effects on the transmitter equipments. High power peaks are usually generated by OFDM transmission leading to distortions at the amplifiers, thus minimizing their efficiency. Two techniques have been included in the standard to limit the PAPR without degrading the transmitted signal: carrier reservation and active constellation extension. The former reserves some subcarriers that can be used to correct the PAPR level of the transmitted signal whereas the latter achieves the same effects modifying the QAM constellation without degrading the signal recovery at reception.

Fig. 2.17 shows the comparative performance of DVB-T and DVB-T2 for similar communication parameters. In order to allow a fair comparison of both standards, quasi error free (QEF) reception is considered, which is defined by BER$= 2 \cdot 10^{-4}$ and BER$= 1 \cdot 10^{-7}$ at the output of the inner decoder for DVB-T and DVB-T2, respectively. If these QEF refer-

ence values are analyzed, a gain of 6 dB can be established between the two standards over AWGN channel and nearly 4 dB over Rayleigh channel. The code rates have been selected in order to approach equivalent data rates.

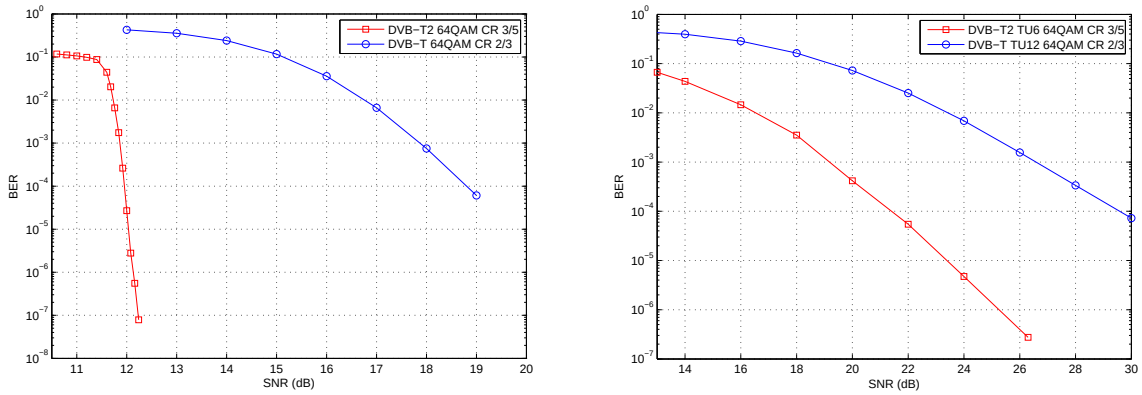


(a) (b)

Figure 2.17: BER performance of DVB-T and DVB-T2 systems over AWGN (a) and Rayleigh (b) channels.

The DVB-NGH standard on the other hand, will be the system for DTV signal reception on mobile handsets. DVB-NGH starts from DVB-T2, already designed in order to correctly operate in the mobile environment, and investigates the possibility of adopting new technologies for the mobile scenario. The new standard is expected to be finished by 2013.

### 2.6.2 Multipath channel models for terrestrial television

Radio channel models are usually derived from field measurements of the channel parameters in reference scenarios. This allows to create realistic models according to the reception environment under study (e.g. outdoor, indoor, etc.). In DTV, due to the variety of scenarios, multiple models have been used to assess the performance at the receiver. Terrestrial DTV standards, such us DVB-T or DVB-T2, define several channel models to provide simulated performance results. The DVB-T2 implementation guidelines document [DVB09] proposes several channel models. In this dissertation, two channel models have been chosen to analyze the performance of the proposed detection techniques in mobile conditions: COST 207 TU6 and 6-tap typical rural area (RA6) channels [COST20789]. These channel models were originally designed for global system for mobile communication (GSM) and adapted to mobile DVB-T. In fact, TU6 is one of the most extended channel models for simulation tests in terrestrial DTV. The Doppler spreading effect is modeled by the Doppler power spectral densities $S_X(f)$ for each of the paths.

The TU6 channel models an urban environment with reflections from buildings without LOS. Assuming the sample frequency of DVB standards, the impulse response has 47 taps

from which only six present significant power. It consists of a frequency-selective Rayleigh channel model. On the other hand, the RA6 channel models a typical rural non hilly terrain, which leads to a less frequency-selective response than the TU6 model's. It considers both LOS and non line-of-sight (NLOS) resulting in Rayleigh and Ricean channel models, respectively. The Doppler power spectral densities and the path characteristics are defined in the COST 207 project [COST20789].

## 2.7 The turbo principle in mobile communications

The 'turbo principle' is a general principle in decoding and detection which can be applied to many detection/decoding problems. It refers to a standard set of rules for exchanging and updating soft decision information between locally optimal processors. It was originally proposed by Berrou and Glaviex [Berrou93] in the early 1990s for suboptimal decoding of "turbo codes" and extended to many detection, decoding and estimation problems soon afterwards. Strictly speaking, there is nothing 'turbo' in the transmitter. Only the receiver uses the 'turbo' feedback. In almost all the cases, the system can be described as a serial concatenation of two decoders, as it is depicted in Fig. 2.18.

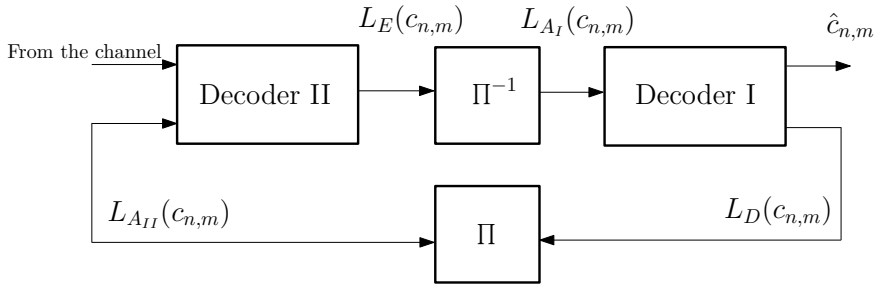


Figure 2.18: Example of a turbo receiver.

The crucial point at the receiver is that the two detectors/decoders are soft-in/soft-out (SISO) processors that accept and deliver probabilities or soft values. The extrinsic part of the soft output of one decoder $L_D(c_{n,m})$ is passed on to the other decoder to be used as a priori input $L_{A_{II}}(c_{n,m})$. We can conclude that, the elements participating in every iterative (turbo) process are the next ones: concatenation of component blocks, interleavers, SISO process and the exchange of extrinsic information. Table 2.1 summarizes different turbo schemes based on serial concatenated systems.

Note that in a wireless communication system the inner 'encoder' could be the multipath channel, or in the case of a mobile OFDM system, as it will be described in Chapter 4, the channel affected by ICI. In this cases, SISO detectors are useful in the design of many wireless systems. In fact, such detectors, when concatenated with a soft channel decoder, can significantly improve the quality of wireless transmission by performing joint, iterative

| configuration | en-/decoder I | en-/decoder II |
|---|---|---|
| serial code concat. | FEC en.-/dec. | FEC en./dec. |
| turbo equalization | FEC en.-/dec. | Multi. chan./det. |
| turbo BICM | FEC en.-/dec. | Mapper/demap. |
| turbo MIMO | FEC en.-/dec. | Mapper/MIMO det. |
| turbo source-channel | source encoder | FEC en.-/dec. |
| LDPC code/decoder | check nodes | variable nodes |

Table 2.1: Serial concatenated systems with iterative detection/decoding.

data detection and channel decoding through the exchange of soft information. However, the exponential complexity of the optimal MAP detector rapidly becomes prohibitive. This motivates the design of suboptimal soft detectors whose complexities are scalable with system dimensions. One recent trend, as it is the scope of this research work, is to design soft detectors for time-varying channels to enable joint channel estimation, data detection, and decoding.

### 2.7.1 BICM-ID

The implementation guidelines document of DVB-T2 [DVB09] proposes the turbo BICM or the so-called bit-interleaved coded modulation-iterative demapping (BICM-ID) as optional reception strategy. It consists of assisting the soft demapping process by considering the extrinsic data at the output of the LDPC decoder as a priori information. The demapping equation (2.11) has been modified to include a priori input as follows,

$$L_D\left(\hat{c}_{n,m}\right) = \log \frac{\sum_{\forall \mathbf{c}_n : c_{n,m}=0} p\left(y_n | s_n\right) \prod_{j=1; j\neq m}^{M} P\left(c_{n,j}\right)}{\sum_{\forall \mathbf{c}_n : c_{n,m}=1} p\left(y_n | s_n\right) \prod_{j=1; j\neq m}^{M} P\left(c_{n,j}\right)} + \log \frac{P\left(c_{n,m}=0\right)}{P\left(c_{n,m}=1\right)}. \tag{2.38}$$

Iterative demapping and decoding strategies have been analyzed for the first generation DVB systems and DVB-S2 in [Suffritti07] and [Lee01] respectively. In Fig. 2.19, performance of DVB-T2 is assessed over a TU6 channel employing iterative demapping. 64800 bit-length LDPC codes have been used and 20 LDPC iterations have been carried out in each of the 3 turbo iterations. In the non-iterative case, 50 LDPC iterations have been carried out.

Fig. 2.19 shows a performance gain of about 0.5 dB of SNR for both 16QAM and 64QAM constellations at BER$=1 \cdot 10^{-4}$. As it is explained in Section 2.3.1, there is a capacity gap between CM and BICM that is negligible when Gray mapping is used. As it is pointed out in [Xie09], such gap decreases as the coding rate increases, and increases as the constellation order increases. Iterative demapping can help to regain such loss. In line with this statement, it can be appreciated a slightly higher performance gain in 64QAM than in 16QAM.

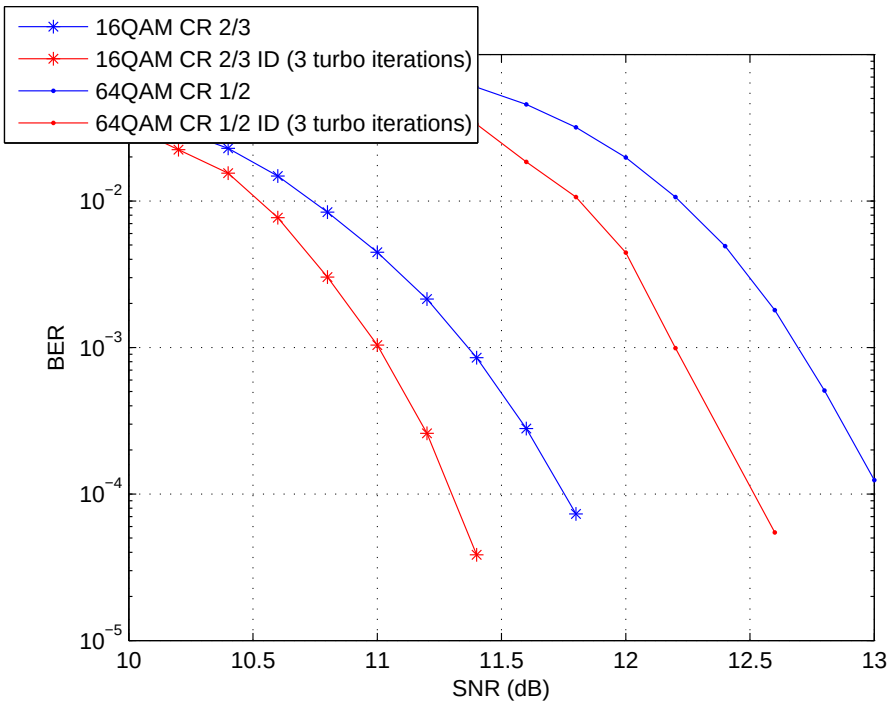


Figure 2.19: DVB.T2 performance with iterative demapping over the TU6 channel. In the iterative case, 3 turbo iterations are considered and 20 LDPC iterations in each turbo iteration. In the non-iterative case, 50 LDPC iterations are carried out.

## 2.8 Intercarrier interference cancellation schemes

In recent years, a wide range of OFDM receiver designs have been proposed in the literature for time-varying multipath channels. We can make a difference between linear equalizers based on zero-forcing (ZF) [Hsu09] or minimum mean-square error (MMSE) criteria [Rugini06, Huang07, Fang08], and non-linear equalizers based on ICI cancellation or decision-feedback [Zhao01, Cai03, Tomasin05, Hou05, Li10, Taubock11]. Linear equalization requires the inversion of the frequency channel matrix, which is prohibitively complex for large OFDM symbols. Although many approaches have been proposed for solving this problem [Fang08, Hsu09], they show, in general terms, poor performance at high-mobility scenarios. Non-linear equalizers outperform linear approaches at the cost of higher complexity. Since there are similarities between the ICI and the multiuser interference (MUI), well-known interference cancellation techniques, such as, successive interference cancellation (SIC) and parallel interference cancellation (PIC), can be directly applied to ICI suppressing. While the former present higher computational complexity and processing delays, the latter suffer from performance loss at high Doppler frequencies. In [Hwang09], a combination of the MMSE method and PIC is presented, which outperforms the conventional PIC schemes. Recently, space alternating generalized expectation maximization (SAGE) has been proposed for ICI cancellation [Panayirci10, Wu11].

Other research works explore optimal or near-optimal solutions, e.g., near-ML approaches [Ohno05, Ku11], sphere decoding (SD) [Kou05], or MAP equalization employing Bahl Cocke Jelinek Raviv (BCJR) algorithm [Liu09]. Apart from the frequency-domain, several time-domain solutions have also been proposed [Stamoulis02, Schniter04, Eva Peiker09].

Most of the techniques mentioned above, either do not show good performance in high-mobility scenarios or they are not suited to large FFT modes in terms of complexity and design constraints. Peng and Ryan suggested a parallel implementation of a two-stage equalizer [Peng06] suitable for large FFT sizes, which has low complexity comparing with other proposals when the OFDM symbol length is very large. Recently, a time-domain per sub-block equalizer has been presented [Baracca11] to tackle the same problem formulated in this paper. One of the drawbacks of this proposal is that pilot tones used in most of wireless communication systems can not be used for channel estimation.

FGs have received the attention of many researchers and have been applied to solve many technical problems in communications [Kschischang01, Wymeersch07]. Essentially, FGs represent graphically the factorization of a function, and have been shown to be a good alternative to solve complex inference problems. Many recent papers address the use of FG-based algorithms (also known as BP algorithms) for detection or equalization in channels with memory [Colavolpe05b, Colavolpe06, Anastasopoulos07]. Recently, this framework has been extended to ICI channels. In fact, a set of detection algorithms have been presented based on the Ungerboeck approach for MAP symbol detection [Haselmayr11], while in [Huang11], progressive parallel ICI cancellation has been proposed based on FGs.

To sum up, the main ICI suppressing approaches are roughly depicted in Fig. 2.20 regarding the performance and the complexity. It is worth noting that there exist a huge amount of variants for each of these families, so that this figure only represents the general idea.

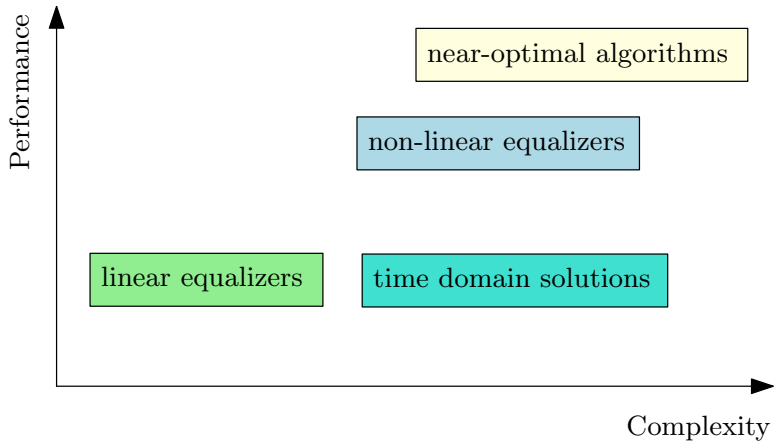


Figure 2.20: Summary of the main ICI suppressing schemes.

ICI mitigation has been also considered for the first generation DVB standards [Leif07, Poggioni09], and recently a novel approach has been proposed for DVB-T2 and DVB-NGH signal reception [Baracca11], where a pre-equalizer operating in sub-blocks of the received OFDM block was proposed in order to combat the time-variation of the channel caused by the Doppler frequency shift.

## 2.9 Chapter Summary

This chapter covers a background of the main theoretical aspects behind this dissertation. The BICM-OFDM communication framework has been briefly described, along with LDPC codes. This communication scheme, sometimes better known as bit-interleaved LDPC coded modulation (BILCM), has been adopted in many last-generation wireless communication standards, as it is the case of the second generation terrestrial DTV systems. We also coped with the challenge of signal reception in mobile environments, and analyzed how an OFDM signal can be deteriorated by the Doppler spread. The main characteristics of DVB-T2 standard have also been described.

On the other hand, we have introduced the 'turbo principle' and iterative receivers, which are the key points of the FG framework. We have discussed a particular case of a turbo receiver (BICM-ID) and analyzed its application in DVB-T2 reception. Last, a summary of the main ICI suppressing schemes developed in recent years has been presented, emphasizing ICI suppressing schemes applied to terrestrial DVB systems.

# Chapter 3

# Factor graph-based detection for channels affected by ICI

## 3.1 Introduction

FGs and the associated *summary propagation algorithms* are a general trend in signal processing, since they present very attractive properties for a wide variety of detection and estimation problems. First of all, they are simple and easy to read in the sense that they allow to represent graphically a bunch of equations. Second, they compute marginals in a mathematically efficient way. Last, but not least, they allow hierarchical modeling and functional decomposition (we can abstract away parts of the function by grouping some parts of the graph into a super-vertex), and they are fully compatible with conventional block diagrams.

The SP algorithm was invented by Gallager [Gallager63] as a decoding algorithm for LDPC codes. Afterwards, Tanner proposed a graphical model to describe and generalize LDPC codes, introducing the MS algorithm [Tanner81]. However, the full power of iterative processing was realized when turbo codes came about [Berrou93] followed by the rediscovery of LDPC codes [MacKay99]. The remarkable work of Wiberg et al. [Wiberg96] provided a new perspective by which means decoding of LDPC codes, turbo codes, as well as the forward-backward (FB) and Viterbi algorithm were viewed as particular instances of the same algorithm. This made new applications like signal detection for channels with memory obvious. It is noteworthy that the literature in this framework is vast, and the brief overview provided here is incomplete, since important contributions have been made from many different fields such as artificial intelligence, statistics or computer sciences.

But, why use FGs for ICI compensation? Which are the benefits of FG-based detection in DVB terrestrial systems? As it will be explained in further sections in this chapter, the physical layer of DVB terrestrial systems present two main characteristics that have to be taken into account for designing the detection strategy: first, a powerful channel code is employed which requires soft detection; second, making use of large OFDM symbol lengths

forces to adopt parallel detection schemes in order to diminish high latencies. FG-based detection fits both requirements.

## 3.2 Basic concepts

A FG is a bipartite graph which describes the factorization of a global function into a product of several local functions. Running a *summary propagation algorithm* in the FG allows to compute marginals of the global function by passing "messages" along the edges of the graph. The main summary propagation algorithms are the SP algorithm and the MP (or MS) algorithm. Originally, FGs were proposed in coding theory, but they consist of an attractive solution for a wide variety of signal processing problems. In fact, HMMs (with the associated FB algorithm), Kalman filtering, the Viterbi algorithm (VA), or even the fast Fourier transform (FFT) can be considered as particular instances of the SP algorithm.

### 3.2.1 Factor graphs and inference

In this dissertation, FGs are used for solving a well-defined inference problem, which is namely an estimation problem. Let us abstract out the OFDM modulation and consider the signal in frequency-domain (before and after the inverse fast Fourier transform (IFFT) and FFT processing, respectively), as shown in the system model described in Fig. 3.1.

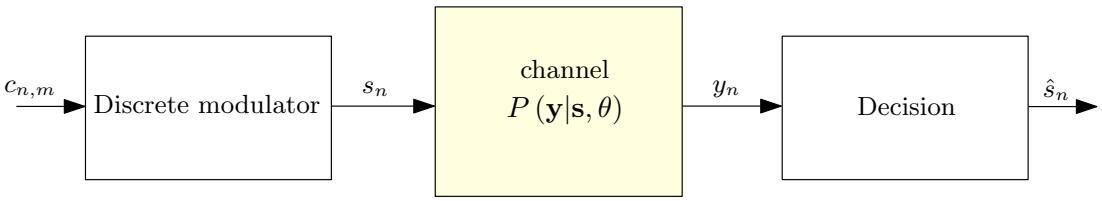


Figure 3.1: Simplified discrete channel model, where neither OFDM modulation nor interleaving has been considered for simplicity.

The modulator formats the messages for transmission over the vector channel by translating the encoded bits $c_{n,m}$ into a N-dimensional vector $\mathbf{s}$ composed of symbols chosen from a complex constellation $\chi$. The conditional probability of the output vector $\mathbf{y}$ given the input vector $\mathbf{s}$, $P(\mathbf{y}|\mathbf{s})$, completely describes the discrete version of the channel. The decision device (in our case, the FG based detector) then translates the output vector $\mathbf{y}$ into an estimate of the transmitted message $\hat{\mathbf{s}}$. The optimal data detector chooses $\hat{s}_n$ to minimize the error probability, which is accomplished by the MAP detection strategy defined by the Bayesian estimation theory, where there is a variable of interest (unknown variable) $\mathbf{s} = [s_1, s_2, ..., s_N]$, an evidence or observation $\mathbf{y} = [y_1, y_2, ..., y_N]$, and an underlying model $\theta$ which somehow describes the relation between $\mathbf{s}$ and $\mathbf{y}$:

$$P(\mathbf{s},\mathbf{y}|\theta) = P(\mathbf{s}|\mathbf{y},\theta)\,P(\mathbf{y}|\theta) = P(\mathbf{y}|\mathbf{s},\theta)\,P(\mathbf{s}|\theta)\,. \tag{3.1}$$

$P(\mathbf{s}|\mathbf{y},\theta)$ is referred as the posterior probability of $\mathbf{s}$, $P(\mathbf{y}|\theta)$ is the likelihood of $\theta$, $P(\mathbf{y}|\mathbf{s},\theta)$ is the likelihood of $\mathbf{s}$ given $\theta$, and $P(\mathbf{s}|\theta)$ is called the a-priori probability, or the prior of $\mathbf{s}$. Within the MAP detection strategy, two variants can be defined depending on the error parameter to be minimized:

1. MAP *sequence* detection which minimizes the error rate of the packet $\mathbf{s}$, which means minimizing the FER:
$$\hat{\mathbf{s}} = \arg\max_{\mathbf{s}} P(\mathbf{s}|\mathbf{y}) \tag{3.2}$$

2. MAP *symbol* detection which minimizes the error rate of the individual symbols $s_n$, which means minimizing the symbol error rate (SER):
$$\hat{s}_n = \arg\max_{s_n} P(s_n|\mathbf{y}) \tag{3.3}$$

In most communication systems, the objective is to maximize over all $\mathbf{s}$. The problem is that its complexity is exponential with the length of $\mathbf{s}$, which is usually prohibitively complex. The solution is to minimize the SER (which implies minimizing the BER), instead of minimizing the FER. But, again, there is a complexity challenge in computing $P(s_n|\mathbf{y})$. It is in this point where FGs gain relevance, since $P(s_n|\mathbf{y})$ is marginal of $P(\mathbf{s}|\mathbf{y})$, and FGs can help in computing marginals. From an statistical inference point of view, there are different problems which could be solved by FGs, but we are going to focus on the subject of interest in this dissertation, which, as mentioned, is the calculation of the marginal a posteriori probabilities expressed as,

$$P(s_n|\mathbf{y},\theta) = \sum_{\sim\{s_n\}} P(\mathbf{s}|\mathbf{y},\theta)\,. \tag{3.4}$$

where $\sim\{s_n\}$ refers to all variables except $s_n$.

### 3.2.2 Building a factor graph

As mentioned, a FG is a diagram that represents the factorization of a function of several variables. Suppose that some function $f(s_1, s_2, ..., s_N)$ is factorized into $J$ factors,

$$f(s_1, s_2, ..., s_N) = \prod_{k=1}^{J} f_k(\psi_k)\,, \tag{3.5}$$

where $\psi_k \subseteq \{s_1, ..., s_D\}$ is the $k$th variable subset and $f_k(\cdot)$ is a real valued function. The factor graph $G = (V, E)$ corresponding to (3.5) is created following the next rules:

- For every variable $s_n$, we create a vertex referred as *variable node*: $s_n \in V$, where $V$ represents the set of vertices of the graph,
- For every factor $f_k$, we create a vertex referred as *function node*: $f_k \in V$, and
- For each factor $f_k$, and every variable $s_n \in \vartheta(f_k)$, we create and edge $e = (s_n, f_k) \in E$, where $E$ is the set of edges, and $\vartheta(v)$ stands for the set of neighbors of a given node $v$.

Once we have factorized the function, we can draw the corresponding FG. Note that there is a one-to-one mapping between a given factorization and the corresponding FG. The representation adopted in this research work, which is shown in Fig. 3.2, corresponds to the conventional FG-type. There is another type of graph introduced by Forney [Forney01] which is considered as a "normal FG". Both types are equivalent in the sense that exactly the same messages are computed, but differ in some graphical aspects.

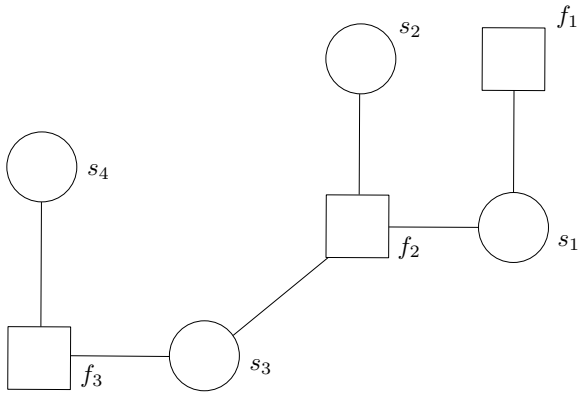


Figure 3.2: FG representing function $f(s_1, s_2, s_3, s_4) = f_1(s_1) f_2(s_1, s_2, s_3) f_3(s_3, s_4)$.

Our goal is to compute marginals of the function $f(\cdot)$ with respect to $N$ variables. The marginal of $s_n$ is given by

$$g_{s_n}(s_n) = \sum_{\sim\{s_n\}} f(s_1, s_2, ..., s_N), \tag{3.6}$$

This means that the marginalization of $s_n$ involves the summation over the values of all the variables except $s_n$, which is a cumbersome computational task. Making use of the factorization in (3.5) and running the SP algorithm in the corresponding FG allows to compute the $N$ marginals in a computationally attractive way by passing messages over the edges of the graph. Note that applying the SP algorithm in a FG means local computation in basic blocks: once we have identified the local processing rule, we only have to remind the SP rule. The intrinsic benefits of this approach are, actually, the reason of the wide usage of FGs by the digital communication community. In fact, as mentioned, well-known algorithms such as VA or FB algorithms can be cast to the FG framework in a very natural way.

### 3.2.3 SP algorithm

The SP algorithm computes two messages for each edge in the graph, one in each direction. Considering the FG defined as in the previous section, we can distinguish two types of messages: the ones going from a variable node to a function node $\mu_{s_n \to f_l}(s_n)$, and the ones from a function node to a variable node $\mu_{f_k \to s_m}(s_m)$.

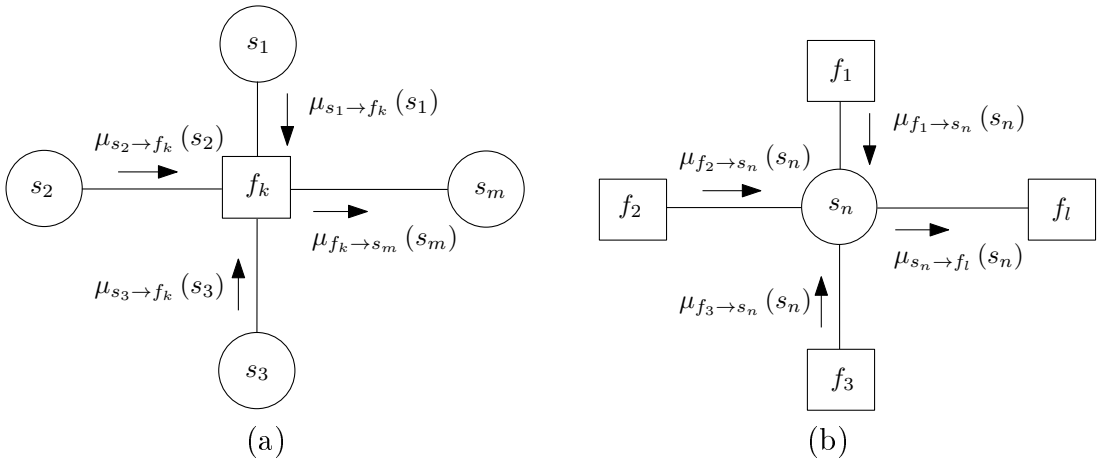


Figure 3.3: The SP algorithm: message computation rule from function node $f_k$ to variable node $s_m$ (a), and from variable node $s_n$ to function node $f_l$ (b).

There are three phases in the SP algorithm: initialization, message computation and termination. For convenience, we will start the algorithm from the leaves:

*Inizialization:*

- Every leaf function node $f_k$, with $\{s_m\} = \vartheta(f_k)$, sends a message to variable node $s_m$, with $\mu_{f_k \to s_m}(s_m) = f_k(s_m)$.
- Every leaf variable node $s_n$, with $\{f_l\} = \vartheta(s_n)$, sends a message to function node $f_l$, with $\mu_{s_n \to f_l}(s_n) = 1$.

*Message computation:*

- Every function node $f_k$ of degree $D$ has received incoming messages from $D-1$ distinct variable nodes $s_n \in \vartheta(f_k)$. Then, node $f_k$ computes the outgoing message $\mu_{f_k \to s_m}(s_m)$ as

$$\mu_{f_k \to s_m}(s_m) = \sum_{\sim\{s_m\}} f_k\left(\{s_n\}_{s_n \in \vartheta(f_k)}\right) \prod_{s_n \in \vartheta(f_k)\setminus\{s_m\}} \mu_{s_n \to f_k}(s_n). \tag{3.7}$$

  Message propagation is depicted in Fig. 3.3a.

- Every variable node $s_n$ of degree $D$ has received incoming messages from $D-1$ distinct function nodes $f_k \in \vartheta(s_n)$. Then, node $s_n$ computes the outgoing messages $\mu_{s_n \to f_l}(s_n)$

as

$$\mu_{s_n \to f_l}(s_n) = \prod_{f_k \in \vartheta(s_n) \setminus \{f_l\}} \mu_{f_k \to s_n}(s_n) \tag{3.8}$$

Message propagation is depicted in Fig. 3.3b.

*Termination:*

- The algorithm terminates computing the marginal of $s_n$ by multiplying the messages in both direction on the edge $(s_n, f_k)$,

$$g_{s_n}(s_n) = P(s_n, \mathbf{y}) = \mu_{f_k \to s_n}(s_n)\, \mu_{s_n \to f_k}(s_n). \tag{3.9}$$

- From the Bayesian estimation theory, and taking into account that

$$P(\mathbf{y}) = \sum_{s_n \in \chi} P(s_n, \mathbf{y}), \tag{3.10}$$

the marginal a posteriori distributions, necessary to evaluate the MAP symbol detection rule, are given by

$$P(s_n|\mathbf{y}) = \frac{P(s_n, \mathbf{y})}{P(\mathbf{y})} = \frac{g_{s_n}(s_n)}{\sum_{s_n \in \chi} g_{s_n}(s_n)}. \tag{3.11}$$

### 3.2.4 Messages and their representation

When FGs are used to solve inference problems, there is usually a common problem related to the dynamic range of the messages: they tend to get smaller as the algorithm proceeds. This turns out to be a real problem in computer simulation or hardware implementation. To get around this problem, it is a common approach to implement the SP algorithm in logarithmic-domain, which yields an increase of the dynamic range, and therefore makes the algorithm more stable. In such case, expressions in (3.7) and (3.8) become

$$\bar{\mu}_{f_k \to s_m}(s_m) = \ln \left\{ \sum_{\sim \{s_m\}} \exp \left[ \ln f_k \left( \{s_n\}_{s_n \in \vartheta(f_k)} \right) + \sum_{s_n \in \vartheta(f_k) \setminus \{s_m\}} \bar{\mu}_{s_n \to f_k}(s_n) \right] \right\}, \tag{3.12}$$

and

$$\bar{\mu}_{s_n \to f_l}(s_n) = \sum_{f_k \in \vartheta(s_n) \setminus \{f_l\}} \bar{\mu}_{f_k \to s_n}(s_n), \tag{3.13}$$

The implementation of these latter rules does not require multiplications, and besides, can be assessed recursively in a very efficient way using the Jacobian logarithm:

$$\mathbb{M}(a_1, a_2) = \ln(\exp(a_1) + \exp(a_1)) = \max(a_1, a_2) + \ln(1 + \exp(-|a_2 - a_1|)), \quad (3.14)$$

where $a_1$ and $a_2$ are real numbers, and $\ln(1 + \exp(-|a_2 - a_1|))$ is a nonlinear function which can be evaluated by means of a lookup table. There is a noteworthy particular case of logarithmic-domain implementation, which consists of approximating the Jacobian algorithm by the max function:

$$\max(a_1, a_2) + \ln(1 + \exp(-|a_2 - a_1|)) = \max(a_1, a_2). \quad (3.15)$$

This approximation leads to the MS algorithm, which, as we will explain in Section 3.5.1, plays an important role: it can be interpreted as an optimization technique/algorithm, since it allows to locate the maximum of a function, as well as the values of the variables that achieve this maximum. Note that this takes us back to the MAP sequence detection strategy [Wymeersch07].

#### 3.2.4.1 Message-scaling

Another approach to get around the problem of messages getting smaller is *message scaling*. Messages can be scaled arbitrarily without altering the outcome of the algorithm. This is done multiplying messages by constants in the SP algorithm, and adding constants to the messages in the logarithmic-domain version. Interestingly, we do not need to keep track of all the scaling factors when we are interested in computing marginal a posteriori probabilities. In fact, assuming scaled marginals $\tilde{g}_{s_n} = \gamma g_{s_n}$, marginal a-posteriori distributions calculated in (3.11) remain the same

$$P(s_n|\mathbf{y}) = \frac{P(s_n, \mathbf{y})}{P(\mathbf{y})} = \frac{\tilde{g}_{s_n}(s_n)}{\sum_{s_n \in \chi} \tilde{g}_{s_n}(s_n)}. \quad (3.16)$$

A particular type of scaling which has some interesting consequences is the *normalization*, which fullfils

$$\sum_{s_m \in \chi} \gamma \mu_{f_k \to s_m}(s_m) = 1. \quad (3.17)$$

The main implication of normalizing messages is that they can be interpreted as probability distributions (pmfs or pdfs). Let assume that $s_n$ are independent random variables with a priori distributions $P(s_n) = \mu_{s_n \to f_k}(s_n)$. Therefore, we can interpret (3.7) as [Wymeersch07]

$$\mu_{f_k \to s_m}(s_m) = P(s_m) = \sum_{\{\sim s_m\}} P\left(s_m, \{s_n\}_{n \neq m}\right) = \sum_{\sim\{s_m\}} \underbrace{P\left(s_m | \{s_n\}_{n \neq m}\right)}_{\propto f_k(s_1,\ldots,s_D)} \prod_{n \neq m} \underbrace{P(s_n)}_{\mu_{s_n \to f_k(s_n)}} . \tag{3.18}$$

Finally, note that in this dissertation, we consider discrete variables and therefore the problem behind processing continuous variables in a FG is out of the scope of this thesis. This issue is extensively addressed in [Wymeersch07].

## 3.3 Loopy factor graphs

The theory described in the previous section holds when the FG is cycle-free. Nevertheless, this is not the case of interest in many cases, including the receivers considered in this dissertation. Moreover, the most promising applications in digital communications are based on *cyclic* FGs, or *loopy* FGs. But, which are the consequences of having loops in a FG? The very first conclusion is that the SP algorithm leads to *iterative processing* or *turbo processing*, which requires the establishment of initialization and termination criteria. A natural way to do that is to initialize the SP algorithm with the variable nodes sending trivial messages to the function nodes, and artificially halting the SP algorithm after a certain amount of iterations (after which we hope that messages have converged in some sense).

However, the main problem in loopy FGs is that the output of SP algorithm operating in a FG with cycles can not in general be interpreted as exact function summaries, which means that the outputs can not be considered as true marginal a posteriori distributions. These approximate marginal a posteriori distributions are sometimes referred as *beliefs*, which leads to the term BP algorithm. In general, little is known about the performance of message passing algorithms in loopy FGs. What is the relationship between the marginals obtained and the true marginal a posteriori distributions? Do the messages converge at all? It is fair to say that the answer of these questions is not fully known yet.

There are three main strategies that can be followed to cope with loopy FGs:

1. Run the algorithm and hope for the best: There is no guarantee that the algorithm will converge, and if it does, it will be to the correct marginal a posteriori distributions. In general, the marginal a posteriori distributions obtained in a loopy FG are too optimistic, since they assume that all messages come from independent inputs, whereas messages enter constantly into sum-product updates because of the presence of cycles in the graph. In [Wymeersch07], it is proven analytically for the most simple loopy FG that the SP algorithm gives correct marginal a posteriori distributions up to an additive error.

In that sense, it can be stated that the performance of the SP algorithm in a loopy FG is suboptimal. Obviously, the performance is worse when the graph has many short cycles, and becomes negligible as cycles get longer and, therefore, the graph turns out to be sparse (this is the case of LDPC codes). Regarding the applications based on physical models with inherent short cycles, the FG-based framework has for a long time been considered useless due to its poor performance. However, empirical results have proven that, for many practical scenarios, implementing the SP algorithm for inference on loopy FGs provides excellent performance, and hence, turns out to be a feasible alternative for designing near-optimal algorithms [Kaynak05].

2. Modify the FG by removing cycles: it consists of agglomerating parts of the graph with the aim of eliminating some cycles. Note that, the total agglomeration of the graph, leads to a trellis-based structure. There are two main techniques of agglomeration: stretching and clustering [Kschischang01]. The drawback of agglomerating the graph is the complexity increase, since it comes at the expense of a (often substantial) rise of the variable alphabets' complexity.

3. Beef up the SP algorithm to perform better in graphs with cycles: the goal is that the SP algorithm still could perform well on certain classes of cyclic graphs. This is a current research topic with applications in artificial intelligence, optimization and physics. In particular, [Yedidia05] proposes a generalization of the SP algorithm that may perform better, and reveals a link with free-energy minimization in statistical physics.

## 3.4 System description

As it has been already explained, the first reason for using the FG framework in signal detection is the fact that it allows the evaluation of the MAP symbol detection rule in a computationally efficient manner. The second is that the BP algorithm has an inherent parallel structure, which is an interesting feature for high-speed detection and decoding in turbo receiver schemes in order to reduce excessive latencies. This intrinsic parallel structure of the detection scheme turns out to be a necessary characteristic when large FFT sizes are employed.

With the aim of increasing spectral efficiency or enhancing the robustness in SFN, there is a growing trend toward using large OFDM symbol lengths (which means densely spaced subcarriers) in most of the new wireless communication systems (e.g., 32K subcarriers in DVB-T2). As the delay spread increases, symbol duration must also be increased in order to maintain a near-flat channel in every subcarrier. Nevertheless, since ICI power depends on the subcarrier spacing, the effect of time-varying channels becomes critical when large OFDM

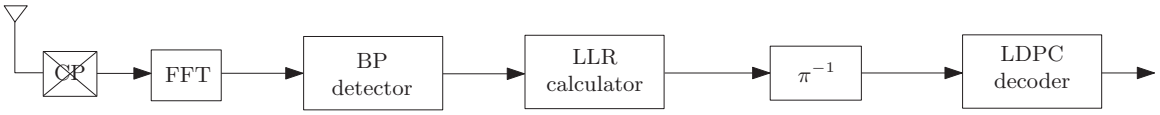


Figure 3.4: Block diagram of the BICM-OFDM reception scheme including the BP detector.

symbols are used and it is necessary to develop appropriate signal processing techniques to combat the mobility-induced ICI problem. Hence, from an ICI cancellation perspective, the most challenging scenario is a high-mobility environment when a large FFT mode is employed.

In this chapter, we consider a single user BICM-OFDM system over a frequency selective time-varying channel (Fig. 3.4). Throughout this chapter, ideal CSI and perfect synchronization are assumed. No ISI is considered since it is assumed that the CP is longer than the channel delay spread. According to the COST 207 model, the channel taps are considered independent random processes with Rayleigh statistics, and the Doppler frequency $F_d$ is modeled with the widely used Jakes' spectrum. The mobile scenarios considered throughout the thesis are characterized by the normalized Doppler frequency $f_d = F_d\Delta_f$, where $\Delta_f$ refers to the subcarrier spacing.

At this point, we will reformulate the system description in Section (2.5.1.1) introducing matrix notation. The received signal after CP removal can be expressed in matrix form as [Fang08]

$$\mathbf{r} = \overline{\mathbf{H}}\mathbf{F}^H\mathbf{s} + \mathbf{z}, \tag{3.19}$$

where $\overline{\mathbf{H}}$ is a $N \times N$ time-domain channel matrix, $\mathbf{F}$ stands for the standard $N$-point DFT matrix, and vectors $\mathbf{s}$, $\mathbf{r}$ and $\mathbf{z}$ contain the transmitted signal, the received signal and AWGN discrete samples, respectively. We assume that $\mathbf{z}$ is a complex Gaussian noise vector with zero mean and covariance $E\left\{\mathbf{z}\mathbf{z}^H\right\} = \sigma_n^2\mathbf{I}_\mathrm{N}$. Applying the DFT to the received signal $\mathbf{r}$ leads to the received signal in frequency-domain

$$\mathbf{y} = \mathbf{F}\mathbf{r} = \mathbf{F}\overline{\mathbf{H}}\mathbf{F}^H\mathbf{s} + \mathbf{F}\mathbf{z} = \mathbf{H}\mathbf{s} + \mathbf{z}_f, \tag{3.20}$$

where $\mathbf{H} = \mathbf{F}\overline{\mathbf{H}}\mathbf{F}^H$ is the frequency-domain channel matrix, and $\mathbf{z}_f = \mathbf{F}\mathbf{z}$ is the frequency-domain noise vector which has the same statistics as time-domain noise $\mathbf{z}$.

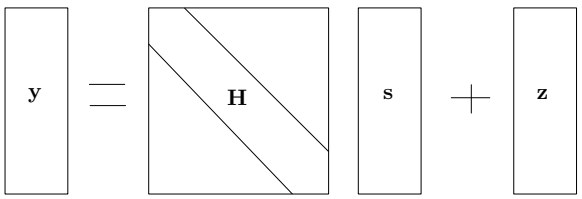


Figure 3.5: Frequency-domain system input-output relation after CP removal.

In time-invariant channels, the inclusion of the CP makes $\overline{\overline{\mathbf{H}}}$ circulant and therefore $\mathbf{H}$ becomes diagonal, leading to the low-complexity per-subcarrier equalization that characterizes OFDM systems. Nevertheless, when the channel is time-variant, the off-diagonal elements of $\mathbf{H}$ are not zero anymore, and ICI comes up making the implementation of conventional equalizers prohibitively complex. Fig. 3.6 shows how the energy leaks out to the off-diagonal elements of $\mathbf{H}$ as the Doppler frequency increases, giving rise to ICI.

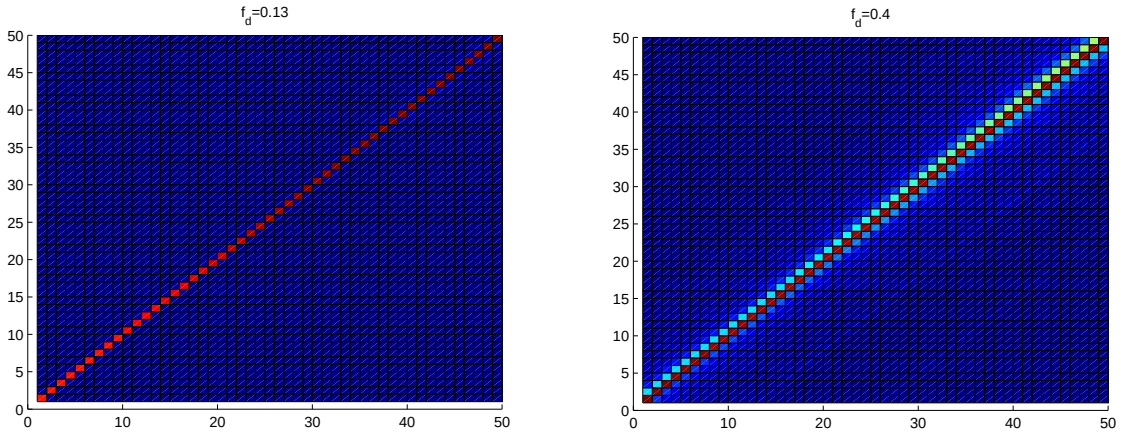


(a) (b)

Figure 3.6: Representation of part of the channel frequency response $\mathbf{H}$ for $f_d = 0.13$ (a) and $f_d = 0.4$ (b). Higher power is represented by lighter color. TU6 channel has been considered.

Many ICI compensation schemes mentioned in Section 2.8 consider ICI just as interference and try to subtract it out. Nevertheless, there is another strategy which can bring more benefits: ICI can be considered as a frequency-domain diversity source instead of interference. That means that ICI introduces an additional frequency-domain diversity in the received signal, which is defined by the $\mathbf{H}$ matrix. We stress the importance of this fact, since this frequency-diversity can be exploited with the aim of increasing the system performance. And this is (resuming the analysis at the beginning of this chapter) the third reason for using FGs for ICI compensation: a properly defined FG describes the correlation in frequency-domain due to ICI, and running the SP algorithm on the FG achieves a very good diversity order.

Tab. 3.1 summarizes the rest of the simulation parameters considered throughout this chapter.

## 3.5 Maximum a posteriori symbol detection based on factor graphs

In this section, FG-based detection is described and assessed for broadcast channels affected by ICI. Forney and Ungerboeck approaches will be considered for MAP symbol detection

Table 3.1: Simulation parameters in Chapter 3.

| **Parameter** | **Value** |
|---|---|
| Carrier frequency | 760 MHz |
| Bandwidth | 8 MHz |
| Number of subcarriers ($N$) | 32784 |
| Subcarrier spacing | 280 Hz |
| Length of one OFDM block ($T_u$) | $3584\mu s$ |
| Length of the guard interval ($T_u/4$) | $896\mu s$ |
| Modulation | quadrature phase-shift keying (QPSK) |
| FEC length (LDPC) | 64800 bits |
| Code rate | 2/3 |
| Channel model | TU6 |

and analyzed the exact update rules and their associated complexity.

As it has been described in Section 3.4, most of the energy of $\mathbf{H}$ is confined around the main diagonal. This is a crucial observation, since processing the whole matrix $\mathbf{H}$ turns out to be unfeasible in terms of complexity. Therefore, we are forced to define a banded version of $\mathbf{H}$, where $q$ defines how many off-diagonals above and below the main diagonal are taken into consideration. We know that, as a result of increasing the normalized Doppler frequency, more energy leaks into the off-diagonal elements of $\mathbf{H}$, and it is necessary to define a proper value of $q$ to get a trade-off between performance and computational complexity. In this work $q = 1$ is further assumed and as it will be shown by simulation results in this chapter, this value is enough to achieve good BER performance in high-mobility scenarios. Note that the $q$ parameter describes the ICI channel memory, which leads to the presence of a residual ICI defined by the rest of the off-diagonal elements of $\mathbf{H}$ not included in $q$. In that way, in comparison to the ISI channel, the ICI channel can be considered as "non-causal" *finite-memory* channel (in the sense that, in frequency-domain, the received symbol $y_k$ depends on the prior $s_{k-1}$, current $s_k$ and posterior $s_{k+1}$ transmitted symbols).

### 3.5.1 Optimal maximum a posteriori symbol detection

In this section, we will present the FB algorithm as the optimal MAP symbol detector. Since FG-based detector turns into sub-optimality because of the existence of short loops, we need a reference to compute the performance loss due to this sub-optimality. Note that FB algorithm involves sequential processing, thus it is not suited to large FFT sizes. The FB algorithm, also known as BCJR algorithm in coding theory, can be interpreted as the

application of the SP algorithm to a HMM or a trellis. Indeed, chain graphs like trellises or Markov models constitute an important family of FGs [Kschischang01].

In the FB algorithm, messages are propagated in both directions at the same time. Fig. 3.7 depicts the corresponding HMM with the forward and backward messages. We immediately see that the FG has no cycles, and the SP leads to sequential processing.

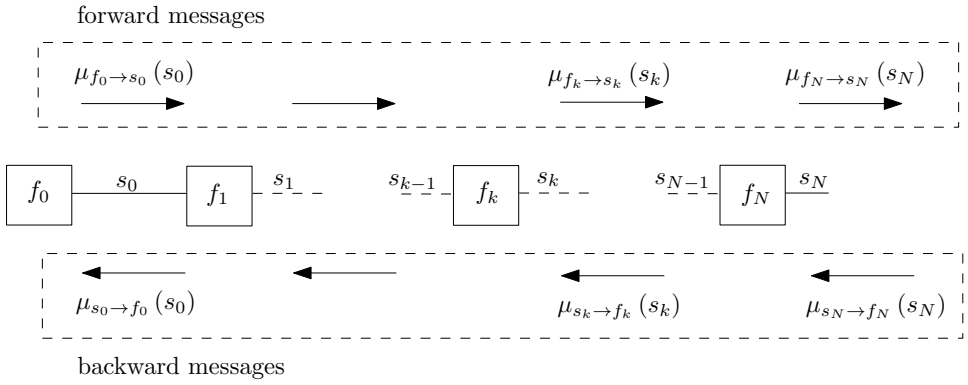


Figure 3.7: The SP algorithm on a HMM with forward and backward phases.

Once the phases have been completed, the marginals are computed multiplying the messages in both directions on every edge. In conclusion, with the SP algorithm implemented on a HMM, inference problems (like determining the marginal a posteriori distributions) can be solved exactly. Hence, assuming the same parameter model, the performance difference of the FB algorithm with respect to the FG-based algorithms, equals the performance loss of the latter due to the presence of short loops in the FG.

On the other hand, it is noteworthy that the implementation of the MS algorithm in a HMM is equivalent to the VA, which, as we have seen before, can be implemented through the SP algorithm in logarithmic-domain by means of the Jacobian logarithm and approximating it with the max function.

### 3.5.2 Forney approach

For the system model described in Section 3.2.2 and assuming $q = 1$, the $\psi$ variable subset is defined as $\psi_k = \{s_{k-1}, s_k, s_{k+1}\}$. Based on the Forney observation model [Forney72], the likelihood $P(\mathbf{y}|\mathbf{s})$ introduced in (3.1) is factorized as follows:

$$P(\mathbf{y}|\mathbf{s}) \propto \prod_{k=1}^{N} f_k(s_{k-1}, s_k, s_{k+1}), \tag{3.21}$$

where implicitly $s_k = 0$ for $k \leq 0$ and $k > N$, and

$$f_k\left(s_{k-1}, s_k, s_{k+1}\right) \propto \exp\left(-\frac{\left|y_k - \sum_{n=k-1}^{k+1} H_{kn} s_n\right|^2}{\sigma_n^2}\right). \tag{3.22}$$

Part of the corresponding FG is depicted in Fig. 3.8, where it is clear that the shortest cycle in the graph is length-4, i.e., the graph has girth 4.

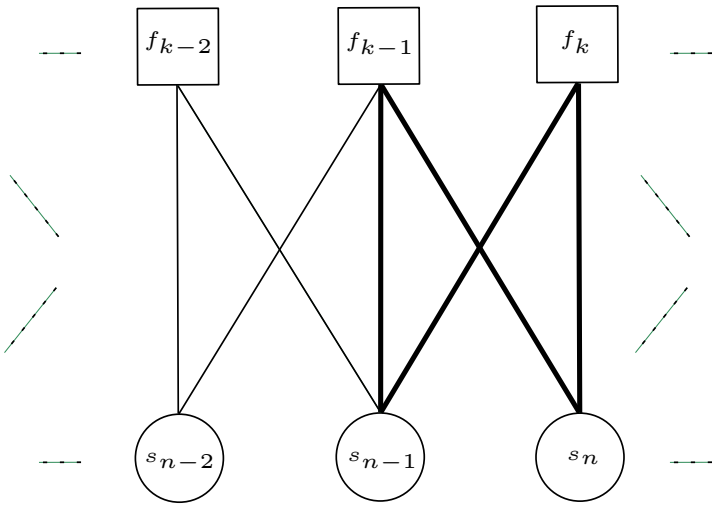


Figure 3.8: Factor Graph for the Forney approach-based MAP symbol detection.

After running the SP algorithm on this FG following (3.7) and (3.8), the marginal a posteriori probabilities are computed by means of (3.9). Note that the order in which messages are updated in the FG can be very diverse. This is stated by the message-passing schedule: the specification of messages to be passed during each clock tick. The performance of the message-passing algorithm varies depending on the selected schedule. The two extreme message passing schedules are the so-called flooding (parallel) and the serial schedule. In the former, a message is passed in each direction over each edge at each clock tick. In the latter, at most one message is passed anywhere in the graph at each clock tick. Obviously, a wide variety of hybrid message-passing schedules can be defined. In this dissertation, we are interested in parallel processing in order to diminish latencies in the detection process due to the usage of large OFDM symbol lengths. Hence, the flooding schedule has been adopted.

#### 3.5.2.1 Convergence analysis

The convergence analysis aims to observe the behavior of the algorithm as iterations are performed in the FG. Fig. 3.9 depicts the BER performance over iterations for different Doppler frequencies (0.1, 0.3, 0.4, 0.5) at turbo cliff region. As it is shown, the behavior of the algorithm differs at low and high Doppler frequencies. On one hand, both SP and MS algorithms converge in the second iteration at $f_d = 0.1$, whereas, for higher Doppler frequencies, the best BER performance is achieved in the third iteration. This behavior

is directly connected with the length-4 cycles in the graph: at the third iteration, each node in the FG receives messages which carry information already processed by it. This leads to message-correlation causing significant performance loss. In the case of low Doppler frequencies, since the weights of the edges (determined by the channel coefficients defined in $\mathbf{H}$) are less significant, two iterations are enough to converge. Fortunately, as it will be shown in the next section, few iterations are enough to get a high level of ICI suppression.

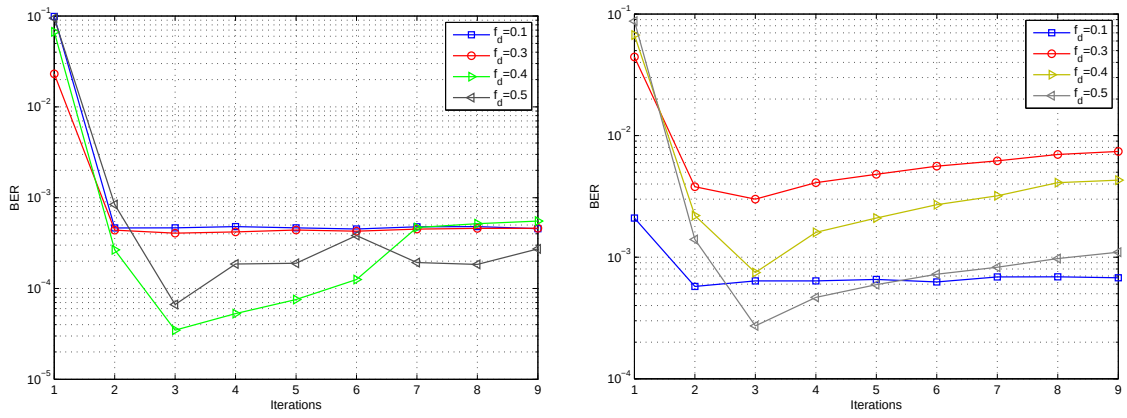


Figure 3.9: Convergence analysis by means of BER performance vs number of iterations for SP (a) and MS (b) algorithms at turbo cliff region. TU6 channel is assumed.

On the other hand, note that the algorithm is more stable at low Doppler frequencies, where, as it can be seen in Fig. 3.9, SP behaves more stably than MS.

#### 3.5.2.2 Exploiting frequency-diversity

As it was pointed out in Section 3.4, the BP detector exploits the frequency-diversity introduced by ICI, and this is the reason of the good performance in high-mobility scenarios. Since this frequency-diversity increases with the Doppler frequency, ICI suppressing capacity gets higher as the Doppler frequency increases. Fig. 3.10a shows this behavior in terms of percentage of suppressed ICI, non-suppressed ICI and residual ICI. The suppressed ICI is the portion of the total ICI that the algorithm is capable of suppressing. The non-suppressed ICI refers to the amount of ICI that remains after detection because the algorithm is not able to suppress due to its sub-optimality. In the case of optimal FB algorithm, the non-suppressed ICI turns into zero. Finally, as a consequence of considering finite ICI channel memory ($q = 1$), there is a residual ICI which cannot be removed by the BP detector.

Fig. 3.10a shows that, in terms of percentage, the suppressed ICI grows substantially with the Doppler frequency, causing as a consequence, the drop of the residual ICI. That is to say, since the correction capacity grows, there is less residual ICI at high Doppler

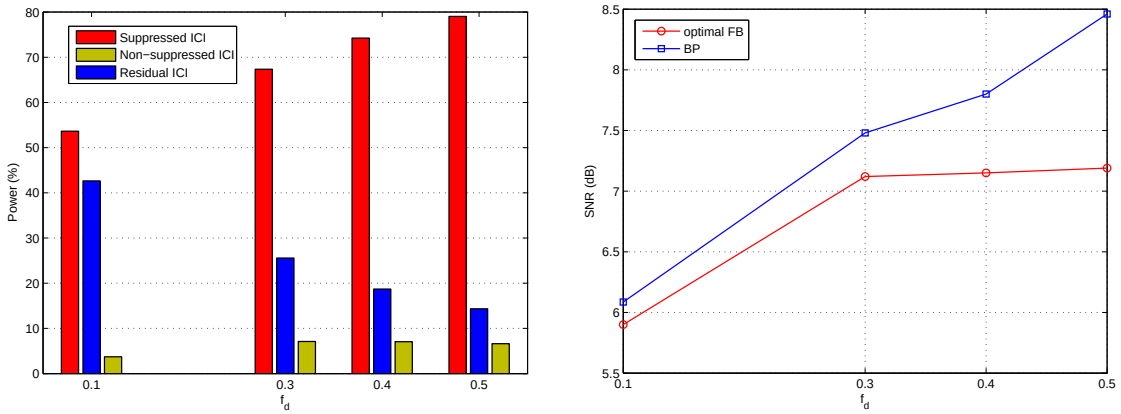


(a) (b)

Figure 3.10: Percentages of suppressed ICI, non-suppressed ICI and residual ICI for different $f_d$ (a) and SNR vs $f_d$ at BER $= 10^{-4}$ (b). MS algorithm is assumed.

frequencies. On the other hand, it is shown that, the non-suppressed ICI gets stuck at a certain level beyond $f_d = 0.3$.

Note that, although the percentage analysis helps to understand the ICI suppression capacity of the algorithm, we have to take care of the ICI power in absolute terms. For example, although based on the percentage analysis residual ICI is much smaller at $f_d = 0.5$ than at $f_d = 0.1$, in absolute terms, this does not hold: 15% of the total ICI at $f_d = 0.5$ represents more power of ICI than 40% at $f_d = 0.1$. The same happens with the non-suppressed ICI, and therefore, system performance loss due to sub-optimality is higher at high Doppler frequencies. This is shown is Fig. 3.10b, where the necessary SNR to get BER=$10^{-4}$ is depicted for different Doppler frequencies, both for BP algorithm and optimal FB algorithm. As it can be seen, the gap between both curves increases with the Doppler frequency becoming around 1.3 dB at $f_d = 0.5$.

#### 3.5.2.3 BER and FER analysis

In this section, the proposed BP algorithm is assessed by means of BER and FER. This is depicted in Fig. 3.11 for different Doppler frequencies. Based on the convergence analysis in the previous section, two iterations are performed for $f_d = 0.1$ and three for higher Doppler frequencies.

Due to the existence of non-suppressed and residual ICI, BER curves shift to the right side as the Doppler frequency increases, causing as a consequence a performance loss of about 1.5/2 dB (SP/MS) with respect to the free-ICI case for $f_d = 0.5$. Regarding the $f_d = 0.1$ case, note that BP algorithm outperforms the free-ICI case giving a slight performance gain as a result of the diversity order gain.

On the other hand, as it is shown in Fig. 3.11, BER and FER behave in the same way

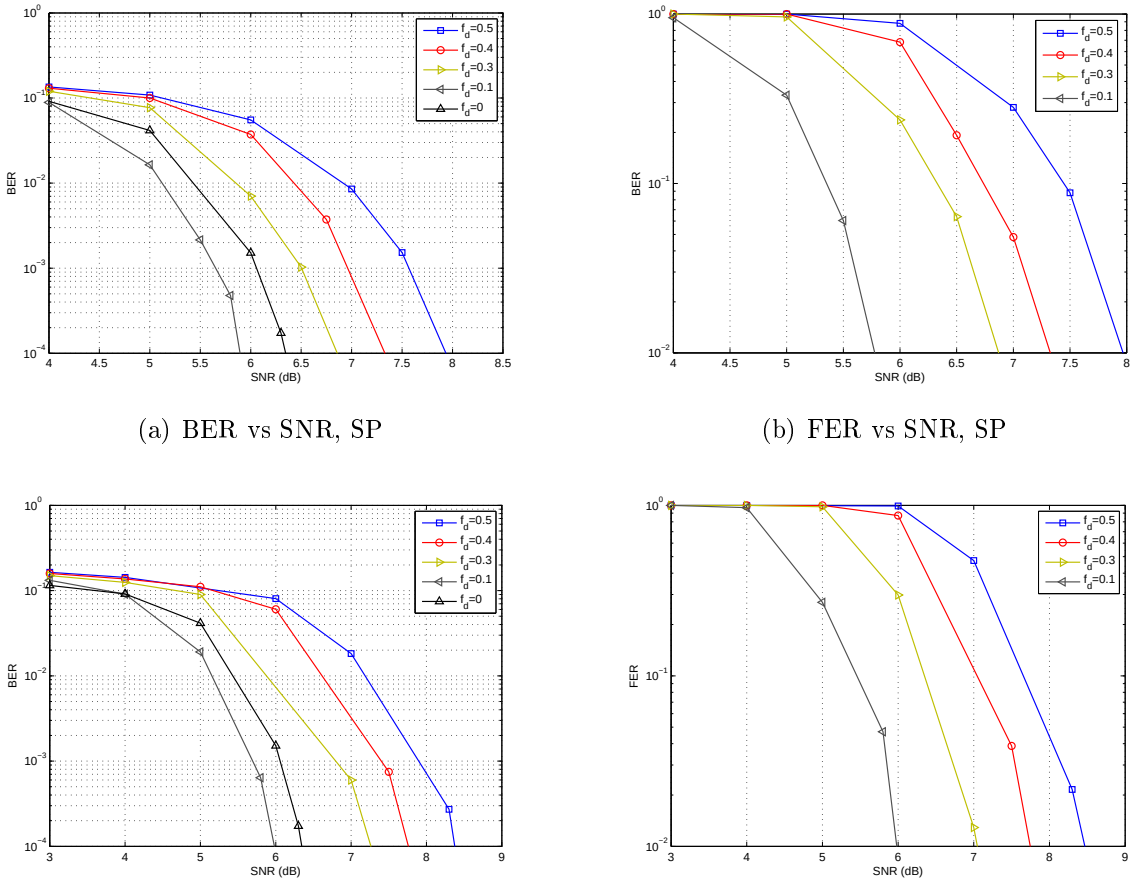


(a) BER vs SNR, SP

(b) FER vs SNR, SP

(c) BER vs SNR, MS

(d) FER vs SNR, MS

Figure 3.11: BER vs SNR and FER vs SNR performance.

both for SP and MS algorithms. This is not consistent with the statement in Section 3.2.1, whereby MS algorithm yields FER minimization and SP algorithm BER minimization. In the first sight, the FER performance should be better for MS algorithm than for SP algorithm, and from Fig. 3.11, it is clear that SP algorithm gives better performance than MS algorithm in terms of BER, as well as in terms of FER. So, what is the matter? The point is that, the BP algorithm is not performing just a single MAP detection task, but, at the same time, it is exploiting the frequency-correlation due to ICI. In that sense, we know that the SP algorithm has more ICI suppression capacity than the MS algorithm, and that is the reason why the statement in Section 3.2.1 does not hold in this case.

Fig. 3.12 deals with BER performance over iterations. On one hand, note that the gap between the second and the third iteration is bigger at higher Doppler frequencies, which means that the performance gain offered by an iteration in the BP algorithm is higher as the Doppler frequency increases. This can also be confirmed from Fig. 3.9. On the other hand, note from Fig. 3.12b the ICI suppression capacity of the BP algorithm, being able to remove the error floor which was at BER=$10^{-1}$ with only three iterations in the FG.

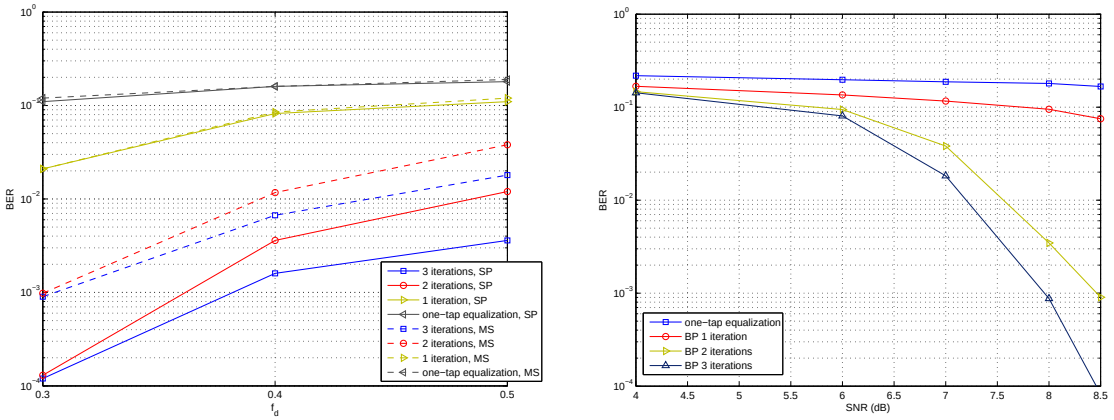


(a) (b)

Figure 3.12: BER vs $f_d$ at SNR=7dB (a) and BER vs SNR for different iterations when MS algorithm is assumed ($f_d = 0.5$) (b).

### 3.5.3 Ungerboeck approach

Both Forney [Forney72] and Ungerboeck [Ungerboeck74] MAP sequence detection strategies are equivalent and only differ in the expression of the VA branch metrics. The former uses the output of a whitened match filter for computing the branch metrics of the VA leading to a Markovian channel model, while the latter can work directly with the output of a filter matched to the received pulse. Nevertheless, when MAP symbol detection strategy is adopted, while the Forney observation model can be directly applied, the extension of the Ungerboeck observation model is not trivial. In [Colavolpe05a], this problem is solved and it is proven that both models are equivalent also for MAP symbol detection. Based on the keen observation made in [Colavolpe05a], a BP detection algorithm based on the Ungerboeck approach [Fertonani08] was proposed for dispersive channels providing impressive complexity reduction comparing with [Colavolpe05b]. Similarly, low-complexity FGs have been derived for channels with memory in [Colavolpe06]. Recently, a novel BP detector employing the Ungerboeck observation model has been presented for ICI channels [Haselmayr11].

Based on the Ungerboeck observation model the likelihood function $P(\mathbf{y}|\mathbf{s})$ can be factorized as follows

$$P(\mathbf{y}|\mathbf{s}) \propto \exp\left(-\frac{|\mathbf{y}-\mathbf{H}\mathbf{s}|^2}{\sigma_n^2}\right) \propto \exp\left(\frac{2\Re\left\{\mathbf{s}^{\mathrm{H}}\mathbf{x}-\mathbf{s}^{\mathrm{H}}\mathbf{G}\mathbf{s}\right\}}{\sigma_n^2}\right), \tag{3.23}$$

where $\mathbf{x} = \mathbf{H}^{\mathrm{H}}\mathbf{y}$ and $\mathbf{G}$ is the Hermitian matrix defined as $\mathbf{G} = \mathbf{H}^{\mathrm{H}}\mathbf{H}$. The same factorization can be expressed in scalar form as

$$P(\mathbf{y}|\mathbf{s}) \propto \prod_{k=1}^{N} \exp\left(\frac{1}{\sigma_n^2}\left[2\Re\left\{s_k^* x_k - \frac{1}{2} g_{k,k}\left|s_k\right|^2 - \sum_{i=1}^{2q} g_{k,k-i} s_k^* s_{k-i}\right\}\right]\right). \tag{3.24}$$

By defining the next functions

$$f_k\left(s_k\right) = \exp\left(\frac{1}{\sigma_n^2} 2\Re\left\{s_k^* x_k - \frac{1}{2} g_{k,k}\left|s_k\right|^2\right\}\right), \tag{3.25}$$

$$u_{k,i}\left(s_k, s_{k-i}\right) = \exp\left(-\frac{1}{\sigma_n^2} 2\Re\left\{g_{k,k-i} s_k^* s_{k-i}\right\}\right), \tag{3.26}$$

the likelihood function can be expressed in a compact form as

$$P\left(\mathbf{y}|\mathbf{s}\right) \propto \prod_{k=1}^{N}\left(f_k\left(s_k\right)\prod_{i=1}^{2q} u_{k,i}\left(s_k, s_{k-i}\right)\right), \tag{3.27}$$

where implicitly $s_k = 0$ for $k \leq 0$ and $k > N$. Part of the FG derived from (3.27) is depicted in Fig. 3.13, where it can be seen that has girth 6. Considering messages depicted in Fig. 3.13 in logarithmic-domain, the marginal a-posteriori probabilities $\overline{\mathrm{APP}}\left(s_k\right) = \ln P\left(s_k|\mathbf{y}\right)$ are computed as

$$\overline{\mathrm{APP}}\left(s_k\right) = \bar{f}_k\left(s_k\right) + \sum_{i=1}^{2q}\left(L_{k,i}^{U} + L_{k,i}^{B}\right), \tag{3.28}$$

while the remaining messages are defined as follows:

$$L_{k,i}^{D}\left(s_k\right) = \overline{\mathrm{APP}}\left(s_k\right) - L_{k,i}^{U}, \tag{3.29}$$

$$L_{k-i,i}^{B}\left(s_{k-i}\right) = \mathbb{M}_{\sim\{s_{k-i}\}}\left(\ln\left(u_{k,i}\left(s_k, s_{k-i}\right)\right) + L_{k,i}^{D}\left(s_k\right)\right), \tag{3.30}$$

$$L_{k,i}^{U}\left(s_k\right) = \mathbb{M}_{\sim\{s_k\}}\left(\ln\left(u_{k,i}\left(s_k, s_{k-i}\right)\right) + L_{k-i,i}^{F}\left(s_{k-i}\right)\right), \tag{3.31}$$

$$L_{k-i,i}^{U}\left(s_{k-i}\right) = \overline{\mathrm{APP}}\left(s_{k-i}\right) - L_{k-i,i}^{B}\left(s_{k-i}\right). \tag{3.32}$$

### 3.5.4 Forney approach vs Ungerboeck approach

The performance of the proposed detector is compared with the Ungerboeck approach-based BP detector presented in [Haselmayr11]. Three iterations have been carried out in the detector in both cases and MS algorithm has been adopted. Both BP algorithms are compared

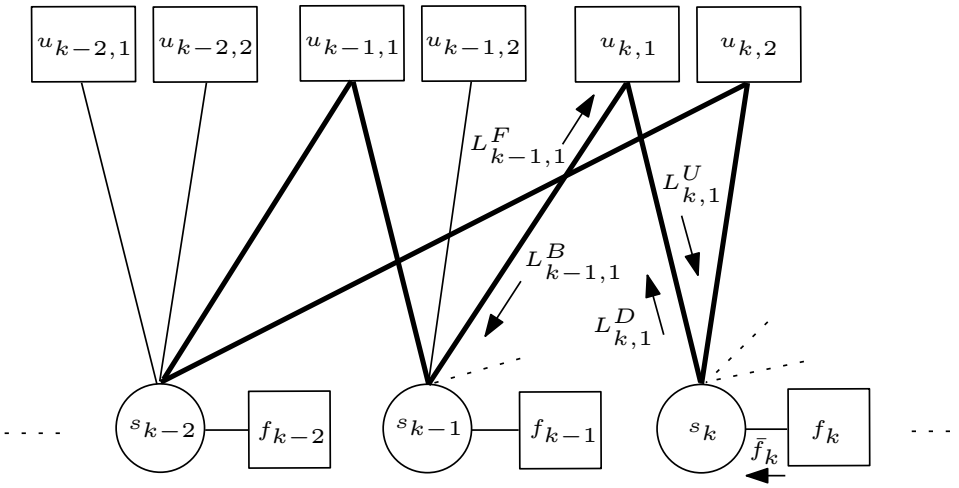


Figure 3.13: Factor Graph for the Ungerboeck approach-based MAP symbol detection.

with the optimal FB algorithm in order to quantize their performance loss with respect to the optimal MAP symbol detection, although it is well-known that FB algorithms can not be considered for large FFT sizes due to their intrinsic serial structure.

As it is shown in Fig. 3.14a, both approaches show almost the same performance for low Doppler frequencies and they are very closed to the optimal FB. Consequently, and taking into account that the Ungerboeck approach is less complex than the proposed Forney approach (deeper explanation is provided in Section 3.6), it is clear that the best option for low mobile scenarios is the Ungerboeck approach-based BP detector [Haselmayr11]. However, it turns out that the performance of the Ungerboeck approach-based BP detector drops down severely at high-mobility scenarios. In Fig. 3.14b, it is shown that the Ungerboeck approach tends to an error floor whereas the Forney approach presents a performance loss of about 0.8 dB at BER = $10^{-4}$ with respect to the optimal FB. A detailed observation of the messages into the FG at asymptotic regime (high SNR and high Doppler frequency) indicates that the factorization based on the Ungerboeck observation model collapses when in the presence of very reliable input information factor nodes output uniform distributions. Therefore, the Ungerboeck approach is not a good candidate for the channels of interest in this dissertation.

#### 3.5.4.1 Kullback-Leibler divergence analysis

This can also be confirmed by means of the Kullback-Leibler (KL) divergence analysis, also known as the relative entropy. Assuming that the outputs of the optimal FB algorithm are exact MAP distributions, the KL divergence offers a measure of the distance between the approximate MAP distributions $Q$ given by the BP algorithms (based on Forney and Ungerboeck approaches) with respect to the "true" distributions $P$ given by the optimal FB algorithm. Being the probability distributions $P$ and $Q$ the discrete marginal a posteriori distributions of the optimal FB and the BP algorithms respectively, their KL divergence is

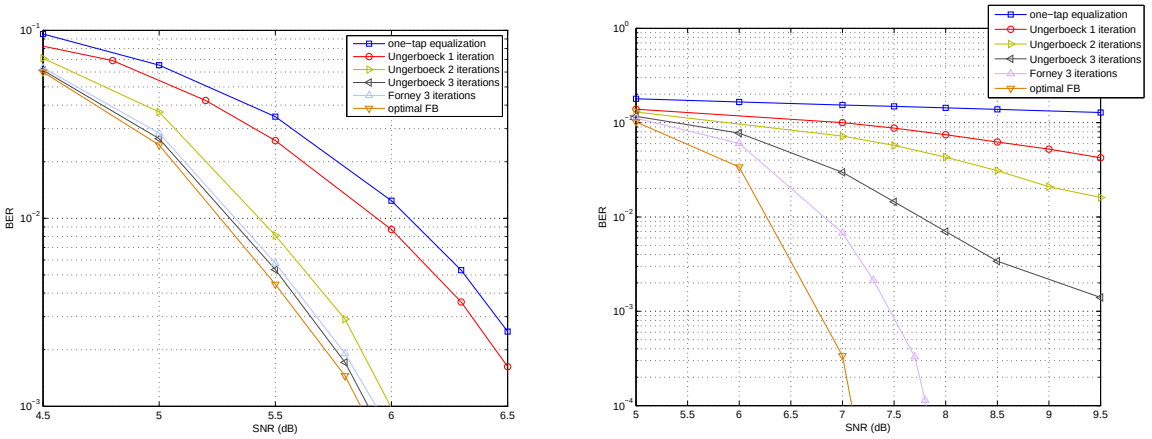


(a) (b)

Figure 3.14: Ungerboeck approach vs Forney approach for $f_d = 0.16$ (a) $f_d = 0.4$ (b).

defined as

$$D_{KL}\left(P||Q\right) = \sum_{s_k \in \chi} P\left(s_k|\mathbf{y}\right) \ln \frac{P\left(s_k|\mathbf{y}\right)}{Q\left(s_k|\mathbf{y}\right)}. \tag{3.33}$$

In words, the previous formula represents the average of the logarithmic difference between the probabilities $P$ and $Q$. It has to be clearly stated that the KL divergence is not a true metric (e.g., it is not symmetric), but even so, it is valid for the purpose of measuring the degradation of the MAP distributions at the output of the BP algorithm due to the existence of cycles in the FG.

Fig. 3.15 shows the evolution of the KL divergence with respect to the normalized Doppler frequency (for 100 different channel realizations). Fig. 3.16, in turn, depicts the evolution of the SNR required for achieving BER=$10^{-4}$ for the three algorithms considered throughout this chapter. As it can be seen, there is a consistence between the behavior of the KL divergence and the BER performance. From Fig. 3.15, it is clear that it is around $f_d = 0.17$ where the KL divergences of both algorithms equalize, and it is also around $f_d = 0.17$ where the same SNR is required to achieve a BER of $10^{-4}$. Both Fig. 3.15 and 3.16 show that the gap between Forney and Ungerboeck BP detectors becomes noticeable beyond $f_d = 0.3$. Therefore, this analysis corroborates the results in Fig. 3.14, and it is definitely concluded that the performance of the Ungerboeck BP detector is insufficient for the channels of interest in this research work.

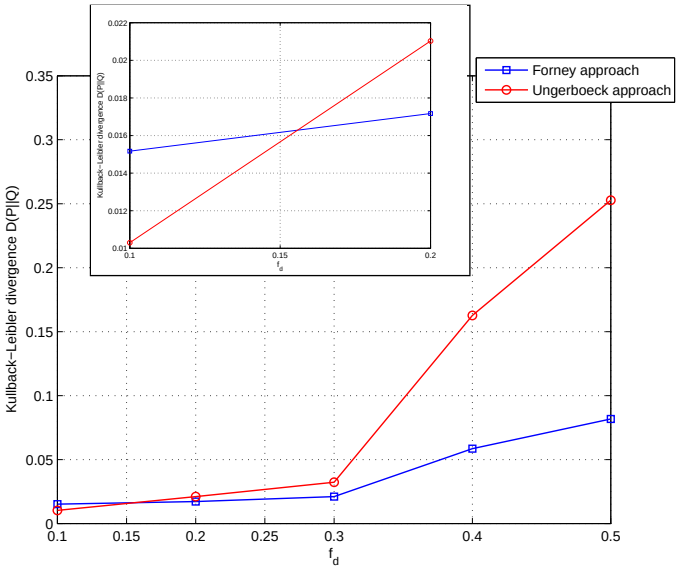


Figure 3.15: Kullback-Leibler divergence $D\,(P||Q)$, where $P$ refers to the optimal FB algorithm and $Q$ represents the Forney approach BP algorithm and the Ungerboeck approach BP algorithm in each case.

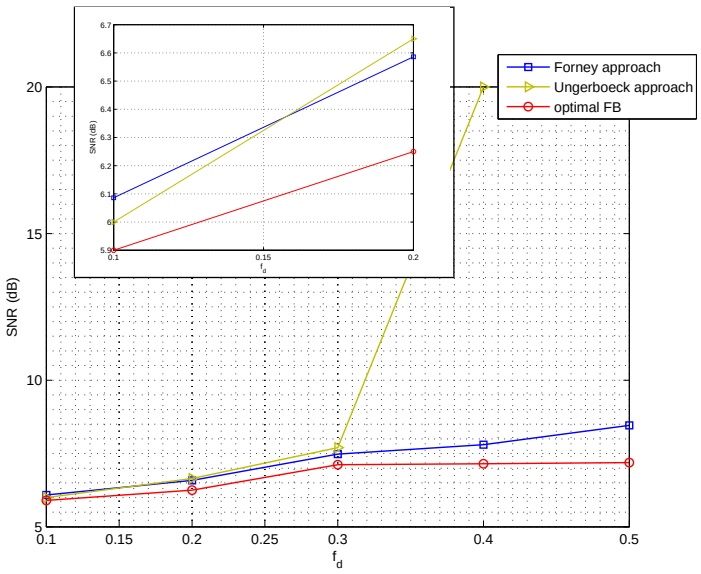


Figure 3.16: SNR vs $f_d$ for the Forney approach BP detector, Ungerboeck approach BP detector and optimal FB algorithm.

### 3.5.5 BP detection vs MAP detection with ICI cancellation

The proposed detector is also compared with the MAP ICI canceler proposed in [Peng06], which presents a fully parallel architecture which accommodates hardware implementation and its complexity is much less than other proposals' in the literature when the OFDM symbol length is very large. As a result, it is a good candidate for ICI compensation when very large OFDM symbols are used. In general terms, it is composed of two stages (Fig. 3.17): the first one estimates the transmitted data by means of a Viterbi-like algorithm (it is a trellis-based symbol detector), and the second one performs the MAP detection suppressing the ICI which was previously reconstructed with the output of stage one (ICI suppressing demapper).

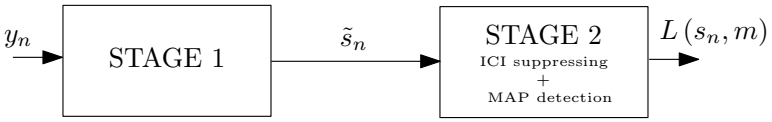


Figure 3.17: Structure of the ICI suppressing soft demapper.

Focusing on stage one, and based on the keen observation that only few subcarriers contribute significantly to ICI, we can simplify the detection process reducing the search dimension to a few dominant terms. With $q = 1$, i.e., three carriers considered for ICI, the trellis has $M^3$ states, three stages, and an auxiliary starting state. Each state consists of a combination of three constellation symbols. Each stage represents each of the three received subcarriers to be considered. The branch cost in the trellis is determined by the Euclidean distance between the received symbols $y_n$ and three symbols (denoted as $s_i$) which determine the branch ending state. The path cost is calculated as

$$\sum_{n=l-q}^{l+q} \left| y_n - \sum_{i=n-q}^{n+q} H_{ni} s_i \right|. \tag{3.34}$$

The VA can be used to find the minimum-cost path if the trellis is defined as in Fig. 3.18.

Stage two computes the LLRs $L(s_n, m)$ in order to suppress ICI and exploit the frequency-diversity introduced by it. Complexity of stage two can be controlled if performance is sacrificed, which is function of parameter $t$. The next equation describes the demapping process, where we consider $t = 2$:

$$L_{lm} \approx \sum_{n=l-t}^{l+t} \log \left[ \frac{\sum_{s_l \in \chi^+} \exp\left[ -\frac{1}{N_0} \left| y_n - \sum_{k=n-t, n\neq l}^{n+q} H_{nk} \widetilde{s}_k - H_{nl} s_l^+ \right|^2 \right]}{\sum_{s_l \in \chi^-} \exp\left[ -\frac{1}{N_0} \left| y_n - \sum_{k=n-t, n\neq l}^{n+q} H_{nk} \widetilde{s}_k - H_{nl} s_l^- \right|^2 \right]} \right]. \tag{3.35}$$

As it is shown in Fig. 3.19, both schemes are very closed to each other for $f_d = 0.1$.

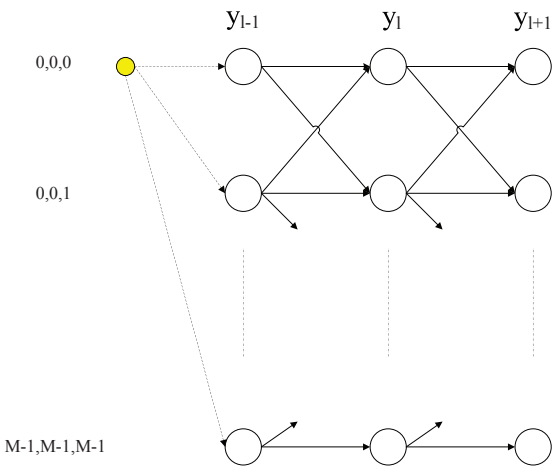


Figure 3.18: Stage 1 computes symbol estimates using a Viterbi-like algorithm.

Nevertheless, the estimates produced by the first stage of the MAP ICI canceler degrade severely at high Doppler frequencies, thus it suffers from a performance loss which leads to an error floor. Hence, although the MAP ICI canceler proposed in [Peng06] is well suited to large FFT sizes from an implementation point of view, it is clearly shown that the proposed BP detector outperforms the MAP ICI canceler in terms of BER performance for the channels of interest in this research work.

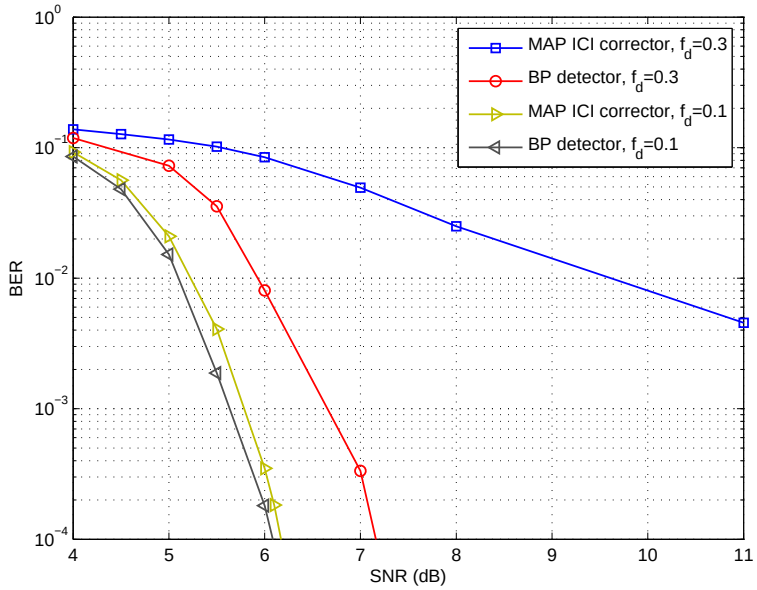


Figure 3.19: MAP ICI canceler [Peng06] vs proposed BP detector for $f_d = 0.1$ and 0.3.

## 3.6 Complexity analysis

As it has been mentioned before, the implementation of the SP algorithm is accomplished in logarithmic domain, and this can be done using the Jacobian logarithm, which only requires additions and the evaluation of a non-linear function.

The complexity of the proposed Forney approach-based BP detection algorithm is mainly a function of the following parameters: constellation size $\Gamma$, number of total subcarriers $N$ and the bandwidth parameter $q$. Table 3.2 describes the complexity of different algorithms considered in this paper. As it is shown, it is obvious the weakness of the proposed algorithm comparing with the Ungerboeck approach-based algorithm presented in [Haselmayr11] in terms of complexity, since the Forney approach is exponentially dependent on $q$, whereas the Ungerboeck approach leads to linear dependence on $q$: we notice that the exponential dependence on the value of $q$ that characterizes the Forney approach, does not appear neither in (3.30), nor in (3.31). Hence, we can state that the complexity of the Ungerboeck approach increases linearly with the value of $q$.

| Algorithm | Complexity | Structure |
|---|---|---|
| Optimal FB | $\mathcal{O}\left(N\Gamma^{2q+1}\right)$ | Serial |
| Forney approach-based BP | $\mathcal{O}\left(N\Gamma^{2q+1}\right)$ | Parallel |
| Ungerboeck approach-based BP [Haselmayr11] | $\mathcal{O}\left(N\Gamma^{2}\left(2q+1\right)\right)$ | Parallel |
| MAP detection with ICI cancellation [Peng06] | $\mathcal{O}\left(4N+N\Gamma^{3}\right)$ | Parallel |

Table 3.2: Complexity analysis.

We can adopt different strategies to reduce the complexity of the algorithm proposed in this work. Two approaches can be distinguished: on one hand, we can replace the SP algorithm by approximations of lower complexity than the original SP algorithm (e.g., the MS algorithm is less complex than the SP algorithm). On the other hand, complexity of message calculation can also be reduced by different means. In this sense, compared with FB algorithms, the complexity reduction is much easier in BP algorithms, since there are no constraints imposed by the trellis structure. Reduced state sequence detection (RSSD) [Eyuboglu88, Chevillat89] can be an effective method for reducing the complexity with a minor performance loss.

## 3.7 Chapter Summary

This chapter can be considered as the central one in this dissertation, since the main theoretical and practical aspects of the proposed FG-based detection are dealt with. Section 3.2 copes with the basic FG framework concepts necessary to understand the design of the BP detector. It is described how FG can solve complex inference problems as the one formu-

lated in this dissertation in a computationally efficient manner. Other fundamental issues related with the FG framework, such as message-representation, are also tackled in this section. Section 3.3 analyzes how short loops affect FG-based algorithms. The problems surrounding loopy FGs play an important role, since the proposed BP detector design does not avoid the presence of the shortest possible loops in a FG. Section 3.4 introduces the main system characteristics as well as the simulation parameters for the BP detector design and assessment.

Three BP algorithms are introduced in Section 3.5 for signal detection in channels affected by ICI: the proposed Forney approach-based BP, the Ungerboeck BP, and the optimal FB detector. Extensive numerical results are provided for different mobile scenarios which show that the proposed Forney approach-based BP detector suits better to the channels of interest in this research work. Finally, a brief complexity analysis is provided in Section 3.6.

# Chapter 4

# Turbo approach for intercarrier interference cancellation

## 4.1 Introduction

In this chapter we integrate the BP detector proposed in Chapter 3 in a higher-order turbo receiver scheme, where soft information is exchanged between the LDPC decoder and the BP detector. A triple iterative scheme is proposed where messages are exchanged among internal LDPC decoder nodes, internal detector nodes, and between the detector and the decoder. Assuming that LDPC codes are decoded with FG-based algorithms, the turbo receiver presents a fully parallel structure which can enable a high-speed detection. This is an interesting feature when long OFDM blocks are employed, which is the case of broadcasting systems where reduced end-to-end delay is required (e.g., use of the DVB-NGH system during sports events) and thus it is necessary to restrain the latency as much as possible.

Once the iterative reception strategy has been defined, the inclusion of pilot symbols is considered in order to analyze how they can be processed in the FG. We assess the system performance adopting a pilot pattern included in the DVB-T2 standard. Considering that LDPC codes are decoded using BP algorithms, the joint data detection and decoding process can be depicted by a higher-order FG where soft decision messages are transferred on cyclic graphical models. We analyze the performance difference between this graphical turbo approach and the classical one, where two independent processors exchange soft extrinsic information.

The convergence behavior of the classical turbo approach is analyzed by means of EXIT charts and extensive numerical results are provided comparing the BER performance curves of both turbo approaches and the non-turbo case. Along with the TU6 channel, we also consider the rural RA6 channel model in order to assess the typical terrestrial broadcasting channel conditions.

## 4.2 System description

The so-called turbo principle, originally developed for decoding turbo codes (concatenated convolutional codes) [Berrou93] has been adapted to various communication problems. Basically, the digital communication receivers based on the turbo principle are the class of decentralized algorithms that drastically improve communication system performance by repeatedly exchanging soft information among the receiver parts. It was first proposed in [Douillard95] with the aim of approaching the optimal joint processing of the detection and decoding steps over a channel affected by ISI with affordable complexity. If no interleaver was introduced, optimal joint detection/decoding would be possible describing the combined operation of the FEC and the ISI channel in a supertrellis. Nevertheless, complexity is unaffordable except for most simple cases.

In this context, the turbo principle leads to the achievement of nearly optimal performance through the application of iterative processing to relatively low-complexity stages. In brief, the turbo principle obeys the criterion known as "divide and conquer" and presents two key ingredients: local optimality of each stage (ML/MAP design) and the exchange of extrinsic soft information between stages. As it is obvious, the number of states in the trellis of the MAP detector grows with the channel memory and the constellation size, so it might be too complex to implement. Hence, other lower complexity suboptimum approaches can be found that allow the application of the turbo principle [Tuchler02].

In Chapter 3, the implementation of the BP detector in a BICM-OFDM communication system has been analyzed as an efficient solution to counteract the effect of the Doppler spread. The BP detector provides soft outputs which are converted into LLRs to be decoded by the LDPC decoder, that consists of a FG-based algorithm as well. Therefore, the receiver scheme is composed of two concatenated MAP SISO stages that allow the exchange of extrinsic soft information between them. Moreover, note that the fact that both the detector and the decoder are FG-based algorithms results in a very well-suited receiver structure for high-speed reception.

For simplicity, we can abstract out the OFDM modulation, and consider that the communication system is composed of the channel code and the ICI channel working as a inner encoder. Indeed, the ICI channel can be regarded as a rate-1 code, and therefore, we can consider the channel code and the ICI channel as a serial concatenation as it is depicted in Fig. 4.1. Note that, assuming three subcarriers contribute to ICI, that is $q = 1$, the ICI channel has memory 3, which determines the complexity of the BP detector.

The receiver scheme presented in Fig. 4.1 is a triple iterative scheme where three turbo processes are running at the same time: in the detector, in the decoder and between them. From now on, we will further refer to the iterations in the detector as *BP iterations*, to the iterations in the LDPC decoder as *LDPC iterations* and to the iterations between the

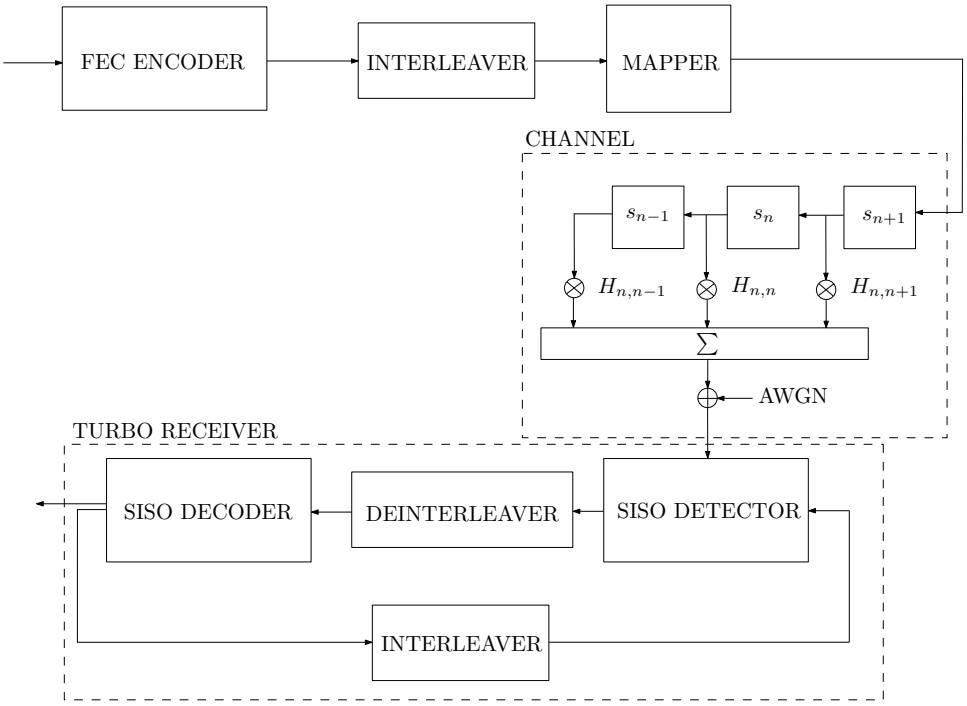


Figure 4.1: Turbo receiver consisting of the concatenation of the detector and the decoder, where the ICI channel works as a rate-1 inner code.

detector and the decoder as *turbo iterations*. A more detailed description of the model depicted in Fig. 4.1 is provided in Fig. 4.2 for the receiver side, where $L_E(c_{n,m})$ denotes the extrinsic LLRs at the output of the detection process which are taken as a priori LLRs in the decoder ($L_A(c_{n,m})$) after having been interleaved. $L_D(c_{n,m})$ refers to the extrinsic LLRs at the output of the decoder which are used to reconstruct symbol likelihoods to be used as a priori information in the detector.

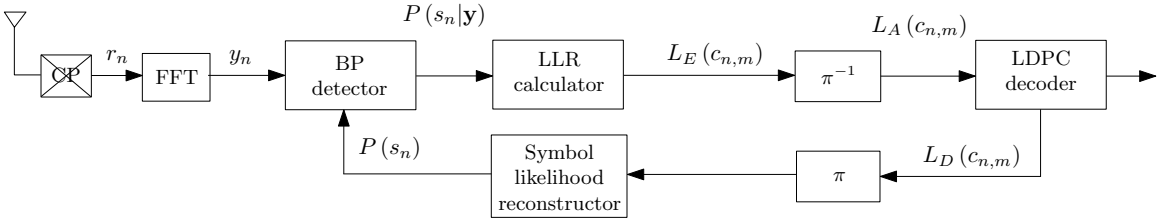


Figure 4.2: Block diagram of the BICM iterative receiver chain including the BP detector.

The BP detector computes the marginal a posteriori probabilities $P(s_n|\mathbf{y})$ given $N$ received symbols applying the SP rule described in (3.7), (3.8) and (3.9). In the initial detection step, it is assumed that no a priori information is available and hence we have $P(s_n) = 0$. Note that the output of the detector and the a priori input are independent to each other, which is the essential feature of any system applying the turbo principle. Hence, the LLR calculator makes use of these marginal a posteriori probabilities to calculate the corresponding LLRs as follows:

$$L_E\left(c_{n,m}\right) = \log \frac{\sum_{\forall \mathbf{c}_n : c_{n,m}=0} P\left(s_n|\mathbf{y}\right) \prod_{j=1;j\neq m}^{M} P\left(c_{n,j}\right)}{\sum_{\forall \mathbf{c}_n : c_{n,m}=1} P\left(s_n|\mathbf{y}\right) \prod_{j=1;j\neq m}^{M} P\left(c_{n,j}\right)}, \tag{4.1}$$

assuming $M$ LLRs for each of the $N$ received symbols. The MAP decoder computes the a posteriori probabilities $P\left(c_{n,m} = \kappa | L\left(c_{1,1}\right), L\left(c_{1,2}\right), ..., L\left(c_{N,M}\right)\right)$, $\kappa = \{0, 1\}$, and outputs the difference

$$L_D\left(c_{n,m}\right) = \ln \frac{P\left(c_{n,m=1}|L_A\left(c_{1,1}\right), ..., L_A\left(c_{N,M}\right)\right)}{P\left(c_{n,m=0}|L_A\left(c_{1,1}\right), ..., L_A\left(c_{N,M}\right)\right)} - \ln \frac{P\left(c_{n,m}=1\right)}{P\left(c_{n,m}=0\right)}, \tag{4.2}$$

where the detector output is considered to be a priori information to the decoder. The next step in the turbo procedure is to feed the detector back considering as a priori information the extrinsic information at the output of the decoder. For that purpose, taking into account that the SP rule in the detector is performed in the symbol domain, we have to generate soft symbols from the LLRs. Basic LLR algebra shows that the bit probabilities are obtained from the LLRs by evaluating

$$P\left(c_{n,m}\right) = \frac{1}{1+\exp\left(-L_D\left(c_{n,m}\right)\right)} \exp\left(-c_{n,m} \cdot L_D\left(c_{n,m}\right)\right). \tag{4.3}$$

The a priori inputs $P\left(s_n\right)$ for a given constellation are obtained multiplying all the bit probabilities corresponding to the symbol $P\left(s_n\right) = \prod_{m=1}^{M} P\left(c_{n,m}\right)$. Finally these a priori probabilities are multiplied in each variable node of the detector FG with the rest of incoming messages as it is depicted in Fig.4.3.

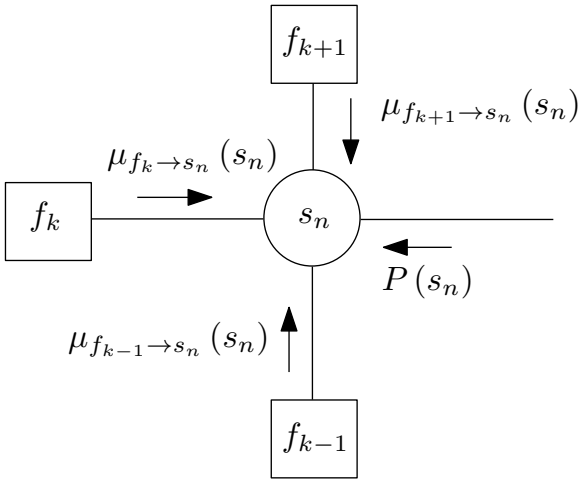


Figure 4.3: Example of a variable node processing a priori information of the corresponding symbol.

Once we have built the turbo scheme, there are two major questions to be answered:

- Under what circumstances can we guarantee convergence to the ML solution?
- How long will it take to converge?

Both questions are hard to answer and we can only try to get the optimum solution by simulation. A *turbo schedule* has to be defined for this purpose, that is, the amount of iterations to be performed in each of the stages for each of the turbo iteration must be expected.

The turbo procedure explained so far corresponds to the original one, typically viewed as two processors running MAP algorithms and exchanging soft decision information. In this work, we will further refer to this first approach as *classical approach*. There is an alternative derived from Wiberg's PhD dissertation [Wiberg96] and further advances, which is commonly described as passing soft decision messages on cyclic graphical models. This second approach will be further denoted as *graphical approach*.

## 4.3 Pilot-assisted factor graph based detection

Many wireless communication systems use training data sequences for channel estimation. For instance, DVB standards consider different pilot patterns in order to adjust the transmission requirements to different channel conditions. The inclusion of pilot carriers has some implications in signal detection based on FGs, which have to be taken into account. The first one is that detection has to be performed before pilot removal. This is obvious, since otherwise the FG representation does not reflect the symbol correlation caused by the ICI channel. This fact makes the FG longer since variable and function nodes corresponding to pilot carriers have to be taken into account. However, at the same time, there is known information that we can use in order to assist the detection process. This gives rise to the term *pilot-assisted FG-based detection*. Fig. 4.4 shows how to deal with pilot carriers in the message passing process, where $s_n$ and $f_k$ are the variable and function nodes corresponding to a given pilot symbol, respectively.

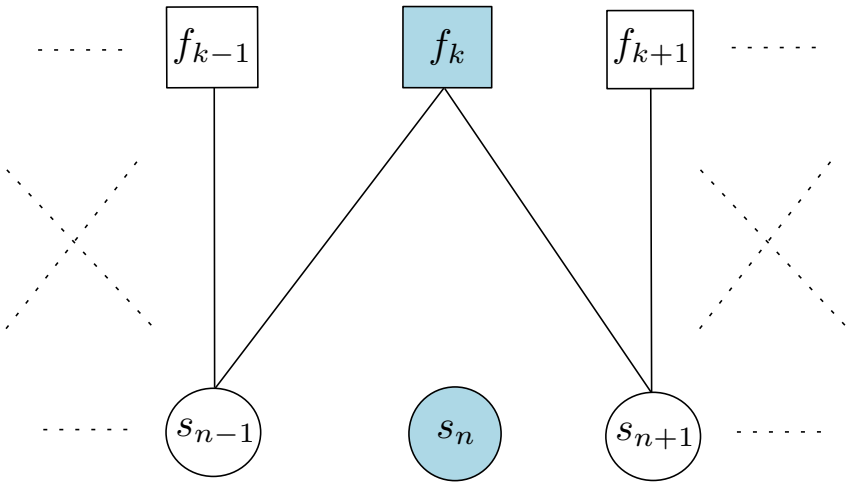


Figure 4.4: Pilot processing in the factor graph.

On one hand, outgoing messages from $f_k$ are more accurate representations of marginal distributions since known information corresponding to $s_n$ has been used in (3.7). On the other hand, messages transmitted by variable node $s_n$ are uniform distributions of the corresponding pilot symbol, which are useless for data symbol detection. Thus, we can consider variable node $s_n$ as an idle node and disconnect it from its neighbors. As we can see in Fig. 4.4, some cycles are straightforwardly removed from the FG as a consequence of disconnecting variable nodes corresponding to pilot symbols. As an example, considering the PP1 pilot pattern of DVB-T2, where pilot carriers represent the 8% of the total carriers, 8% of length-4 cycles are directly removed, which yields an additional performance improvement.

Note that the use of clusters of pilot carriers (consecutive pilot carriers), as it is usual for channel estimation in mobile receivers, would cause the FG to be split into several partitions with no connection among them. This is not something desirable for the SP algorithm since it prevents messages from spreading over the FG. In other words, it provokes messages to be confined in a reduced portion of the FG. Of course, the performance degradation due to this fact depends on the convergence behavior of the algorithm, being negligible if the algorithm tends to converge fast (in few iterations).

There are other alternatives to deal with pilot carriers in the FG. For example, it is possible to extend the message-alphabet by including new points in the constellation that refer to pilot tones. Obviously, this would increase the complexity of the algorithm. In this work, considering that the BP detector converges relatively fast, we have adopted the former way of proceeding.

## 4.4 Classical approach

This is the original turbo receiver approach typically viewed as two processors exchanging soft decision information as it is represented in Fig. 4.2. Note that, in our receiver design, this implies resetting all messages in the detector and decoder FGs each time they are provided with a priori information, so that any memory of the previous iterations is removed. Therefore, when the detector FG is provided with a priori information, it is considered that the value of the messages coming from factor nodes is zero, as it is depicted in Fig. 4.5. Thus, the detection process resumes with the variable nodes transmitting messages to their neighboring factor nodes. The procedure is equivalent in the decoder FG where it is considered that messages coming from check nodes are zero.

This way of proceeding is interesting when channel estimation is considered into a turbo scheme which reestimates the channel in each turbo iteration. Note that, in such a receiver scheme, unless the detector is reset, the factor nodes would propagate new messages computed with the reestimated channel frequency response and these would merge with old messages from the previous turbo iteration, which had been computed with a different chan-

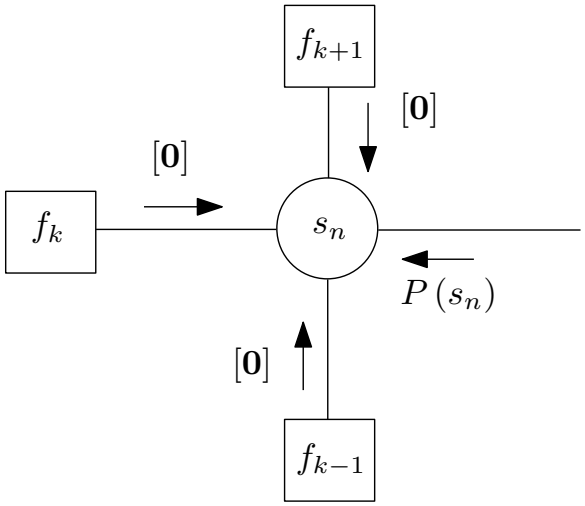


Figure 4.5: Example of a variable node processing a priori information of the corresponding symbol in the classical turbo approach.

nel frequency response. This fact could cause the SP algorithm to become unstable and therefore degrade the detector performance.

### 4.4.1 EXIT chart analysis

Two very well-known tools can be used to analyze the convergence behavior of a turbo process at cliff region: the EXIT charts introduced by Stephan ten Brink [tenBrink01] and the so-called density evolution [Richardson01]. The former visualize the exchange of extrinsic information between the constituent decoders, while the latter analyzes the decoding behavior by tracking the densities of the messages throughout the iterations, being mainly used for the analysis and optimization of LDPC codes. Calculating and tracking the densities can be difficult, specially, if more complicated component codes are used like the ones in our receiver design. Note that we are analyzing a serially concatenated scheme over an AWGN channel with the LDPC as the outer constituent decoder and the BP detector as the inner constituent decoder. Assuming that the bit interleaver is sufficiently large, the EXIT charts provide an accurate prediction of the convergence behavior. Due to the complexity of the system, EXIT functions have to be assessed by Montecarlo simulation.

The EXIT chart characterizes the relation between input and output LLRs of the component decoders in terms of mutual information. To measure the information contents of the a priori knowledge, Shannon's mutual information $I = I(S;L)$ between the transmitted bits $S$ and the LLR values $L$ is used. For simplicity, let us assume binary phase-shift keying (BPSK) modulation and a large interleaver, which assures statistical independence and Gaussian distribution for the input $L$ with parameter $\sigma^2 \leftrightarrow I(L;S)$. As it is depicted in Fig. 4.6, we vary the quality of the a priori information and observe the extrinsic output information. $LA$ denotes the a priori input LLR and $LE$ refers to the extrinsic output LLR.

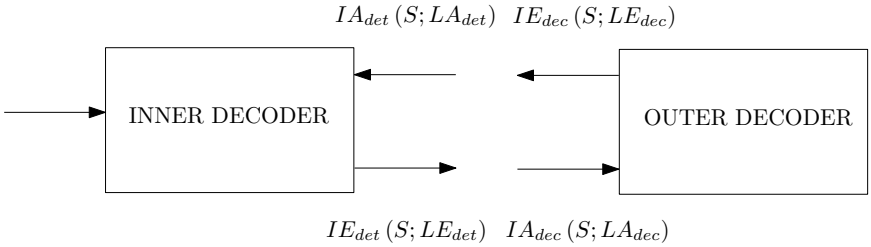


Figure 4.6: Modeling a serial concatenated system with EXIT functions.

Considering $S$ and $Y$ to be two real valued random variables, the Shannon's mutual information is defined as

$$I(S;Y) = \int\int f(s,y) \log \frac{f(s,y)}{f(s)\, f(y)} ds dy, \tag{4.4}$$

If we restrict ourselves to BPSK, $s \in \{+1,-1\}$, and equally likely inputs $s$, the mutual information becomes

$$I(S;Y) = \frac{1}{2} \sum_{s=+1,-1} \int_{-\infty}^{\infty} f(y|s) \log \frac{f(y|s)}{f(y)} dy. \tag{4.5}$$

The integral in 4.5 has to be evaluated numerically. Applying additional assumptions on the distributions $p(y|s)$, such as considering they are symmetric and consistent, we can compute the mutual information as time a average and avoid numerical integration. Due to suboptimal detectors, often distributions are not exactly consistent. However, it turns out that we can mostly assume consistency and still obtain accurate results. On the other hand, because of the nonlinearity of the decoder, the L-value distribution of the output is in general unknown and no longer Gaussian. Nevertheless, by invoking the ergodicity theorem, we can measure the mutual information from a large number $N$ of samples even for non-Gaussian or unknown distributions. Combining these constraints with 4.5 and invoking the ergodicity theorem leads to estimating the mutual information only from the magnitudes without knowing the correct data [tenBrink01] as

$$I(L;S) = 1 - E\left\{\log_2\left(1+\exp\left(-L\right)\right)\right\} \approx 1 - \frac{1}{N}\sum_{n=1}^{N} \log_2\left(1+\exp\left(-s_n L_n\right)\right). \tag{4.6}$$

#### 4.4.1.1 Numerical results

Simulation parameters in this chapter are the same as in Chapter 3, except that we incorporate the RA6 channel model and the 16QAM modulation, which is simulated in combination with CR=1/2. The PP1 DVB-T2 [ETSI09] pilot pattern has been adopted. We consider ideal CSI as well as perfect synchronization throughout this chapter. From extensive simu-

lation results, we know that the best BER result is achieved with the next turbo schedule: 2 BP iterations and 20 LDPC iterations in each turbo iteration.

Fig. 4.7a and 4.7b depict the EXIT functions for both QPSK and 16QAM modulations. Fig. 4.7a shows the behavior of detector EXIT function in the ICI-free case and when a high Doppler frequency is considered. We notice that when the Doppler frequency is zero the curve is flat, and that the Doppler frequency provides a slight slope. The absence of Doppler frequency equals removing the inner encoder from the system, so that the only purpose of the BP detector is to carried out the MAP detection. In other words, the system equals a BICM communication system with iterative MAP demapping. As is it well-known, when Gray mapping is used (as it is the case), the detector EXIT function is flat, so that performing the turbo principle between the decoder and the demapper is useless [Schreckenbach03]. However, the detector EXIT function becomes steeper as the Doppler frequency increases.

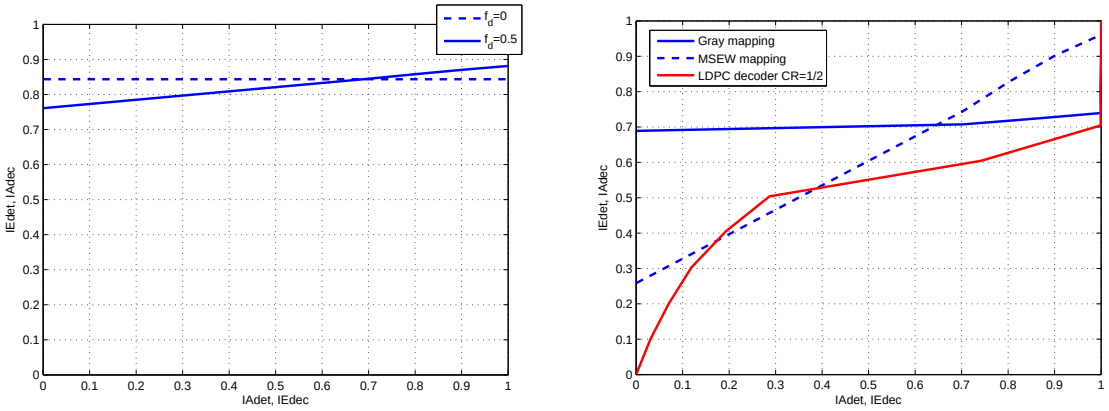


(a) (b)

Figure 4.7: Detector EXIT function for QPSK modulation (a) and detector and decoder EXIT functions for 16QAM modulation with different mapping schemes when $f_d = 0.22$ (b). TU6 channel has been considered in both cases.

Fig. 4.7b shows detector and decoder EXIT functions for the 16QAM modulation. Two mapping labels have been assessed: Gray and maximum squared euclidian weight (MSEW). It is shown that for $f_d = 0.22$, the detector function is almost flat when Gray mapping is considered. Again, the Gray mapping does not give any gain when the a priori mutual information is increased and iterations do not give any benefits. For the MSEW label, the function starts at a lower value and ends up almost in the (1,1) point. However, detector and decoder functions cross each other preventing from any gain in the iterative process. From Fig. 4.7, we conclude that when LDPC codes are adopted the best mapping is Gray and in such case the performance gain provided by the turbo scheme is higher for higher Doppler frequencies.

Fig. 4.8a shows the EXIT chart for QPSK modulation and $f_d = 0.5$. The system is

performing in the turbo-cliff region (SNR=8 dB). As it can be seen, the slight slope of the detector function allows to gain performance in three turbo iterations. Fig. 4.8b shows the corresponding BER performance versus LDPC iterations, where it is shown that the LDPC decoder provides free-error output at the fourth turbo iteration. Although the EXIT chart model is no exact, it provides a reliable reference in order to design the turbo schedule.

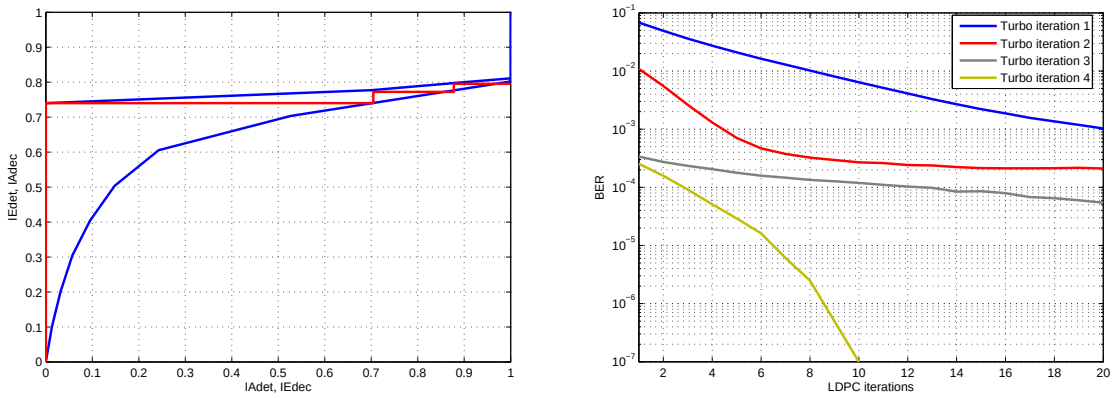


(a) (b)

Figure 4.8: EXIT chart (a) and BER vs LDPC iterations (b). QPSK modulation, TU6 channel, $f_d = 0.5$ and SNR $= 8$ dB has been considered.

As a conclusion, based on the EXIT chart analysis, it can be stated that the turbo scheme operating at high Doppler frequencies converges at few iterations, no more than five.

## 4.5 Graphical approach

The second turbo approach, referred to as *graphical approach*, was introduced in [Wiberg96] and is commonly described as passing soft decision messages on cyclic graphical models. Considering that LDPC codes are decoded using BP algorithms, a joint data detection and decoding process can be carried out by a higher-order FG as it is depicted in Fig. 4.9. Note that the EXIT charts cannot be used to analyze the convergence behavior of this approach as in the previous section, since detection and decoding are not independent anymore. That is, detector and decoder FGs are not reset, but they keep memory from previous turbo iterations.

We now compare the classical and graphical approaches with the non-turbo case as it was conceived in Chapter 3. The selected turbo schedule is the following for each case: 2 BP iterations and 20 LDPC iterations have been carried out in each turbo iteration in both turbo approaches, and 3 BP iterations and 50 LDPC iterations are performed in the non-turbo case.

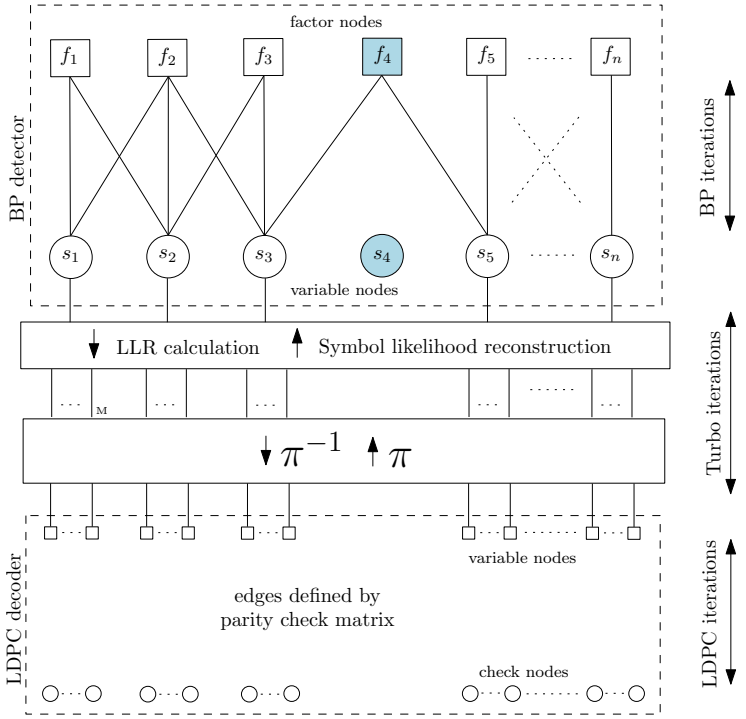


Figure 4.9: High order FG performing joint data detection and decoding following the graphical approach for turbo reeption.

Fig. 4.10 shows BER versus SNR performance for TU6 and RA6 channels. As it can be seen, the graphical approach outperforms the classical one in both cases, providing a performance gain of about 0.8 dB at BER= $10^{-4}$. On the other hand, there is a slight difference between the non-turbo case and the classical turbo approach for the turbo schedule adopted here.

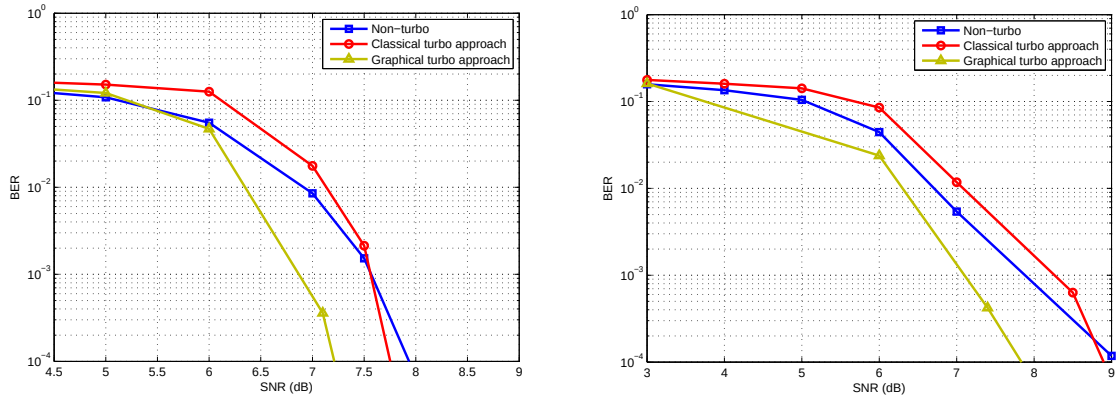


Figure 4.10: Performance comparison of non-turbo reception, classical turbo approach and the graphical turbo approach for TU6 (a) and RA6 (b) channels. $f_d = 0.5$ has been considered.

The performance gain introduced by the turbo iterations is shown in Fig. 4.11, where BER curves are depicted for the five turbo iterations when TU6 channel is considered. As it can be seen, the performance gain between the first and the fifth iteration is more than 1 dB at BER= $10^{-4}$. Besides, it is noteworthy that the graphical approach outperforms the non-turbo case at the second iteration, which means that better BER result is achieved with less amount of total iterations (BP iterations + LDPC iterations).

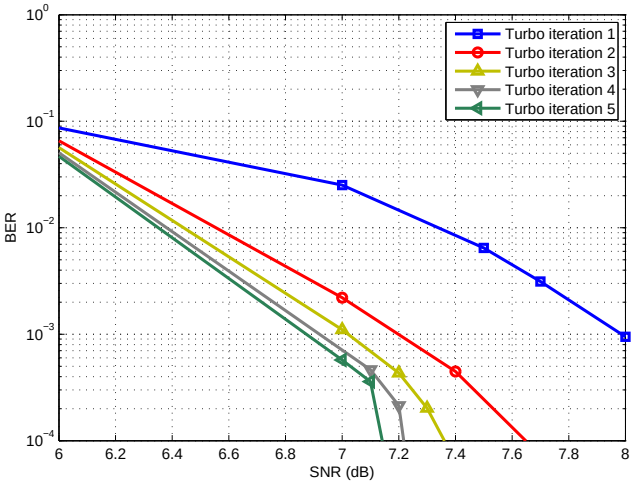


Figure 4.11: BER vs SNR performance of the graphical approach for the five turbo iterations.

Fig. 4.12 shows the graphical approach performance for QPSK. From Fig. 4.12a, we can see that the BER performance is better than the ICI-free case up to $f_d = 0.3$. This can be explained by the fact that the proposed BP exploits the available frequency-diversity, improving the diversity order with respect to the standard BICM-OFDM system. On the other hand, note that the BER curve shifts to the right side as the Doppler frequency increases. This is mostly caused by the residual ICI due to not considering more subcarriers contributing to ICI, which would enhance the BER performance at the cost of much higher complexity. The BER behavior is quite different over the RA6 channel (Fig. 4.12b). It can be seen that the performance for $f_d = 0.3$ is substantially better than for $f_d = 0.1$. The reason behind this apparently strange behavior is that wireless channels with short delay spread can largely degrade the BER performance of a BICM-OFDM systems due to the high correlation between contiguous subcarriers. In [May04] it is shown that the maximum diversity order that a BICM-OFDM system can achieve is $\min(d_{free}, L)$, where $d_{free}$ refers to the Hamming distance of the channel code and $L$ stands for the number of channel taps. Note from Fig. 4.12 that the BER performance of the ICI-free case is much worse over the RA6 channel. Therefore, the diversity order gain due to the inclusion of the BP detector is more evident in the RA6 channel case.

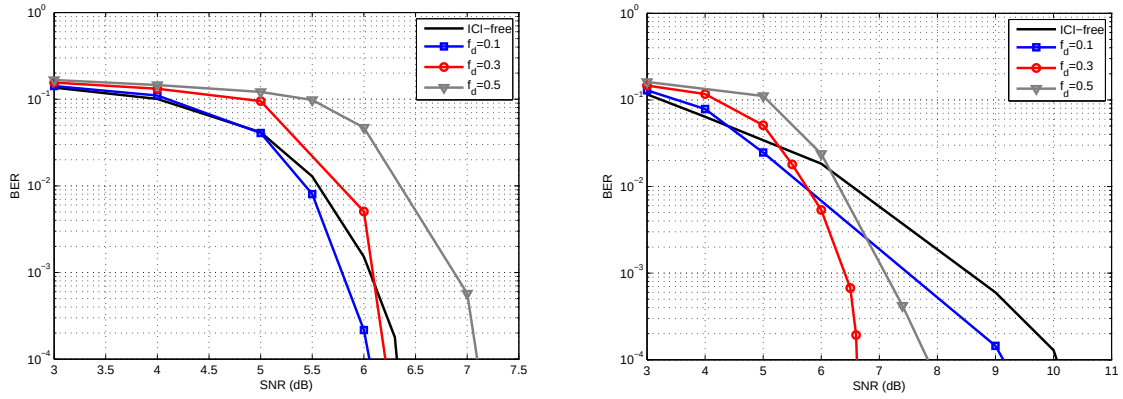


(a) (b)

Figure 4.12: Graphical turbo approach performance for different Doppler frequencies over TU6 channel (a) and RA6 channel (b) when QPSK modulation is considered.

Last, we provide BER versus SNR results for 16QAM in order to assess the proposed receiver design with a higher constellation order. In this case, the mentioned residual ICI, which can be modeled as a near-Gaussian noise, affects much more to the signal, preventing from achieving the free-ICI case at the Doppler frequencies considered for the QPSK modulation. Fig. 4.13 shows that the BP detector is able to remove the error-floor caused by the Doppler spread at $f_d = 0.22$ over both channel models considered here. BER results over TU6 channel indicate that there is a performance loss of about 1.2 dB at BER$= 10^{-4}$ with respect to the ICI-free case. Regarding the RA6 channel, it is shown that the BP detector achieves ICI-free performance at such Doppler frequency.

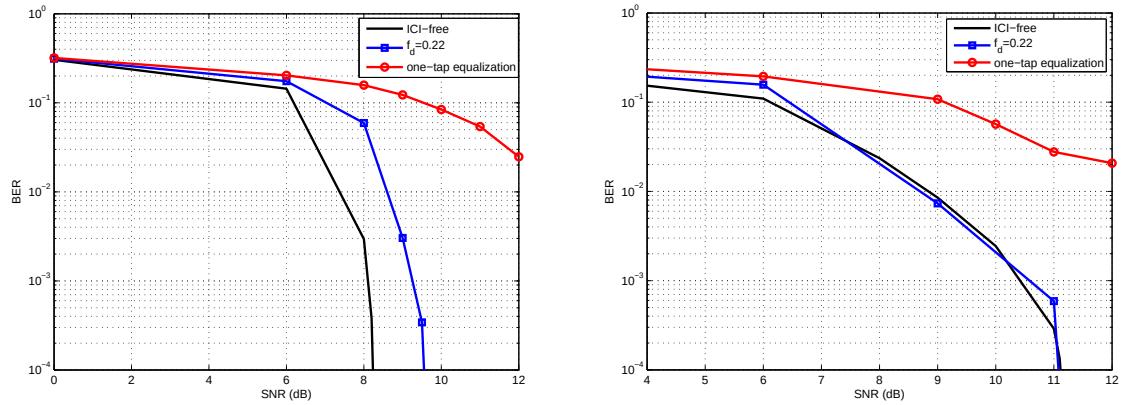


(a) (b)

Figure 4.13: Graphical turbo approach performance for different Doppler frequencies over TU6 channel (a) and RA6 channel (b) when 16QAM modulation is considered.

## 4.6 Chapter Summary

This chapter analyzes the performance of the proposed BP detector as part of a turbo receiver design along with the LDPC decoder, where extrinsic soft information is exchanged between the decoder and the detector. The fact that both detection and decoding are performed by BP algorithms allows high speed joint detection and decoding.

Section 4.2 describes the turbo receiver scheme, where the ICI channel works as an inner encoder concatenated with the LDPC as the outer constituent code. Section 4.3 describes how to deal with pilots in the FG and which are the benefits and drawbacks of the presence of pilots in the detection process are described. Section 4.4 presents the classical turbo approach, according to which soft decision information is exchanged between independent processes. The convergence behavior of the classical approach is analyzed using EXIT charts. The classical approach is compared to the generalized view of the graphical approach and the non-turbo case in Section 4.5. Extensive numerical results are provided considering QPSK and 16QAM modulation, as well as TU6 and RA6 channel models. It is shown that the proposed receiver scheme provides excellent performance at high mobility scenarios

# Chapter 5

# Impact of BP-based ICI cancellation in mobile DVB-T2

## 5.1 Introduction

Second generation DVB specifications have provided increased robustness and spectral efficiency yielding the fully incorporation of multimedia broadcasting and high definition (HD) television to the terrestrial mean. Predictably, terrestrial (DVB-T2) and handheld (DVB-NGH) versions will be the two leading standards for terrestrial broadcasting all over the world. Mobility support is one of the key features of the advent of the second generation DVB systems, which try to deal with the challenge of enabling mobile broadband services at high vehicular speed. Although initially DVB-T2 was designed for fixed receivers, it is supposed to allow mobile reception with the same spectrum characteristics as DVB-T, since the combination of LDPC codes, as part of the FEC strategy, and time interleaving makes this standard very robust against signal distortion due to the time variation of the channel.

The DVB-T2 specification allows for the possibility of maximizing the performance in SFN applications. Compared with DVB-T standard, longer OFDM blocks have been added (e.g. 32K) to improve the performance of SFNs and increase the symbol period. This increase in the symbol period, in turn, allows for a reduction in the proportional size of the GI while still handling multipath reflections. In fact, new standards appearing in recent years propose very long OFDM blocks with the aim of increasing spectral efficiency or enhance the robustness in SFNs. However, long blocks are more vulnerable to time variations of the channel, which in high mobility scenarios destroy orthogonality among subcarriers, resulting in ICI. The use of long OFDM blocks represents a challenging technical problem when it is combined with mobile signal reception.

In this chapter, the DVB-T2 specification is taken as a reference for DVB technology, and the proposed BP detector is assessed over its physical layer. Along with ideal CSI, channel estimation is also considered in order to analyze its impact on the BP detection process in a realistic receiver.

## 5.2 DVB-T2 to pave the way of DVB-NGH

Since the introduction of DVB-H, significant changes have taken place in the delivery and consumption of multimedia content. On one hand, the multimedia content market is going through a big change towards a range of rich multimedia traffic (various video and audio contents, images and text messages). On the other hand, there is another significant recent change: the convergence of the fixed and mobile paradigms. With the introduction of DVB-T2, there is a need to look at ways of leveraging its advantages in developing NGH. Radio spectrum is a scarce resource and its use by different networks without interfering with each other is essential. Therefore, spectrum sharing of future broadcasting and cellular networks and effective utilization of this resource in delivering services via different networks is essential for next generation systems.

Considering the above, the aim of this thesis dissertation is to take the current terrestrial TV standards a step forward providing improvements in two directions: increase the spectral efficiency and enhance the robustness. Fig. 5.1 depicts the trade-off between the spectral efficiency and robustness in mobile terrestrial DTV.

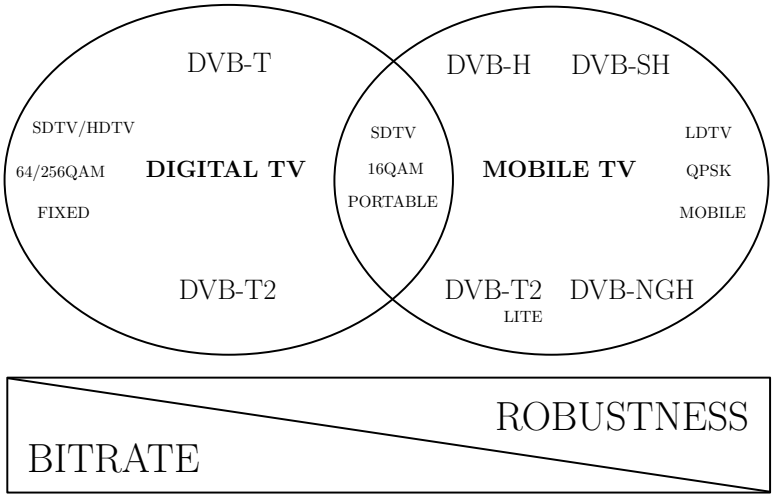


Figure 5.1: Bitrate vs robustness trade-off.

At this point, it is of interest to analyze the commercial and technical requirements defined for the development of the upcoming DVB-NGH specification. We enumerate the most significant ones:

- Wide coverage: a user access services across an entire territory. The implication is that networks aimed at wide area coverage must be efficient and affordable to build.

- Robust reception: it must be possible to access services for either indoor or outdoor, and stationary, walking or traveling at speed.

- Responsive: it must be quick to start up and to access audio-visual and interactive services, fast channel change times.
- Extremely fast moving usage scenarios: mobile vehicular reception is considered at speeds from 15 to 350 km/h.
- Low system end-to-end delay: important for live events; e.g. use of the NGH system during sports events.
- Extended battery life: it must be able to offer extended viewing sessions.
- Quality improvement: it is likely that in the medium term the terminals will have larger screens (e.g., smartphones, tablets, etc.).
- Capacity improvement: recognizing that capacity can be traded for robustness, the overall capacity improvement, shall be at least 50% compared to DVB-H for a given robustness.

### 5.2.1 The benefits of employing long OFDM blocks in terrestrial broadcasting systems

Considering the technical and commercial requirements imposed to future mobile terrestrial DTV specifications, the use of long OFDM blocks presents a bunch of interesting advantages. In fact, there is a growing trend toward employing long OFDM blocks in terrestrial broadcasting systems. On one hand, it allows to provide wider coverage using SFNs. A document from Mobile Multi-Meda (M3) [Gallard11], a French collaborative project, shows why DVB-NGH is better than the LTE/3GPP E-MBMS ("Evolved Multimedia Broadcast Multicast Services") in terms of spectrum efficiency and reuse of existing broadcast antennas. DVB-NGH can include much larger GIs, allowing a maximum cell radius of up to 107 km, suitable for a high power, high antenna transmitter site and multiple low/medium power transmitters in a SFN, leading to efficient and affordable network design.

Secondly, the use of long OFDM blocks leads to maximizing the net throughput, fulfilling the technical requirement by which means overheads such as packet headers should be minimized, without losing functionality. Last, but not least, taking into account that 32K-length symbols are already being used for fix terrestrial DTV (e.g., UK), the same symbol length could be used for mobile reception with different PLPs that could enable service specific robustness without occupying other frequency bands.

Of course, a trade-off among efficiency, SFN performance and mobile robustness must be obtained. Using long OFDM blocks leads to increasing the robustness in SFNs and the net throughput, but has at least two counterparts at the same time: the effect of the Doppler frequency is much higher, which restricts the use of high constellation orders and

it can provoke high latencies if the receiver design is not properly constrained. Therefore, advanced signal processing techniques have to be considered in order to counteract the severe effect of the Doppler frequency keeping latency and complexity at reasonable levels.

System performance of first generation DVB systems in mobile scenarios has been widely addressed by previous literature [Poggioni09, Herlekar05, Lu08, Wilhelmsson07]. At the same time, many different schemes have been proposed for signal reception with possible application to DVB systems [Tomasin05, Hwang09]. However, for the best of our knowledge, little has been done regarding the second generation DVB standards [Ochandiano10]. Recently, a time-domain per sub-block equalizer has been presented [Baracca11] which tackles the same problem formulated in this work. The main drawbacks of this proposal are its limited performance and the impossibility of employing pilot tones for channel estimation.

## 5.3 DVB-T2 performance in mobile scenarios

We highlight two features of the DVB-T2 physical layer due to their importance when combating the signal distortion caused by ICI: LDPC codes as part of the FEC scheme, and the time interleaver. It is well-known that when the codeword is sufficiently large, ICI can be modeled as an additive Gaussian random noise [Wang06], which can be effectively counteracted by the LDPC code at low and moderate Doppler frequencies. On the other hand, the primary objective of the time interleaver is to provide time-domain diversity when used along with powerful error correction coding. As it is usual, the maximum time interleaver span is restricted by the standard in order to limit the receiver latency.

Fig. 5.2 shows the simplified block diagram of the conventional DVB-T2 receiver. In this research work, assuming the first option for time interleaving defined in the DVB-T2 standard, we consider that each interleaving frame contains one TI-block and is mapped directly to one T2-frame [ETSI09].

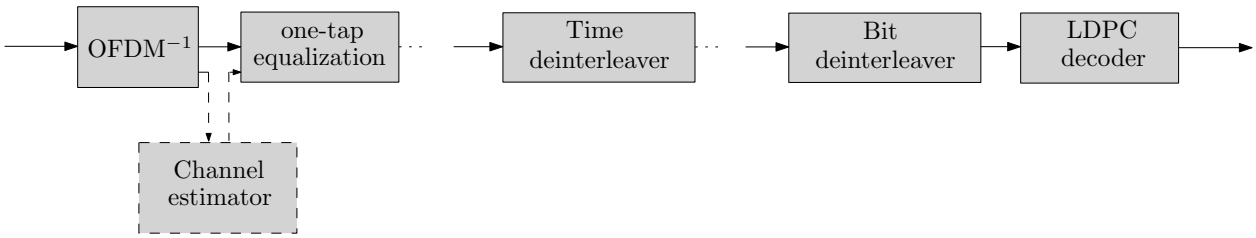


Figure 5.2: Simplified block diagram of the conventional DVB-T2 receiver (CONV).

The DVB-T2 implementation guidelines document [DVB09] proposes several channel models, from which two have been chosen to analyze the performance of the proposed detection techniques in mobile conditions: COST 207 TU6 and RA6 channels [COST20789]. We

consider maximum normalized Doppler frequency $f_d = 0.5$. Table 5.1 describes the simulation parameters adopted throughout this work. Under such conditions, $f_d = 0.5$ corresponds to about 200 km/h of vehicular speed. The BER is computed after at the output of the LDPC decoder.

Table 5.1: Simulation parameters in Chapter 5.

| **Parameter** | **Value** |
|---|---|
| Carrier frequency | 760 MHz |
| Bandwidth | 8 MHz |
| Number of subcarriers ($N$) | 32784 |
| Subcarrier spacing | 280 Hz |
| Length of one OFDM block ($T_u$) | $3584\mu s$ |
| Length of the guard interval ($T_u/4$) | $896\mu s$ |
| Modulation | QPSK, 16QAM |
| FEC length (LDPC) | 64800 bits |
| Code rate | 2/3 (QPSK), 1/2 (16QAM) |
| Channel model | RA6, TU6 |

As it is shown in Fig. 5.3, the time interleaver, in conjunction with LDPC codes, makes DVB-T2 very robust in a wide range of mobile communication scenarios. Mobile reception of DVB-T2 is assessed according to the number of FEC blocks considered in the TI-block. Note that for the time interleaving configuration and transmission parameters adopted in this paper, the maximum number of FEC blocks in the TI-block is limited to 17 by the standard [ETSI09].

According to Fig. 5.3a, error-free reception is possible for the RA6 channel up to $f_d = 0.3$ when QPSK modulation is considered without the inclusion of any specific signal processing technique for ICI suppression. However, beyond this Doppler frequency, the performance crashes giving rise to a high error floor. The BER curves for TU6 channel follow similar trends. In this case, the maximum Doppler frequency for error-free communication is even lower.

Fig. 5.3b shows the same performance results for 16QAM modulation. As it is known, the distortion caused by ICI becomes severer as the modulation order increases. Therefore, the maximum Doppler frequency that allows error-free communication is lower in 16QAM than in QPSK. It can be seen that error-free communication is possible over RA6 channel for $f_d = 0.23$ when 19 FEC blocks are used in the TI-block. As in the QPSK case, the maximum Doppler frequency for error-free communication is lower for TU6 channel.

From this analysis, it is concluded that the physical layer of DVB-T2 allows good mobile signal reception in a wide variety of mobile environments. However, for the channels of

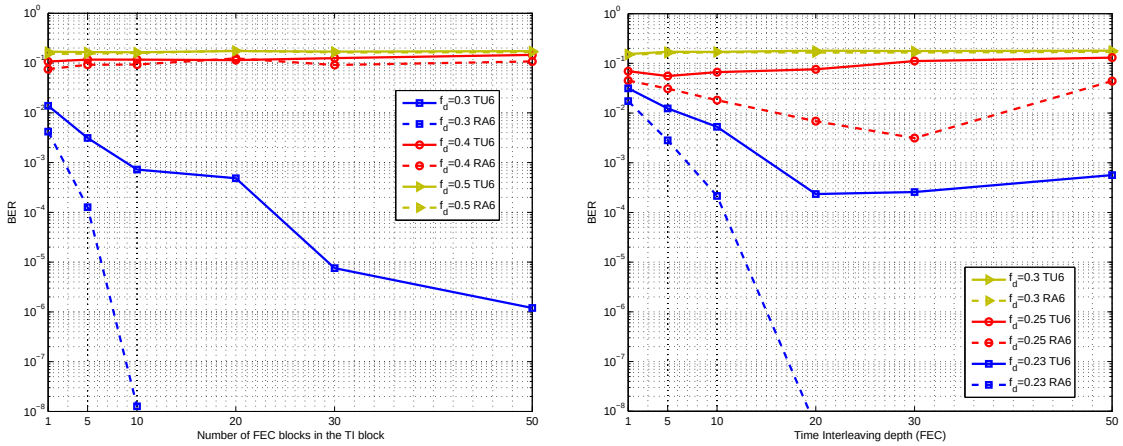


(a) (b)

Figure 5.3: DVB-T2 performance versus different number of FEC blocks in the TI-block (time interleaving depth) at high SNR regime (SNR=30dB) for QPSK (a) and 16QAM (b).

interest in this research work, it is not able to provide free-error communication by itself. Therefore, advanced signal detection strategies need to be included for that purpose at the expense of increasing the complexity of the receiver.

## 5.4 Belief propagation detection over DVB-T2

Two things have to be taken into account to design detection strategies for DVB standards: first, the use of long OFDM blocks forces to adopt parallel structures in order to fulfill stringent latency requirements, and second, since LDPC codes are decoded by means of SISO decoders, soft values are required at the output of the detector. BP algorithm fits both requirements and therefore suits very well to second generation terrestrial DVB standards.

Two reception schemes are here proposed, both based on the traditional DVB-T2 physical layer. The first proposed scheme (PS1) substitutes the MAP one-tap equalizer in the conventional DVB-T2 receiver (CONV) by the BP detector, and maintains the time interleaver. In the second proposed scheme (PS2), the time interleaver is subtracted out and the turbo approach is applied exchanging soft information between the decoder, the detector and the channel estimator. The aim of both proposed schemes is to achieve a reasonable trade-off among performance, complexity and latency. The last gains in importance when real-time multimedia traffic requires stringent end-to-end delays. The combination of the turbo approach and the inclusion of the time interleaver would cause excessive time-delays in signal reception, and it is therefore discarded.

The mechanism behind the proposed schemes combating ICI is the exploitation of the frequency and time-diversity provided by the time-varying channel. PS1 makes use of

both frequency-diversity (frequency correlation in the received signal due to ICI) and time-diversity (due to the use of time interleaver along with error correction coding in a time-varying channel) to provide free-error reception (see Fig. 5.4). In PS2, the lack of the time interleaver is replaced by the performance gain offered by the turbo approach (see Fig. 5.7). Note that in the PS2 scheme, the whole reception process, except channel estimation, can be understood in terms of a high-order FG including joint signal detection and decoding, where soft decision messages are exchanged on a cyclic graphical model. Optional signal processing stages included in the standard (e.g., constellation rotation) are not considered in this research work.

### 5.4.1 First proposed reception scheme (PS1)

A simplified block diagram of PS1 reception scheme is shown in Fig. 5.4, where the one-tap MAP equalizer has been replaced by the BP detector. Based on the simulation results analyzed in Chapter 3, three iterations have been carried out in the BP detector and 50 iterations in the LDPC decoder.

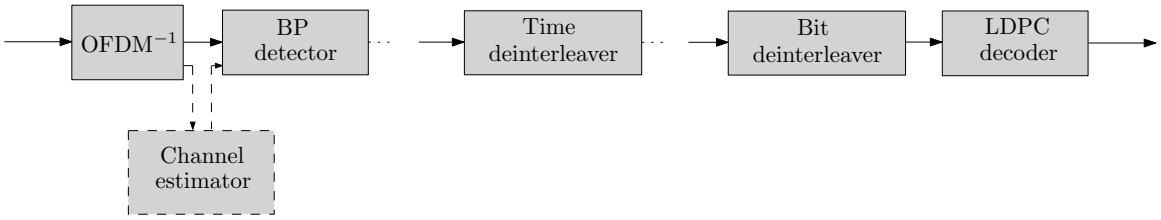


Figure 5.4: Simplified block diagram of the first proposed scheme (PS1).

#### 5.4.1.1 Performance with ideal CSI

Fig. 5.5 shows the BER performance of PS1 for TU6 channel. As it was mentioned, this scheme profits from both frequency-diversity (BP detector) and time-diversity (time interleaver). In Fig. 5.5a BER results are depicted for the three iterations carried out in the detector considering 10 FEC blocks per TI-block. As it can be seen, the second iteration is able to remove the error floor caused by the Doppler spread, and the third iteration gives a tight performance gain of about 0.3 dB at BER= $10^{-4}$, approaching the ICI-free curve up to 1 dB. This corroborates the efficiency of the proposed BP detector in such channel conditions.

In turn, time interleaving performance is assessed in Fig. 5.5b by keeping the number of BP iterations fixed and varying time interleaving depths (1, 5 and 10 FEC blocks per TI-block). As it is shown, the maximum performance gain that time interleaving can offer is

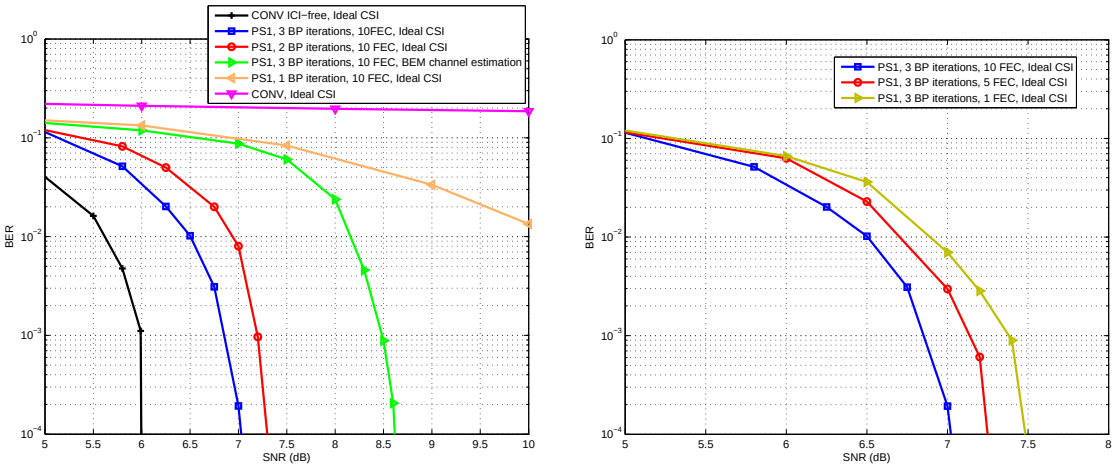


(a) (b)

Figure 5.5: PS1 BER performance comparison for different number of BP iterations, with $f_d = 0.5$ over TU6 channel, considering ideal and partial CSI. 10 FEC blocks per TI-block are assumed (a). PS1 BER performance for different number of FEC blocks per TI-block, with $f_d = 0.5$ over TU6 channel, considering 3 BP iterations (b).

around 0.5 dB. Consequently, for the TU6 channel model, the frequency-diversity exploitation offered by the BP detector is much more efficient than the effects of the time-diversity provided by the time interleaver.

Fig. 5.6a and 5.6b show the analogue analysis for RA6 channel model. As it is well-known, the BER behavior of a BICM-OFDM scheme is substantially worse in less selective channels. Therefore, it is interesting to extend the simulation results of Fig. 5.5a and5.5b to the RA6 channel model. The high correlation in the frequency domain due to the short delay spread of the channel can largely degrade the BER performance, that is, the lower delay spread leads to frequency-diversity loss. Therefore, as it is shown in Fig. 5.6a, PS1 scheme produces a remarkable impact on the BER, giving a performance gain of about 4 dB with respect to the ICI-free case at BER$= 10^{-4}$.

On the other hand, comparing Fig. 5.5b and 5.6b, we can observe that the contribution of the time interleaver is higher in RA6 than in TU6. The reason behind this behavior is that spreading out symbols by means of the time interleaver emulates an ergodic channel [Poggioni09], offering a high diversity order gain with respect to the RA6 channel. Besides, it is worth noting that there is no performance gain beyond 5 FEC blocks per TI-block.

#### 5.4.1.2 Performance with channel estimation

Non-ideal CSI is considered in order to analyze how the detector performs in a realistic receiver. Channel estimation based on basic expansion model (BEM) is considered [Tang07], which consists of one of the most promising channel estimation techniques to be applied

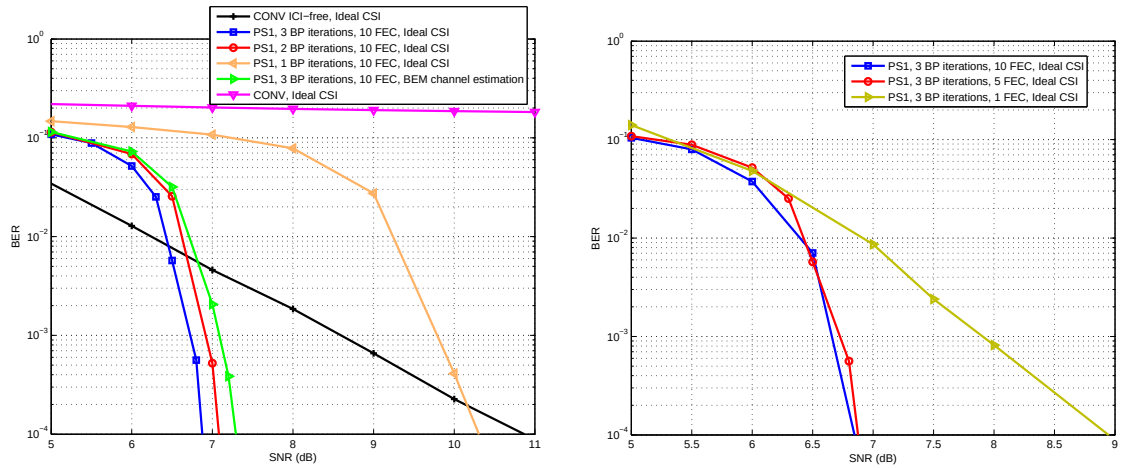


(a) (b)

Figure 5.6: PS1 BER performance comparison for different numbers of BP iterations, with $f_d = 0.5$ over RA6 channel, considering ideal and partial CSI. 10 FEC blocks per TI-block are assumed (a). PS1 BER performance for different number of FEC blocks per TI-block, with $f_d = 0.5$ over RA6 channel, considering 3 BP iterations (b).

to OFDM communication systems operating in rapidly time-varying channels. Channel estimation is out of the scope of this thesis, so that the aim of including channel estimation is not analyzing a given channel estimation technique itself, but assessing how the BP detector behaves in such conditions in comparison with ideal CSI.

When the channel is assumed to be time-varying, suitable techniques are needed to estimate the complete channel parameters, including the ICI terms. The channel can be approximated as

$$\overline{\mathbf{h}}_l = \mathbf{B} \cdot \mathbf{h}_{u,l}, \tag{5.1}$$

where $\overline{\mathbf{h}}_l = [\overline{h}_{0,mod(0+l,N)}, \cdots, \overline{h}_{N-1,mod(N-1,N)}]^T$, is an $N \times 1$ vector that contains the channel coefficients for the $l$-th channel tap from time indexes 0 to $N$-1. This way, instead of estimating all the channel coefficients $N \times L$, we only need to estimate the BEM coefficients $\mathbf{h}_{u,l} = [h_{0,l}, \cdots, h_{Q,l}]^T$, resulting in a significant reduction of the number of parameters to be estimated, which are equal to $(Q+1) \times L$ for each OFDM symbol and $Q$ is the amount of diagonals in the frequency response channel considered to describe the ICI excluding the main diagonal. $\mathbf{B} = [\mathbf{b}_0, \cdots, \mathbf{b}_Q]$ is an $N \times (Q+1)$ matrix that contains $Q+1$ basis functions $\mathbf{b}_q$ as columns, where $\mathbf{b}_q = [b_{q,0}, \cdots, b_{q,N-1}]^T$ whose coefficients are obtained following [Tang07]. Stacking all the channel taps, $\mathbf{h}_u = [h_{0,0}, \cdots, h_{0,L-1}, \cdots, h_{Q,0}, \cdots, h_{Q,L-1}]$, yields

$$\overline{\mathbf{H}} = (\mathbf{B} \otimes \mathbf{I}_L)\mathbf{h}_u. \tag{5.2}$$

In order to adapt the previous channel estimation scheme to DVB-T2, pilots have to be

clustered in $C$ groups of $L_p$ pilots each. Inside each cluster $\mathbf{s}_c^{(p)}, c = 0, 1, \cdots, C-1$, the frequency-domain Kronecker delta (FDKD) scheme has been adopted, where a nonzero pilot is placed in the middle, with zero guard bands on both sides [Kannu05]. Stacking all the pilot clusters together into a pilot vector yields $\mathbf{s}^{(p)} = \left[\mathbf{s}_0^{(p)T}, \cdots, \mathbf{s}_{C-1}^{(p)T}\right]^T$. A performance improvement can be seen with larger cluster lengths for high normalized Doppler frequencies at the expense of higher complexity. Note from Fig. 5.7 that, in PS2 scheme, the channel estimation can be improved making use of the soft data from the channel decoder as it is proposed in [Fang10], where not only the pilot carriers are used to estimate the channel, but also the soft data estimates from detected data symbols. Simulation parameters related with channel estimation adopted in this work are further explained in [Ochandiano12a].

Taking a look at the BER curves with channel estimation in Fig. 5.5 and 5.6, we notice that the performance loss due to non-ideal CSI depends on the channel model: following the track of a highly-selective channel is harder than of a less-selective one. Therefore, the performance loss in RA6 with respect to the ideal CSI is less than 0.3 dB at BER= $10^{-4}$, whereas TU6 leads to a performance loss of about 1.5 dB at BER=$10^{-4}$. We conclude that the estimation error does not cause destructive effects to the BP algorithm and it behaves as an additional noise source leading to the displacement of the BER curve to the right side.

### 5.4.2 Second proposed reception scheme (PS2)

A simplified block diagram of PS2 reception scheme is shown in Fig. 5.7, where the time interleaver has been subtracted out and the turbo approach has been included, exchanging soft information between the LDPC decoder, the detector and the channel estimator. Based on the simulation results in Chapter 4, 2 iterations have been carried out within the BP detector and 20 iterations within the LDPC decoder for each of the 5 turbo iterations.

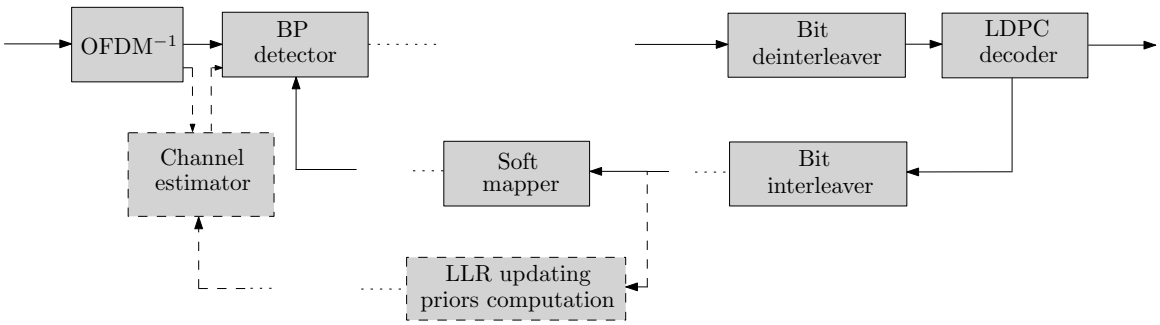


Figure 5.7: Simplified block diagram of the second proposed scheme (PS2).

#### 5.4.2.1 Performance with ideal CSI

Fig. 5.8a and 5.8b show BER results for PS2 reception scheme over TU6 and RA6, respectively. Note that comparing Fig. 5.8a and 5.5a, PS1 outperforms PS2 up to 0.5 dB over TU6 channel. In the same way, an analogue behavior can be seen over RA6, where PS1 presents a gain of 1.2 dB with respect to PS2. Therefore, PS1 turns out to be the best solution in terms of performance for both channel models when ideal CSI is assumed. It is worth noting that, due to the higher contribution of the time interleaver, the conjunction of BP detector and time interleaver (PS1) provides higher gains with respect to PS2 in less frequency-selective channels.

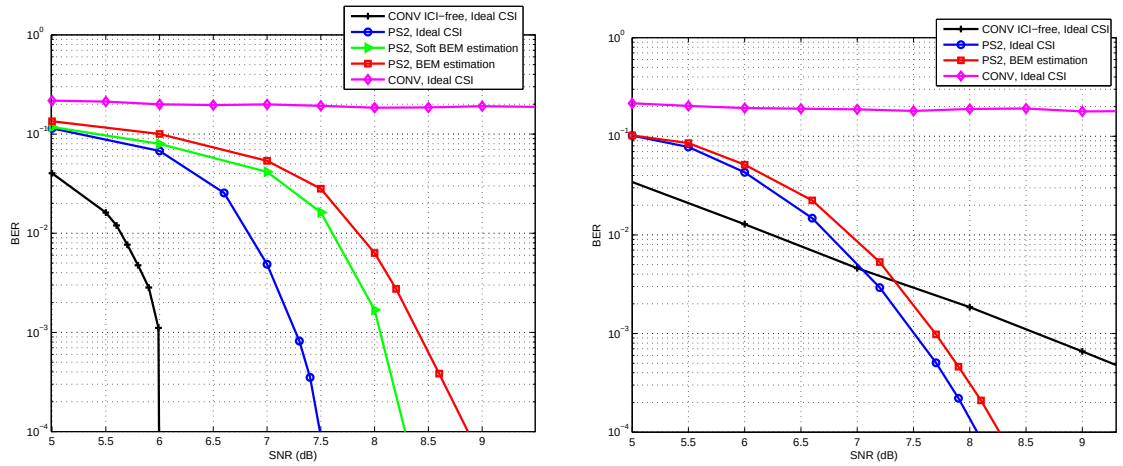


Figure 5.8: PS2 BER performance for 3 BP iterations. $f_d = 0.5$ over TU6 channel (a) and RA6 channel (b).

#### 5.4.2.2 Performance with channel estimation

Fig. 5.8a depicts the evolution of the BER for various SNR values over TU6, showing the performance of PS2 scheme with two different approaches for channel estimation. The first one combines solely the BEM channel estimator and the BP detector, while the second reconstructs soft symbols using extrinsic information from the decoder to reestimate the channel in the turbo process. The results in Fig. 5.8a clearly show that a huge profit is obtained when compared with no ICI compensation scheme (CONV scheme). The degradation of PS2 considering BEM estimation is approximately 1.3 dB compared to the ideal CSI case. Moreover, when soft data estimates are taken into account, the system performance can be further improved up to 0.5 dB, moving closer to the ideal channel case.

Fig. 5.8b shows results for RA6 channel. In this case, the soft data estimates are not taken into consideration since the BEM channel estimation itself is good enough, and adding

soft estimates would only increase complexity. PS2 including the BEM channel estimation algorithm suffers a degradation of 0.2 dB compared to the ideal channel knowledge case.

To sum up, the overall system performance of both schemes is compared: regarding TU6 channel (Fig. 5.5a and 5.8a), due to the performance gain introduced by the inclusion of soft data estimates in BEM channel estimation, PS2 shows a performance improvement of 0.3 dB over PS1. Therefore, although in the case of ideal CSI PS1 outperforms PS2, when channel estimation is considered, PS2 turns out to be the most effective solution. In contrast, since channel estimation is much more accurate in RA6 channel, PS1 outperforms PS2 (Fig. 5.6a and 5.8b), and hence we conclude that PS1 is better suited to less selective channels.

## 5.5 Chapter Summary

In this chapter, we propose the BP detector to deal with the problem of mobile terrestrial DTV signal reception when long OFDM blocks are used. First, a thorough analysis of the DVB-T2 chain under high-mobility has been presented. The time interleaver performance has been assessed showing that it is not possible to achieve error-free communication for the channels of interest in this research work. Therefore, we conclude that specific signal processing techniques have to be applied to the reception chain in order to suppress ICI when long OFDM blocks are employed, such as 32K mode.

Two reception schemes have been proposed combining the time interleaver, the BP detector and the turbo approach by which extrinsic soft information is exchanged between the LDPC decoder and the BP detector. The first proposed scheme (PS1) substitutes the conventional one-tap MAP equalizer by the BP detector and maintains the time interleaver. In the second proposed scheme (PS2), the time interleaver has been replaced by the turbo approach. The principle behind these schemes is the exploitation of the time and the frequency diversity available in time-varying channels. The proposed reception schemes have been assessed over DVB-T2 physical layer in realistic broadcasting channel conditions, for which well-known TU6 and RA6 channel models have been used. A real channel estimation error has also been considered with the aim of analyzing its impact on the BP algorithm.

Extensive numerical results show the effectiveness of the BP algorithm over DVB-T2 physical layer, where the error floor due to Doppler spread is removed and error-free communication can be provided. We also conclude that PS1 is better suited to less-selective channels, whereas PS2 behaves better in highly-selective ones.

In conclusion, we have proposed a very robust receiver of DVB-T2 being able to provide error-free reception at high receiver speeds (up to 200 km/h) when the effect of the Doppler frequency is severest (32K OFDM mode). Therefore, we can take advantage of the benefits of using long OFDM blocks at high-mobility conditions. On the other hand, for the signal bandwidth considered in this work, the BP detector is not able to provide error-free commu-

nication at such receiver speeds (200 km/h) when higher constellation orders are used. We might consider a higher signal bandwidth in order to increase the capacity. Design specifications of DVB-NGH propose up to 20 MHz of signal bandwidth, for which the effect of a given Doppler frequency is fairly reduced. We consider that employing the signal processing techniques analyzed in this thesis dissertation over the physical layer of DVB-T2 fulfills the technical and commercial requirements imposed to the next generation mobile terrestrial DTV.

# Chapter 6

# Conclusions and Further Research

## 6.1 Summary

In this PhD dissertation, we have proposed a novel detector design for BICM-OFDM systems over ICI channels. The proposed detection scheme, which is based on FG theory, makes use of the frequency-domain diversity available in the received signal affected by ICI, achieving high diversity order, and thus, turning into a very efficient detection algorithm when the distortion caused by the Doppler spread is very high.

There is a growing trend toward using long OFDM blocks with the aim of increasing spectral efficiency or enhancing the robustness in SFN. However, it represents a technical challenge when it is applied to mobile signal reception, since the effect of time-varying channels becomes critical when large OFDM symbols are used, and it is necessary to develop appropriate signal processing techniques to combat the mobility-induced ICI problem. In fact, from signal detection and channel estimation perspective, the most challenging scenario includes high-mobility and long OFDM blocks. In addition to its performance efficiency, the proposed BP detector suits very well to long OFDM blocks, allowing fully parallel implementation, necessary when high speed and low latency reception is required.

As a starting point, the physical layer of DVB-T2 transmission and reception chains has been implemented in Matlab and the system performance has been assessed for different realistic broadcasting channel conditions. The iterative demapping scheme proposed in the implementation guidelines document [DVB09] has also been considered, showing by simulations that it does not provide substantial performance improvement for the channels of interest in this work.

Chapter 3 focuses on the design of the novel BP detector. We have considered the two existing approaches for MAP detection: the Forney approach and the Ungerboeck approach. It is concluded that, although the Ungerboeck approach is less complex and presents better design characteristics at the first sight, it turns out to be inefficient for the channel conditions considered in this dissertation. Both MAP detection approaches have been compared to the optimal FB algorithm with the aim of computing the performance loss due to the presence

of short cycles in the FG. Note that the FB algorithm is not a good candidate because it has an inherent serial structure which it is not suited to the employment of long OFDM blocks. The proposed BP algorithm has also been compared to best MAP detector design proposed in the literature. Simulation results show that the BP detector outperforms this proposal over the channels of interest. Finally, we deal with the complexity issue and point a procedure to reduce the computational load of the proposed algorithm at the expense of an affordable performance loss.

In Chapter 4, we consider the proposed BP detector as part of a turbo scheme along with the LDPC decoder. Since LDPC codes are decoded by means of FG-based algorithms, joint data detection and decoding can be carried out into the same FG framework. In fact, a higher order FG can be drawn including both signal detection and decoding processes. Simulation results show that this turbo scheme enhances the BER performance of the system with a lower amount of total iterations (considering the sum of BP and LDPC iterations) comparing to the non-turbo case (Chapter 3). On the other hand, we also propose how to deal with pilot tones in the FG and show that the presence of pilot carriers can increase the performance of the BP algorithm.

Unlike in Chapters 3 and 4, where a general BICM-OFDM communication scheme has been considered in order to assess the proposed algorithm, we have implemented the BP detector over the DVB-T2 chain in Chapter 5. First of all, we show by numerical results that the physical layer of DVB-T2 is not able to provide error-free communication for the channels of interest in this work when 32K-length OFDM blocks are used. Therefore, it is concluded that advanced signal processing techniques are required. We propose two reception schemes which exploit the frequency and time-domain diversity available in the received signal affected by ICI. Along with the ideal CSI, we consider the inclusion of channel estimation as well, with the aim of analyzing the impact of a realistic scenario in the detection process. Simulation results confirm that the implementation of the proposed BP detector allows error-free detection of DVB-T2 signal at high receiver speeds, up to 200 km/h, when 32K-length OFDM blocks are employed.

## 6.2 Thesis Contributions

The main contributions of this research work are the following:

- Analysis of the DVB-T2 physical layer performance over broadcasting channel models. Iterative MAP detection proposed in [DVB09] has been assessed. This work was published in [Mendicute10].

- Analysis of signal detection and ICI cancellation algorithms proposed in the literature. Namely, the performance of the MAP detector in [Peng06] has been assessed over the

receiver chain of DVB-T2. This work was published in [Ochandiano10].

- Design of a novel iterative detection algorithm based on FGs suitable for reception of terrestrial DTV signal in mobile environments. The detector performance has been assessed over a general BICM-OFDM communication scheme. This work was published in [Ochandiano11a].

- Development of a turbo receiver scheme enabling joint data detection and decoding into the same FG framework and its analysis using EXIT charts. This work was published in [Ochandiano11b].

- Performance study of FG-based detection by means of the two existing MAP strategies proposed in this thesis: Forney and Ungerboeck. It has been shown that the Forney MAP detection outperforms the Ungerboeck approach in terms of performance. This work has been submitted for its possible publication in [Ochandiano12b].

- Simulation-based analysis of the implementation of the proposed BP detector over the DVB-T2 receiver chain. We have compared two receiver schemes combining the turbo scheme and the time interleaver. This work has been submitted for its possible publication in [Ochandiano12a].

## 6.3 Suggestions for Further Research

Many issues described in this PhD dissertation can be addressed as future extension of the current work. These are some of the suggestions for further research:

- As we have seen, the capacity of combating ICI increases with the Doppler frequency when QPSK modulation is considered with the proposed FG-based detector. That is what makes it suitable for long OFDM blocks. Nevertheless, as it is well-known, the signal distortion caused by a given Doppler frequency is much severer when higher constellation are adopted. In our case, $f_d = 0.5$ is destructive for 16QAM constellation. Therefore, an extension of this work can be carried out focusing on trying to make the BP algorithm efficient for 16QAM at the considered high Doppler frequencies.

- Channel estimation has been dropped out of the FG framework for complexity reasons. An improvement of the receiver design should consider the incorporation of the channel estimation into this framework, performing the main stages of the receiver chain by means of a higher-order FG.

- Complexity considerations: the performance loss due to the implementation of different complexity reduction techniques could be assessed.

- Hardware implementation of the proposed receiver design. Broadcasting of Live events requires low latency, which is a technical challenge at the receiver side when long OFDM blocks are used. Therefore, it is of interest to develop high speed and low-complexity hardware implementation techniques.

# Appendix A
# Publications

The following papers have been published or are under preparation for publication in refereed journal and conference proceedings.

**Book Chapter:**

- M. Mendicute, I. Sobrón, L. Martínez and P. Ochandiano, "Digital Video" chap. DVB-T2: New signal processing algorithms for a challenging digital video broadcasting standard, pp. 185-206, InTech, Feb. 2010.

**Journal papers:**

- P. Ochandiano, H. Wymeersch, M. Mendicute, L. Martínez and I. Sobrón "Factor graph based detection approach for high-mobility OFDM systems with large FFT sizes", submitted to *EURASIP Wireless Communications and Networking* (under review).
- P. Ochandiano, L. Martínez, I. Sobrón and M. Mendicute, "Iterative detection and channel estimation for mobile terrestrial TV with long OFDM blocks", submitted to *IEEE Transactions on Broadcasting* (under review).

**International conference papers:**

- I. Sobrón, M. Mendicute, L. Martínez and P. Ochandiano, "Impact of self interference in DVB-T2 broadcasting single frequency networks", in *Proc. 9th International Workshop on Electronics, Control, Modeling, Measurement and Signals (ECMS '09)*, pp. 97-103, Mondragon, Spain, Jul. 2009.
- P. Ochandiano, I. Sobrón, L. Martínez, M. Mendicute and J. Altuna, "Analysis of ICI compensation for DVB-T2", in *Proc. 7th International Symposium on Wireless*

*Communication Systems (ISWCS '10)*, pp. 427-430, York, United Kingdom, Sep. 2010.

- I. Sobrón, M. Barrenechea, P. Ochandiano, L. Martínez, M. Mendicute and J. Altuna, "Low-complexity detection of golden codes in LDPC-coded OFDM systems", submitted to *IEEE International Conference on Acoustics, Speech and Signal Processing (ICASSP '11)*, Prague, Czech Republic, May 2011.

- P. Ochandiano, H. Wymeersch, I. Sobrón, L. Martínez and M. Mendicute, "Novel ICI suppressing receiver for high-mobility DVB-T2 reception with large FFT modes", in *Proc. IEEE International Symposium on Broadband Multimedia Systems and Broadcasting (ISBMSB '11)*, Nuremberg, Germany, June 2011.

- L. Martínez, P. Ochandiano, I. Sobrón and M. Mendicute, "Novel pilot structures for BEM channel estimation and ICI compensation in high-mobility DVB", in *Proc. IEEE International Symposium on Broadband Multimedia Systems and Broadcasting (ISBMSB'11)*, Nuremberg, Germany, June 2011.

- P. Ochandiano, H. Wymeersch, M. Mendicute, L. Martínez and I. Sobrón, "Iterative ICI Cancellation Based on Factor Graphs for Large FFT Sizes", in *Proc. EURASIP European Signal Processing Conference (EUSIPCO'11)*, Barcelona, Spain, Aug. 2011.

- L. Martínez, P. Ochandiano, I. Sobrón and M. Mendicute, "Iterative BEM channel estimation and BP detection for ICI cancellation in DVB systems with very high-mobility", in *Proc. IEEE International Symposium on Broadband Multimedia Systems and Broadcasting (ISBMSB'12)*, Seoul, South Korea, June 2012.

**National conference papers:**

- I. Sobrón, P. Ochandiano, L. Martínez, M. Mendicute and J. Altuna, "Análisis de robustez de DVB-T2 en redes SFN", in *Proc. XXII Simposium Nacional de la Unión Científica Internacional de Radio (URSI '09)*, Cantabria, Spain, Sep. 2009.

- L. Martínez, I. Sobrón, P. Ochandiano, M. Mendicute and J. Altuna, "Estimación de canal para transmisión multiantena y recepción móvil en DVB-T2", in *Proc. XXIII Simposium Nacional de la Unión Científica Internacional de Radio (URSI '10)*, Bilbao, Spain, Sep. 2010.

- P. Ochandiano, I. Sobrón, L. Martínez, M. Mendicute and J. Altuna, "Detección iterativa en receptores DVB-T2", in *Proc. XXIII Simposium Nacional de la Unión Científica Internacional de Radio (URSI '10)*, Bilbao, Spain, Sep. 2010.

- I. Sobrón, P. Ochandiano, L. Martínez, M. Mendicute and J. Altuna, "Transmisión SFBC distribuida en redes SFN de DVB-T2", in *Proc. XXIII Simposium Nacional de la Unión Científica Internacional de Radio (URSI '10)*, Bilbao, Spain, Sep. 2010.

# References


[Anastasopoulos07] A. Anastasopoulos, K. M. Chugg, G. Colavolpe, G. Ferrari, and R. Raheli, "Iterative detection for channels with memory", *Proceedings of the IEEE*, vol. 95, 1272–1294, 2007.

[ARIB01] ARIB, "Transmission System for Digital Terrestrial Television Broadcasting STD-B31 v1.0", 2001.

[ATSC05] ATSC, "ATSC Digital Television Standard (A/53) Revision E, with Amendments No. 1 and 2", December 2005.

[Baracca11] P. Baracca, S. Tomasin, L. Vangelista, N. Benvenuto, and A. Morello, "Per Sub-block Equalization of Very Long OFDM Blocks in Mobile Communications", *IEEE Transactions on Communications*, vol. 59, 2011.

[Berrou93] C. Berrou, A. Glavieux, and P. Thitimajshima, "Near Shannon limit error-correcting coding and decoding: Turbo-codes", pp. 1064–70, New York, NY, USA, 1993.

[Cai03] X. Cai and G. Giannakis, "Bounding performance and suppressing intercarrier interference in wireless mobile OFDM", *IEEE Transactions on Communications*, vol. 51, 2047–56, 2003.

[Caire98] G. Caire, G. Taricco, and E. Biglieri, "Bit-interleaved coded modulation", *IEEE Transactions on Information Theory*, vol. 44, 927–46, 1998.

[Chevillat89] P. R. Chevillat and E. Eleftheriou, "Decoding of trellis-encoded signals in the presence of intersymbol interference and noise", *IEEE Transactions on Communications*, vol. 37, 669–676, 1989.

[Clarke68] R. H. Clarke, "A Statistical Theory of Mobile-Radio Reception", *Bell Systems Technical Journal*, vol. 47, 957–1000, 1968.

[Colavolpe05a] G. Colavolpe and A. Barbieri, "On MAP symbol detection for ISI channels using the Ungerboeck observation model", *IEEE Communications Letters*, vol. 9, 720–2, 2005.

[Colavolpe05b] G. Colavolpe and G. Germi, "On the application of factor graphs and the sum-product algorithm to ISI channels", *IEEE Transactions on Communications*, vol. 53, 818–825, 2005.

[Colavolpe06] G. Colavolpe, "On LDPC codes over channels with memory", *IEEE Transactions on Wireless Communications*, vol. 5, 1757–66, 2006.

[COST20789] COST207, "Digital land mobile radio communications (final report)", Tech. rep., Commision of the European Communities, Directorate General Telecommunications, Information Industries and Innovation, 1989.

[Douillard95] C. Douillard, M. Jezequel, C. Berrou, A. Picart, P. Didier, and A. Glavieux, "Iterative correction of intersymbol interference: turbo-equalization", *European Transactions on Telecommunications*, vol. 6, 507–11, 1995.

[DVB08] DVB, "Framing structure, channel coding and modulation for a second generation digital terrestrial television broadcasting system (DVB-T2)", Document A122, June 2008.

[DVB09] DVB, "Implementation guidelines for a second generation digital terrestrial television broadcasting system (DVB-T2)", Document A133, February 2009.

[ETSI94] E. B. U. ETSI, "Digital Broadcasting Systems for Television, Sound and Data services; Framing structure, channel coding and modulation for cable systems", Tech. rep., ETSI, 1994.

[ETSI95] E. B. U. ETSI, "Digital Video Broadcasting (DVB); Framing structure, channel coding and modulation for 11/12 GHz satellite services", Tech. rep., ETSI, 1995.

[ETSI97] ETSI, "Digital video Broadcasting (DVB); Framing structure, channel coding and modulation for digital terrestrial television (DVB-T) ETS EN 300 744", March 1997.

[ETSI04] E. B. U. ETSI, "Digital Video Broadcasting (DVB); Transmission System for Handheld Terminals (DVB-H)", Tech. rep., ETSI, 2004.

[ETSI05] E. B. U. ETSI, "Digital Video Broadcasting (DVB); Second generation framing structure, channel coding and modulation systems for broadcasting, interactive services, news gathering and other broadband satellite applications", Tech. rep., ETSI, 2005.

[ETSI09] ETSI, "Digital Video Broadcasting (DVB); Frame structure channel coding and modulation for a second generation digital terrestrial television broadcasting system (DVB-T2)", Tech. rep., ETSI, 2009.

[Eva Peiker09] J. L. Eva Peiker, Werner G. Teich, "Windowing in the receiver for OFDM systems in high-mobility scenarios", in *MCSS*, pp. pp.57–65, 2009.

[Eyuboglu88] M. Eyuboglu and S. Qureshi, "Reduced-state sequence estimation with set partitioning and decision feedback", *IEEE Transactions on Communications*, vol. 36, 13–20, 1988.

[Fang08] K. Fang, L. Rugini, and G. Leus, "Low-complexity block turbo equalization for OFDM systems in time-varying channels", *IEEE Transactions on Signal Processing*, vol. 56, 5555–66, 2008.

[Fang10] K. Fang, L. Rugini, and G. Leus, "Block transmissions over doubly selective channels: iterative channel estimation and turbo equalization", *EURASIP Journal on Advances in Signal Processing*, p. 974652 (13 pp.), 2010.

[Fertonani08] D. Fertonani, A. Barbieri, and G. Colavolpe, "Novel graph-based algorithms for soft-output detection over dispersive channels", in *IEEE Global Telecommunications Conference*, p. 5 pp., Piscataway, NJ, USA, 2008.

[Forney72] J. Forney, G.D., "Lower bounds on error probability in the presence of large intersymbol interference", *IEEE Transactions on Communications*, vol. 20, 76–7, 1972.

[Forney01] J. Forney, G.D., "Codes on graphs: normal realizations", *IEEE Transactions on Information Theory*, vol. 47, 520–48, 2001.

[Gallager63] R. G. Gallager, "Low density parity check codes", *IRE Trans. Inf. Theory*, vol. 8, 21–28, 1963.

[Gallard11] C. Gallard, "D21.1 Ű Analysis on 3GPP E-MBMS/DVB-NGH Physical Layer Convergence", Tech. rep., France Telecom, 2011.

[Haselmayr11] H. Haselmayr, B. Etzlinger, and A. Springer, "Factor-graph-based detection algorithms for coded OFDM over time-varying channels", in *Newcom++*, 2011.

[Herlekar05] S. Herlekar, K. Matarneh, H.-C. Wu, Y. Wu, and X. Wang, "Performance evaluation of an ICI self-cancellation coded transceiver for mobile DVB-T applications", *IEEE Transactions on Consumer Electronics*, vol. 51, 1110–20, 2005.

[Hou05] W.-S. Hou and B.-S. Chen, "ICI cancellation for OFDM communication systems in time-varying multipath fading channels", *IEEE Transactions on Wireless Communications*, vol. 4, 2100–10, 2005.

[Hsu09] C.-Y. Hsu and W.-R. Wu, "Low-complexity ICI mitigation methods for high-mobility SISO/MIMO-OFDM systems", *IEEE Transactions on Vehicular Technology*, vol. 58, 2755–68, 2009.

[Huang07] X. Huang and H.-C. Wu, "Robust and efficient intercarrier interference mitigation for OFDM systems in time-varying fading channels", *IEEE Transactions on Vehicular Technology*, vol. 56, 2517–28, 2007.

[Huang11] C.-W. Huang, P.-A. Ting, and C.-C. Huang, "A novel message passing based MIMO-OFDM data detector with a progressive parallel ICI canceller", *IEEE Transactions on Wireless Communications*, vol. 10, 1260–8, 2011.

[Hwang09] S. U. Hwang, J. H. Lee, and J. Seo, "Low complexity iterative ICI cancellation and equalization for OFDM systems over doubly selective channels", *IEEE Transactions on Broadcasting*, vol. 55, 132–139, 2009.

[IEEE05] IEEE, "IEEE 802.16e. Air interface for fixed and mobile broadband wireless access systems", Tech. rep., IEEE, 2005.

[IEEE06] IEEE, "IEEE 802.11n. Wireless LAN medium access control and physical layer specifications: enhancements for higher throughput", Tech. rep., IEEE, 2006.

[Imai77] H. Imai and S. Hirakawa, "A new multilevel coding method using error-correcting codes", *IEEE Transactions on Information Theory*, vol. IT-23, 371–7, 1977.

[Kannu05] A. Kannu and P. Schniter, "MSE-optimal training for linear time-varying channels", in *IEEE International Conference on Acoustics, Speech, and Signal Processing (ICASSP)*, 2005.

[Kaynak05] M. Kaynak, T. Duman, and E. Kurtas, "Belief propagation over MIMO frequency selective fading channels", p. 6 pp., 2005.

[Kou05] Y. Kou, W.-S. Lu, and A. Antoniou, "Application of sphere decoding in intercarrier-interference reduction for OFDM systems", in *2005 IEEE Pacific Rim Conference on Communications, Computers and Signal Processing (PACRIM)*, pp. 360–3, 2005.

[Kschischang01] F. Kschischang, B. Frey, and H.-A. Loeliger, "Factor graphs and the sum-product algorithm", *IEEE Transactions on Information Theory*, vol. 47, 498–519, 2001.

[Ku11] M.-L. Ku, W.-C. Chen, and C.-C. Huang, "EM-based iterative receivers for OFDM and BICM/OFDM systems in doubly selective Channels", *IEEE Transactions on Wireless Communications*, vol. 10, 1405–1415, 2011.

[Lee01] C. Lee, S. Ng, L. Piazzo, and L. Hanzo, "TCM, TTCM, BICM and iterative BICM assisted OFDM-based digital video broadcasting to mobile receivers", vol. vol.1, pp. 732–6, Piscataway, NJ, USA, 2001.

[Leif07] Leif, J. Svensson, A. Nevalainen, and M. Faulkner, "Some results on implementing low-complex ICI cancellation for DVB-H", *IEEE 65th Vehicular Tech. Conf. - VTC2007-Spring*, pp. 2931–2935, 2007.

[Li10] X. Li, R. Zhou, V. Chakravarthy, S. Hong, and Z. Wu, "Total intercarrier interference cancellation for OFDM mobile communication systems", Piscataway, NJ, USA, 2010.

[Liu09] D. Liu and M. Fitz, "Iterative MAP equalization and decoding in wireless mobile coded OFDM", *IEEE Transactions on Communications*, vol. 57, 2042–51, 2009.

[Lu08] S. Lu and N. Al-Dhahir, "Coherent and differential ICI cancellation for mobile OFDM with application to DVB-H", *IEEE Transactions on Wireless Communications*, vol. 7, 4110–16, 2008.

[MacKay99] D. MacKay, "Good error-correcting codes based on very sparse matrices", *IEEE Transactions on Information Theory*, vol. 45, 399–431, 1999.

[Massey74] J. Massey, "Coding and modulation in digital communications", in *International Zurich Seminar on Digital Communications*, pp. 2–4, 1974.

[May04] E. May and E. Ayanoglu, "Full frequency diversity codes for single input single output systems", in *IEEE 60th Vehicular Technology Conference*, vol. 3, pp. 1870–4, 2004.

[Mendicute10] M. Mendicute, I. Sobrón, L. Martínez, and P. Ochandiano, *DVB-T2: New Signal Processing Algorithms for a Challenging Digital Video Broadcasting Standard*, Intech, 2010.

[Ochandiano10] P. Ochandiano, I. Sobrón, L. Martínez, M. Mendicute, and J. Altuna., "Analysis of ICI compensation for DVB-T2", in *IEEE International Symposium on Wireless Communication Systems (ISWCS)*, 2010.

[Ochandiano11a] P. Ochandiano, H. Wymeersch, M. Mendicute, L. Martínez, and I. Sobrón, "Iterative ICI cancellation based on factor graphs for large FFT sizes", in *European Signal Processing Conference (EUSIPCO)*, 2011.

[Ochandiano11b] P. Ochandiano, H. Wymeersch, I. Sobron, L. Martinez, and M. Mendicute, "Novel ICI suppressing receiver for high-mobility DVB-T2 reception with large FFT modes", in *IEEE International Symposium on Broadband Multimedia Systems and Broadcasting*, 2011.

[Ochandiano12a] P. Ochandiano, L. Martínez, I. Sobrón, and M. Mendicute, "Iterative detection and channel estimation for mobile terretrial TV with long OFDM blocks", *Submitted to IEEE Transactions on Broadcasting*, 2012.

[Ochandiano12b] P. Ochandiano, H. Wymeersch, I. Sobron, L. Martinez, and M. Mendicute, "Factor graph based detection approach for high-mobility OFDM systems with large FFT modes", *Submitted to EURASIP Wireless Communications and Networking*, 2012.

[Ohno05] S. Ohno, "Maximum likelihood inter-carrier interference suppression for wireless OFDM with null subcarriers", pp. 849–52, 2005.

[Panayirci10] E. Panayirci, H. Senol, and H. V. Poor, "Joint channel estimation, equalization, and data detection for OFDM systems in the presence of very high mobility", *IEEE Transactions on Signal Processing*, vol. 58, 4225–4238, 2010.

[Peng06] F. Peng and W. Ryan, "A low-complexity soft demapper for OFDM fading channels with ICI", pp. 1549–54, 2006.

[Poggioni09] M. Poggioni, L. Rugini, and P. Banelli, "DVB-T/H and T-DMB: physical layer performance comparison in fast mobile channels", *IEEE Transactions on Broadcasting*, vol. 55, 719–30, 2009.

[Richardson01] T. Richardson, M. Shokrollahi, and R. Urbanke, "Design of capacity-approaching irregular low-density parity-check codes", *IEEE Transactions on Information Theory*, vol. 47, 619–37, 2001.

[Rugini06] L. Rugini, P. Banelli, and G. Leus, "Low-complexity banded equalizers for OFDM systems in Doppler spread channels", *EURASIP Journal on Applied Signal Processing*, vol. 2006, 13, 2006.

[Russell95] M. Russell and G. Stuber, "Interchannel interference analysis of OFDM in a mobile environment", vol. vol.2, pp. 820–4, New York, NY, USA, 1995.

[SAC06] SAC, "GB20600-2006 Framing structure, Channel coding and modulation for digital television terrestrial broadcasting system", 2006.

[Schniter04] P. Schniter, "Low-complexity equalization of OFDM in doubly selective channels", *IEEE Transactions on Signal Processing*, vol. 52, 1002–11, 2004.

[Schreckenbach03] F. Schreckenbach, N. Gortz, J. Hagenauer, and G. Bauch, "Optimized symbol mappings for bit-interleaved coded modulation with iterative decoding", pp. 3316–20, Piscataway, NJ, USA, 2003.

[Stamoulis02] A. Stamoulis, S. Diggavi, and N. Al-Dhahir, "Intercarrier interference in MIMO OFDM", *IEEE Transactions on Signal Processing*, vol. 50, 2451–64, 2002.

[Suffritti07] R. Suffritti, E. Del Re, and S. Morosi, "Soft demapping and turbo decoding for satellite broadcasting communications", pp. 92–6, Piscataway, NJ, USA, 2007.

[Tang07] Z. Tang, R.-C. Cannizzaro, G. Leus, and P. Banelli, "Pilot-Assisted Time-Varying Channel Estimation for OFDM Systems", *IEEE Transactions on Signal Processing*, vol. 55, 2007.

[Tanner81] R. Tanner, "A recursive approach to low complexity codes", *IEEE Transactions on Information Theory*, vol. IT-27, 533–47, 1981.

[Taubock11] G. Taubock, M. Hampejs, P. Svac, G. Matz, F. Hlawatsch, and K. Grochenig, "Low-complexity ICI/ISI equalization in doubly dispersive multicarrier systems using a decision-feedback LSQR algorithm", *IEEE Transactions on Signal Processing*, vol. 59, 2432–6, 2011.

[tenBrink01] S. ten Brink, "Convergence behavior of iteratively decoded parallel concatenated codes", *IEEE Transactions on Communications*, vol. 49, 1727–37, 2001.

[Tomasin05] S. Tomasin, A. Gorokhov, H. Yang, and J.-P. Linnartz, "Iterative interference cancellation and channel estimation for mobile OFDM", *IEEE Transactions on Wireless Communications*, vol. 4, 238–45, 2005.

[Tuchler02] M. Tuchler, R. Koetter, and A. Singer, "Turbo equalization: principles and new results", *IEEE Transactions on Communications*, vol. 50, 754–67, 2002.

[Ungerboeck74] G. Ungerboeck, "Adaptive maximum-likelihood receiver for carrier-modulated data-transmission systems", *IEEE Transactions on Communications*, vol. 22, 624–36, 1974.

[Ungerboeck76] G. Ungerboeck and I. Csajka, "On improving data link performance by increasing the channel alphabet and introducing sequence coding", 1976.

[Wang06] T. Wang, J. Proakis, E. Masry, and J. Zeidler, "Performance degradation of OFDM systems due to Doppler spreading", *IEEE Transactions on Wireless Communications*, vol. 5, 1422–32, 2006.

[Wiberg96] N. Wiberg, *Codes and decoding on general graphs*, Ph.D. thesis, Linkoping Univ., Sweden, 1996.

[Wilhelmsson07] L. Wilhelmsson, J. Svensson, A. Nevalainen, and M. Faulkner, "Some results on implementing low-complex ICI cancellation for DVB-H", pp. 2931–2935, 2007.

[Wu11] H. Wu, S. Yang, J. Ou, and L. Yang, "Improved ICI mitigation scheme over time-varying channels for high-mobility OFDM systems", *Journal of Convergence Information Technology*, vol. 6, 264–272, 2011.

[Wymeersch07] H. Wymeersch, *Iterative receiver design*, Cambridge University Press, 2007.

[Xie09] Q. Xie, K. Peng, C. Pan, and Z. Yang, "Bit-interleaved LDPC coded modulation with iterative demapping and decoding", *Qinghua Daxue Xuebao/Journal of Tsinghua University*, vol. 49, no. 8, 1201–1204, 2009.

[Yang04] M. Yang, W. Ryan, and Y. Li, "Design of efficiently encodable moderate-length high-rate irregular LDPC codes", *IEEE Transactions on Communications*, vol. 52, 564–71, 2004.

[Yedidia05] J. Yedidia, W. Freeman, and Y. Weiss, "Constructing free-energy approximations and generalized belief propagation algorithms", *IEEE Transactions on Information Theory*, vol. 51, 2282–312, 2005.

[Zehavi92] E. Zehavi, "8-PSK trellis codes for a Rayleigh channel", *IEEE Transactions on Communications*, vol. 40, 873–84, 1992.

[Zhao01] Y. Zhao and S.-G. Haggman, "Intercarrier interference self-cancellation scheme for OFDM mobile communication systems", *IEEE Transactions on Communications*, vol. 49, 1185–91, 2001.